SATURATED TEARING MODES IN LOW ASPECT RATIO TOKAMAKS

A THESIS
Presented to
The Faculty of the Division
of Graduate Studies

By

Robert N. Morris

In Partial Fulfillment
of the Requirements for the Degree
of Doctor of Philosopy
in the School of Nuclear Engineering
and Health Physics

Georgia Institute of Technology

March, 1984

SATURATED TEARING MODES IN LOW
ASPECT RATIO TOKAMAKS

Approved:

Dr. G. Bateman, Chairman

Dr. W. M. Stacey

Dr. W. O. Carlson

Dr. J. N. Davidson

Dr. R. R. Davey

Date approved by Chairman 20 FEB 84

Acknowledgment

I would like to extend my thanks to my thesis advisor, Dr. Bateman, for the suggestion of saturated tearing modes as a thesis topic and for the many hours of help and discussion he gave. I also wish to extend my thanks to my wife Rebecca for her patience and support during the course of this project. My reading committee members, Dr. Carlson, Dr. Davey, Dr. Davidson, and Dr. Stacey, deserve recognition for their time spent reading my thesis and for their useful suggestions. Special notice goes to Bruce DeWald whose colorful personality and special ability to locate taverns frequented by the lower echelons of society provided interest and some much needed diversion. Finally I wish to thank the faculty of the Nuclear Engineering Department for creating a stimulating environment.

Table of Contents

List of Illustrations

Summary

A quasilinear perturbation analysis of the time independent MHD equations has lead to the formulation of a set of equations suitable for the study of saturated tearing modes. The quasilinear analysis allows the effects of the magnetic island on the background equilibrium to be modelled in a self consistant way in a toroidal plasma of arbitrary aspect ratio, beta, and cross section.

The most important finding of this study is the effect of the current density profile within a magnetic island vs the width of a magnetic island. "Peaking" or "anti-peaking" the current density profile within a magnetic island can cause large differences in the saturated magnetic island width; furthermore the width of the magnetic island is found to be sensitive to this parameter.

Modification of the background current density profile by the presence of multiple islands can and does cause nonlinear destablization of magnetic islands; also toroidicity and elongation are shown to have a linear coupling effect that can also destabilize otherwise stable magnetic islands. By themselves, toroidicity and elongation are shown to modestly reduce the saturated magnetic island width and a general trend of smaller magnetic island width with the inward shift of the mode rational surface is noted.

CHAPTER I

Introduction

Magnetic islands belong to a class of perturbations known as internal modes which are believed to exist in controlled fusion devices such as tokamaks and stellarators. Internal modes differ from other types of perturbations in that their major effects are in the internal rather than the boundary or edge regions of the plasma. These effects may manifest themselves as topological changes to the plasma proper and may radically alter the plasma confinement and its global stability. The major impact of magnetic islands is to alter the internal magnetic field configuration which:

1. causes enhanced transport of plasma particles and energy due to the destruction of closed magnetic surfaces;

2. produces Mirnov oscilations by the torodial rotation of the saturated instability (Tearing mode);

3. causes, in the most pathological cases, the major disruption when two tearing modes of different helicity overlap.

Magnetic islands are resonance phenomena - that is, a relatively small perturbation can have its effect enhanced by resonating, or strongly interacting in very specific regions of the plasma. Specifically, these regions are in the neighborhood of closed magnetic field lines or rational (A closed magnetic field line is a magnetic field line that closes on itself after traversing around the torus an integer number of times.) [1-12]

Spontaneously growing perturbations which cause magnetic islands are known as tearing modes, since they cause the magnetic field lines to "tear" or break and reconnect to form a new and different magnetic configuration. This thesis will be concerned with spontaneously growing magnetic perturbations and will concentrate on the interaction between the magnetic perturbations and the current density profile responsible for the existence of these perturbations. Magnetic islands can also be induced by externally applied nonaxisymmetric magnetic perturbations and by other related instabilities, but these other mechanisms are beyond the scope of this thesis.

Magnetic islands are major topological deviations from the simple nested flux surface model for MHD equilibrium. [1,2,40] Rather than the magnetic surfaces being composed of concentric tori as shown in figure 1-1, an equilibrium with magnetic islands has helically distorted cylinders within the simply nested tori as well. See figure 1-2. The nucleus of each magnetic island is a closed magnetic field line which supports a resonant perturbation. Unlike other types of magnetic perturbations, the tearing mode is capable of large scale effects on the plasma even though the amplitude of the mode itself is many times smaller than the other equlibrium quanities. It is the fact that the background equlibrium can be and is effected by the tearing mode that generates the difficulty and the interest in studying the phenomenon. [1,12,13,14,15]

The two important parameters that characterize an island are its helicity number and its width. The helicity numbers, which are the m and n numbers (i.e. 2/1,3/1,etc.) , indicate the island location and with what magnetic surface it interacts with. The relationship between the m and n numbers is

$$nq - m = 0 \qquad (1\text{-}1)$$

where q is defined as the limit of the ratio of the number of

turns a magnetic field line makes as it travels the long way around the toriod divided by the number of turns it makes as it travels the short way around. The periodicity in the polodial angle is m, while n is the periodicity in the torodial angle.

The width of the island is defined as the maximum radial width across the island region. It is approximately

$$W = 4\left[\frac{B^{1V}_{mn}}{n B^{0\theta}\frac{dq}{dV}}\right]^{1/2} \qquad (2\text{-}2)$$

where all quanties are evaluated at the mode rational surface. The perturbed radial field is B^{1V}_{mn} and $B^{0\theta}$ is the poloidial field. This formula has been tested in various computer experiments with the perturbed amplitude being several percent of the toroidal field and found to be in good agreement. [11,12]

Magnetic islands are observed to rotate in the toroidal direction, in the direction of the electron drift resulting from the plasma current. This thesis will not address this rotation, but rather will assume its existence as it does not enter into the MHD analysis. [19]

The most serious problem speculated to be caused by magnetic islands is the major disruption. [16,17,18,19,71,73] Major disruptions can be classified in two ways: A hard disruption in which the entire plasma is

dumped out on a microsecond to hundreds of microseconds time scale and a soft disruption in which the plasma confinement decreases suddenly, but not to a point from which recovery is impossible. [16,21,73] The mechanism for the hard disruption is thought to be the overlap of two islands which generates a large stochastic magnetic region within the plasma volume destroying the plasma confinement. The soft disruption is a more benign effect, in which an island may interact with the plasma interior and the wall limiter providing a transport short circuit, which may or may not be fatal to the discharge. [16,17,18-28,73]

Magnetic islands, when uncoupled or only loosely coupled to each other, grow on a time scale of milliseconds. This growth rate is too slow to explain the sudden nature of the hard disruption which happens on a microsecond time scale. If, however, two magnetic islands of different helicity were to grow and overlap, the resulting region engulfed by the islands may explosively grow into a stochastic magnetic region of poor confinement, and if the initial islands were large enough, a large percentage of the plasma confinement would be destroyed thus terminating the discharge. The most probable causes for the major or "hard" disruption are either the overlapping of the m=2, n=1 island with the m=3, n=2 island and the lack of confinement due to the large stochastic region thus generated, or a combination effect in a high density plasma where the 2/1 island overlaps

both the 3/2 island and the limiter. This occurance destroys the plasma confinement by introducing a large thermal loss and an influx of impurities to the plasma interior. The soft disruption may be the result of a single island connecting the internal plasma volume with the limiter. This will transfer large quanties of plasma energy out of the main plasma volume, but if the island diappears soon enough recovery may be possible. The 2/1 island seems to be the dominant island in this case. [16,73]

Unlike disruptions, Mirnov oscillations are a relativity mild instability. [2,3,29,30,31] They manifest themselves as small oscillating helicial perturbations in the poloidal magnetic field. These perturbations usually settle down to a saturated level as the discharge becomes estabilished and have an oscillation frequency in the neighborhood of 10kHz. This oscillation is believed to be caused by the toroidal rotation of the tearing modes at the electron diamagnetic drift velocity. As the Mirnov oscillations increase in amplitude the energy confinement time of the plasma drops and the sudden reduction in the rotation rate of a tearing mode may be a precurser to a major disruption.

The other major concern is the effect of magnetic islands on transport. Since the islands have a width, they provide a transport short circuit which may be responsible for enhanced transport. [1,2,3] One example of this is the

flattening of the temperature and the density profiles in the plasma interior caused by sawtooth oscillations. These oscillations are caused by a low mode number magnetic island (n=1,m=1) which periodicly dumps plasma particles out of the center of the plasma and into neighboring regions. To analyze this low mode number island requires the inclusion of inertial terms which will not be addressed by this thesis. [3,29,30,31,62] Another example is the above mentioned connection between the plasma interior and edge regions by a 2/1 magnetic island which can cause a large thermal loss under some conditions, especially with contact with the limiter. [16,73] The islands may also enhance particle loss of fast and trapped particles. The situtation becomes even more complex when islands of different helicity overlap and produce a stochastic magnetic field region. This will presumably result in a region with no confinement since the particles will traverse this region on a time scale of the thermal velocities, rather than the diffusion time scale. [3,11,18] Electrons may be effected to a much greater degree than ions, since they have a much smaller gyro radius which allows them to respond to spatially finer scale perturbations. [32]

The analytic study of tearing modes began with a plane slab analysis of a plasma. [11,39,40] The plane slab model examined the singular nature of the problem near the mode rational surface and the resulting boundary layer phenomena.

From this analysis growth rates were estimated by using only the discontinuity of the global solution at the resonant surface rather than by integrating the boundary layer equations. This form of analysis is know as the Δ' analysis and it provided a convenient way to examine an equlibrium for stability to tearing modes and to estimate their saturated widths; unfortunately the plane slab model lacked the ability to model mode mixing and toroidal effects. In order to expand the range of phenomena that could be studied, the reduced MHD equations were developed. [11,18,40,42,62] These equations are the large aspect ratio, low beta limit of the ideal MHD equations with resistivity included, and these equations provided the model that has been of major interest in the study of tearing modes. Several different approaches have been applied to the study of tearing modes using the reduced MHD equations; they are:

1. a linearized model which contains a singularity at the rational surface and relies on a Δ' type of matching;

2. a helical flux model which is limited to a two dimensional formulation, but requires less computational effort;

3. a nonlinear model in which the background is allowed to change as the perturbation develops, thus allowing the perturbation to effect the background; and

4. a quasilinear model in which the background is modified to provide a solution to a linearized tearing mode equation.

The helical flux model is the simplest of these models and has been extensively studied. [4,13,18,43,,53] A simple analytic equlibrium with tearing modes has also been found for a helical flux function. [45] The base model commonly used in the literature for the study of the helical flux function centers around a Δ' type of analysis as in the slab; however saturation effects have been included by using a quaslinear method in which the perturbation is allowed to feedback and influence the functional form for the current; that is, the current profile is modified by the presence of an island. [13] These models have shown that certain current profiles exhibit varying degrees of stability against the formation of tearing modes. The saturation of the resulting island is due to the island sampling different portions of the backgroud equlibrium. The important point made by this quaslinear analysis is that a quaslinear or fully nonlinear model is very useful to compute the saturated island width

since the island width is strongly effected by the current functional form near the island.

The helical flux model, while useful for the study of one harmonic, cannot be used to examine the effects of islands of different helicity on the plasma. It is therefore necessary to use a less stringent form of the reduced MHD equations to address this area. Of particular interest is how the islands effect each other, both in terms of growth rate and saturation width. The dynamics of two islands overlapping and the resulting effect on the plasma is another phenomenon which generates research interest as well.

Solving the reduced MHD equations in cylindrical geometry, with a three dimensional equation set rather than a two dimensional set, allows one to observe the coupling between islands and the resultant effect on the current profile. It has been observed that the 2/1 tearing mode can destablize the 3/2 mode resulting in large increases in the growth rate of the 3/2 mode and the resutant increase in the 3/2 island width. This destablizing effect also extends to other islands as well; one effect of this destablization is to increase the total plasma region occupied by these islands. In fact, if a suitably large number of islands is included, the entire plasma region may be destroyed, from the center to the limiter. [17,18,46,47]

It is generally found that the growth rate of the islands transforms from an exponential growth rate to an

algebraic growth rate as the islands grow in width. [50] The nonlinear coupling may change this result in some cases, resulting in the sudden growth of a favored mode at a much accelerated rate. This may explain the very sudden nature of the major disruption. [17,18,46,76]

Magnetic islands cause sharp deformations in the toroidal current profile near the island x points and this deformation of current becomes even more severe as the number of islands increase. This in fact may have a major coupling effect between islands, since the saturated width of the islands are sensitive to the current density gradient near the island edge. [13,46,48,76] This severe current deformation eventually limits the computer runs, as numeric problems soon develop. [17,18,46] Again this points to the need for a nonlinear or quasilinear approach to the solution.

Toroidal coupling has a profound effect upon the magnetic islands; it introduces a linear coupling effect between neighboring islands. This coupling effect causes normally stable islands to be destabilized by their unstable neighbor. This may cause both islands to grow and is responsible for the generation of satellite islands. Since these satellite islands manifest themselves as an increase in the stochastic magnetic field region, it is clear that this effect is important even in the large aspect ratio approximation. [17,46,47] Mathematically this comes about from the off diagonal terms of the metric tensor relating the

contravariant and covariant vector components of the equilibrium magnetic field. Unfortunately this effect is very difficult to handle for small aspect ratios and has been only formulated in the time independent case. [14]

It is clear that both the nonlinear mode coupling and the geometric mode coupling (toroidal) greatly effect the growth and saturation of magnetic islands. It is this nature of tearing modes that puts the stringent conditions on the equations used to study magnetic islands; apparently higher order terms (toroidal geometry, current profile modifications) must be included to form a reasonable approximation to the physical case.

The set of equations this thesis will concentrate on are the quasilinear equations. In contrast to the reduced MHD equations which generally follow the time evolution of the fields, the quaslinear equations do not follow the time evolution of the fields, but concentrate on the effect of the magnetic island on the background equilibrium. They can, however, handle more complex geometric situations and are useful to find saturated tearing modes in these more physical situations. [8,12,13,14,15,43,48]

The object of this thesis is to apply the quasilinear analysis to cases involving toroidal geometry by using the contravariant and covariant representation of the fields and thus form a system of equations that can be solved without resorting to an aspect ratio approximation. [14] The effect

of the current profile within a magnetic island will be examined along with the effects of plasma elongation. It will be shown that toroidicity causes a small reduction in the width of the magnetic islands and that coupling of magnetic islands with the same n numbers occurs as predicted. The major new finding, however, is that the current density functional form within the magnetic island is one of the most important factors in determining the saturated width of a magnetic island. Since the modelling of a specific current density profile within a magnetic island depends on the local tranport properties of the plasma, which are beyond the scope of this thesis, a parameter study was undertakened to study the saturated magnetic island width that occurred with different levels of current peaking within an island.

The major limit to the accuracy of this model is its confinement to modes that saturate; thus it cannot examine the effect of the m=1, n=1 mode which, in general, does not saturate. This limitation may be most severe when studying toroidal coupling as the m=1, n=1 island may be the most important driving term; it may also play a part in the soft disruptions. [62,73] Other limits include the computer resources available which, at the present time, limit this author to the examination of only two simultaneous modes. Convergence problems may require careful attention to the initial guesses used in the iteration schemes, both in the equilibrium subroutines and the tearing mode subroutines.

Overall, however, the computer code has worked well, effectively used available resources, and provided much useful insight.

CHAPTER II

The Quasilinear Equations

2.1 Derivation

To derive the set of ordinary differential equations that form the basis of the quasilinear model one starts with the static scalar pressure plasma equilibrium force balance equations:

$$\vec{J} \times \vec{B} = \nabla P \tag{2-1}$$

$$\mu_0 \vec{J} = \nabla \times \vec{B} \tag{2-2}$$

$$\nabla \cdot \vec{B} = 0 \tag{2-3}$$

where $\vec{J}$ is the current density, $\vec{B}$ is the magnetic field, and P is the pressure. [12,14] Note that the velocity terms have been omitted; they are not necessary for this model since this model considers only the saturated magnetic island case.

The derivation requires a particular form for the Jacobian of the coordinate system for reasons to be described later. Anticipating this, the form for the two dimensional background equilibrium is written as:

$$\vec{B} = \mathcal{J}(v) B^{0\theta}(v) (\nabla\zeta \times \nabla v) + \mathcal{J}(v) B^{0\zeta}(v) (\nabla v \times \nabla\theta) \qquad (2\text{-}4)$$

$$\vec{J} = \mathcal{J}(v) J^{0\theta}(v) (\nabla\zeta \times \nabla v) + \mathcal{J}(v) J^{0\zeta}(v) (\nabla v \times \nabla\theta) \qquad (2\text{-}5)$$

$$\mathcal{J}^{-1}(v) = \nabla v \cdot (\nabla\theta \times \nabla\zeta) \qquad (2\text{-}6)$$

where $\mathcal{J}(v)$ is the Jacobian of the coordinate system and $B^{0\theta}$, $B^{0\zeta}$, $J^{0\theta}$, $J^{0\zeta}$ are the contravariant components of the vector field. See Chapter III for details of the coordinate system transformations.

In this generalized system the force balance equation reduces to:

$$\mathcal{J}(v) \left[J^{0\theta}(v) B^{0\zeta}(v) - J^{0\zeta}(v) B^{0\theta}(v) \right] = \frac{dP^{0}(v)}{dv} \qquad (2\text{-}7)$$

The derivation of the quasilinear equations is a perturbation analysis of (2-1), (2-2), and (2-3) using the perturbed terms in both their contravariant and covariant vector forms. [41] These forms are:

$$\vec{B}^1 = B^{1V}\mathcal{J}(\nabla\theta\times\nabla\zeta) + B^{1\theta}\mathcal{J}(\nabla\zeta\times\nabla V) + B^{1\zeta}\mathcal{J}(\nabla V\times\nabla\theta) \quad (2\text{-}8)$$

$$\vec{B}^1 = B^1_V\nabla V + B^1_\theta\nabla\theta + B^1_\zeta\nabla\zeta \quad (2\text{-}9)$$

$$\vec{J}^1 = J^{1V}\mathcal{J}(\nabla\theta\times\nabla\zeta) + J^{1\theta}\mathcal{J}(\nabla\zeta\times\nabla V) + J^{1\zeta}\mathcal{J}(\nabla V\times\nabla\theta) \quad (2\text{-}10)$$

Throughout this thesis a superscript "1" will indicate a perturbed term and a superscript "0" will indicate an equilibrium term. All the perturbed variables are written as a Fourier series in harmonics of θ and ζ

$$X^1(V,\theta,\zeta) = \sum_{m,n} X^1_{mn}(V)\exp[i(m\theta - n\zeta)] \quad (2\text{-}11)$$

When using $\vec{J} = \vec{J}^0 + \vec{J}^1$ and $\vec{B} = \vec{B}^0 + \vec{B}^1$ in (2-1) to (2-3) one finds that the divergence equation is most easily written in terms of the contravariant components of $\vec{B}^1$:

$$\frac{d}{dV}\left(-i\mathcal{J}B^{1V}_{mn}\right) = n\mathcal{J}B^{1\zeta}_{mn} - m\mathcal{J}B^{1\theta}_{mn} \quad (2\text{-}12)$$

However Ampere's law is most easily written in terms of the covariant components of $\vec{B}^1$

$$\mu_0 \mathcal{J} J^{1\nu}_{mn} = i\left(m B^1_{\zeta mn} + n B^1_{\theta mn}\right) \tag{2-13}$$

$$\mu_0 \mathcal{J} J^{1\theta}_{mn} = -in B^1_{\nu mn} - \frac{d}{dv} B^1_{\zeta mn} \tag{2-14}$$

$$\mu_0 \mathcal{J} J^{1\zeta}_{mn} = \frac{d}{dv} B^1_{\theta mn} - im B^1_{\nu mn} \tag{2-15}$$

The contravariant components of the current density and magnetic field are used to write the perturbed force balance equations which, when higher order terms are discarded, are:

$$-J^{1\nu}_{mn} \mathcal{J} B^{0\zeta} + J^{0\zeta} \mathcal{J} B^{1\nu}_{mn} = im p^1_{mn} \tag{2-16}$$

$$J^{1\nu}_{mn} \mathcal{J} B^{0\theta} - J^{0\theta} \mathcal{J} B^{1\nu}_{mn} = -in p^1_{mn} \tag{2-17}$$

$$J^{1\theta}_{mn} \mathcal{J} B^{0\zeta} - J^{1\zeta}_{mn} \mathcal{J} B^{0\theta} + J^{0\theta} \mathcal{J} B^{1\zeta}_{mn} - J^{0\zeta}_{mn} \mathcal{J} B^{1\theta}_{mn} = \frac{d}{dv} p^1_{mn} \tag{2-18}$$

Also from the above equations,

$$\left(n B^{0\zeta} - m B^{0\theta}\right) P^{1}_{mn} = i B^{1\nu}_{mn} \frac{dp^{0}}{dv} \tag{2-19}$$

Equation (2-12) is used in (2-15) to obtain

$$B^{1}_{\zeta mn} = \frac{-i\vartheta B^{1\nu}_{mn} \mu_0 J^{0\zeta}}{m B^{0\zeta}} - \frac{\mu_0 P^{1}_{mn}}{B^{0\zeta}} - \frac{n B^{1}_{\theta mn}}{m} \tag{2-20}$$

(2-20) is used with (2-18), (2-14), (2-15) to derive the tearing mode equation:

$$\left(n B^{0\zeta} - m B^{0\theta}\right)\left[\frac{d}{dv} B^{1}_{\theta mn} - im B^{1}_{\nu mn}\right]$$

$$= \mu_0 \left(n J^{0\zeta} - m J^{0\theta}\right) \vartheta B^{1\zeta}_{mn} - i\vartheta B^{1\nu}_{mn} B^{0\zeta} \frac{d}{dv}\left(\frac{\mu_0 J^{0\zeta}}{B^{0\zeta}}\right) \tag{2-21}$$

$$+ m\mu_0 P^{1}_{mn} \frac{1}{B^{0\zeta}} \frac{d}{dv} B^{0\zeta}$$

Equations (2-21) and (2-12) form a coupled pair of ordinary differential equations which can be solved for $-i\vartheta B^{1\nu}_{mn}$ and $B^{1}_{\theta mn}$. P^{1}_{mn} can be eliminated by using (2-19) in (2-21). $B^{1}_{\nu mn}$, $B^{1\theta}_{mn}$, and $B^{1\zeta}_{mn}$ can be written in terms of the other known quantities by relating the contravariant and covariant components in (2-8) and (2-9) as follows:

$$B^{1V} = \frac{B^{1V}}{(\nabla V \cdot \nabla V)} - \frac{B^1_\theta (\nabla\theta \cdot \nabla V)}{(\nabla V \cdot \nabla V)} - \frac{B^1_\varphi (\nabla\varphi \cdot \nabla V)}{(\nabla V \cdot \nabla V)} \qquad (2\text{-}22)$$

$$B^{1\theta} = \frac{B^{1V}(\nabla\theta \cdot \nabla V)}{(\nabla V \cdot \nabla V)} + B^1_\theta \left((\nabla\theta \cdot \nabla\theta) - \frac{(\nabla\theta \cdot \nabla V)^2}{(\nabla V \cdot \nabla V)} \right) \qquad (2\text{-}23)$$

$$+ B^1_\varphi \left((\nabla\theta \cdot \nabla\varphi) - \frac{(\nabla\theta \cdot \nabla V)(\nabla\varphi \cdot \nabla V)}{(\nabla V \cdot \nabla V)} \right)$$

$$B^{1\varphi} = \frac{B^{1V}(\nabla\varphi \cdot \nabla V)}{(\nabla V \cdot \nabla V)} + B^1_\theta \left((\nabla\theta \cdot \nabla\varphi) - \frac{(\nabla\theta \cdot \nabla V)(\nabla\varphi \cdot \nabla V)}{(\nabla V \cdot \nabla V)} \right) \qquad (2\text{-}24)$$

$$+ B^1_\varphi \left((\nabla\varphi \cdot \nabla\varphi) - \frac{(\nabla\varphi \cdot \nabla V)^2}{(\nabla V \cdot \nabla V)} \right)$$

Where (2-22), (2-23), and (2-24) follow from the appropiate combinations of $\vec{B} \cdot \nabla V$, $\vec{B} \cdot \nabla\theta$, and $\vec{B} \cdot \nabla\varphi$.

Thus by using (2-19), (2-20), (2-22), (2-23), and (2-24), (2-21) may be solved. Note that if ϑ were not a

function of v only, the equations would not seperate; this is why a Hamada like coordinate system is required; also note that equations (2-22)-(2-24) must be Fourier analysed to determine the components of B^{1V}_{mn} , $B^{1\Theta}_{mn}$, and $B^{1\zeta}_{mn}$.

The method of solution is as follows: Given $-i\vartheta B^{1V}_{mn}$ and $B^{1}_{\Theta mn}$ find $B^{1}_{\zeta mn}$ using (2-20). Next use B^{1V}_{mn} , $B^{1}_{\zeta mn}$, and $B^{1}_{\Theta mn}$ in (2-22)-(2-24) to find B^{1}_{Vmn} , $B^{1\Theta}_{mn}$, and $B^{1\zeta}_{mn}$. Finally use these results in (2-21) and (2-12) to find $\frac{d}{dv} B^{1}_{\Theta mn}$ and $\frac{d}{dv}\left(-i\vartheta B^{1V}_{mn}\right)$. Note that in general Fourier analysis of (2-22)-(2-24) produces a large number of harmonics. Only the resonant harmonics are used as the nonresonant terms have negligible effect on the island structure.

At this point it must be stressed that the above equations, having been derived in the time independance case, apply only to saturated magnetic islands where the neglected velocity components and time derivatives are unimportant. This set of equations cannot be used to compute magnetic perturbations that oscillate in time such as the m=1, n=1 tearing mode. They are, nonetheless, useful since many modes of interest saturate and these equations, unlike others, can handle toroidal geometry and plasma shaping. In order to include the modes that oscillate in time it is necessary to consider the inertial terms of the MHD equations, such as the mass density and velocity, with the consequence of greater complexity. [17,18,65,66]

If an abritary equlibrium is used in (2-21), (2-21) will be singular at the mode rational surface where $(nB^{0\varphi} - mB^{0\theta}) = 0$; in fact this singularity does not exist because the magnetic island modifies the equilibrium in the vicinity of the mode rational surface to support a resonant perturbation as will be demostrated in the following sections.

2.2 Computational Form for the Tearing Mode Equation

In order to solve (2-21) it is necessary to use (2-19) and the results of Chapter III to put (2-21) into a form that uses variables computed by the equilibrium subroutines. Using

$$\frac{dp}{dV} = \frac{d\psi}{dV}\frac{dp}{d\psi} = \psi' p' \tag{2-25}$$

$$q = B^{0\varphi}/B^{0\theta} \tag{2-26}$$

$$\frac{dF}{dV} = \frac{d\psi}{dV}\frac{dF}{d\psi} = \psi' F' \tag{2-27}$$

(2-21) can be reformulated as

$$\frac{d}{dV}B^{1}_{\theta mn} = imB^{1}_{Vmn} + F'\partial B^{1\varphi}_{mn} - \frac{i\partial B^{1V}_{mn}\psi' q F''}{(nq-m)}$$

$$+\frac{n\mu_0 P' \vartheta B'^{0q}_{mn}}{B^{00}(nq-m)} \qquad (2\text{-}28)$$

$$+\frac{i\vartheta B^{1V}_{mnq}}{(nq-m)}\left[\frac{m\mu_0 P'}{(nq-m)B^{0q2}}\frac{dB^{0q}}{dV}-\frac{d}{dV}\frac{\mu_0 P'}{B^{0q}}\right]$$

This form is useful because F'' is both a function to be given to the equilibrium subroutines and a function, as detailed below, to be modified by the presence of the magnetic island.

2.3 The Magnetic Island Structure

To examine the effect of magnetic islands upon the topology of the plasma confinement consider the equation for magnetic surfaces

$$\vec{B}\cdot\nabla f = 0 \qquad (2\text{-}29)$$

where $\vec{B}$ is the magnetic field and f is the surface mapped out by the magnetic field lines. While this equation, in conjunction with the MHD equations, may have many solutions, the ones of principle interest form a set of simply nested flux surfaces. [1]

If one departs from the simply nested flux surface model f may be forced to take on a very complicated form. The problem at hand is: given a magnetic island, find the simplest form that f can take on consistent with a physical interpretation.

To address this problem let

$$\vec{B} = \mathcal{J} B^{0\theta}(\nabla\zeta \times \nabla V) + \mathcal{J} B^{0\zeta}(\nabla V \times \nabla\theta) + \mathcal{J} B^{1V}(\nabla\theta \times \nabla\zeta) \quad (2\text{-}30)$$

where

θ is the polodial angle,

ζ is the toroidial angle,

V is the radial coordinate, and

$\mathcal{J}$ is the jacobian.

$B^{0\theta}$, $B^{0\zeta}$ are the background equilibrium and B^{1V} is the perturbed radial field (first order correction) of the form

$$B^{1V} \sim \sum_{m,n} B^{1V}_{mn} \exp[i(m\theta - n\zeta)]$$

The perturbations to the toroidal and poloidal field components have been neglected (and thus the divergence of $\vec{B}$ is nonzero) since they make no contribution to the following analysis.

Also let

$$f = f^{\circ}(v) + i f_{mn} \exp[i(m\theta - n\zeta)] \tag{2-31}$$

where f_{mn} is a perturbed term. Use (2-30) and (2-31) in (2-29), linearize, and keep only the first order terms to produce for a single harmonic (isolated island)

$$\frac{1}{(nB^{0\zeta} - mB^{0\theta})} \frac{df^{\circ}}{dv} = \frac{-f_{mn}}{B^{1v}_{mn}} \tag{2-32}$$

Since only the behavior of f° near V=Vmn is of interest (rational surface) replace V with Vmn+X where X=V-Vmn. Introduce $q = B^{0\zeta}/B^{0\theta}$ and rewrite (2-32) as

$$\frac{1}{(nq - m)} \frac{df^{\circ}}{dv} = \frac{-f_{mn} B^{0\theta}}{B^{1v}_{mn}} \tag{2-33}$$

Now, taking the limit of the right hand side of equation (2-33) and assuming that the left hand side is approximately constant across the island, the following second order equation is produced:

$$\frac{d^2 f^{\circ}}{dv^2} = \frac{-nq' B^{0\theta} f_{mn}}{B^{1v}_{mn}} \tag{2-34}$$

In this case one gets for f° (with the condition that $f'(0)=0$)

$$f^{\circ} = f_o - \frac{nq' B^{o\theta} f_{mn}}{2B^{1v}_{mn}} x^2 \qquad (2\text{-}35)$$

Where f_o is a constant. Thus near the island center f has a parabolic profile, which was to be expected since the magnetic island connects plasma on either side of the rational surface, forming an even function across the rational surface.

Using (2-35) in (2-31) and taking only the real parts one gets for f:

$$f = f_o - \frac{nq' B^{o\theta} f_{mn}}{2B^{1v}_{mn}} x^2 - f_{mn} \sin\phi \qquad (2\text{-}36)$$

where $\phi = m\theta - n\zeta$

To determine the halfwidth of the island set the value of f at the seperatrix equal to that at the edge of the island:

$$f(\phi_s, x=0) = f(\phi_H, H) \qquad (2\text{-}37)$$

or using (2-36)

$$H = \left[\left| \frac{2 B_{mn}^{1V}}{n B^{0\Theta} q'} \right| (\sin\phi_S - \sin\phi_H) \right]^{1/2} \qquad (2\text{-}38)$$

where

ϕ_S is the value of ϕ at the seperatrix

ϕ_H is the value of ϕ at the half width

The maximum excursion occurs when

$$\phi_S = \pi/2 \;, \quad \phi_H = 3\pi/2$$

giving for the half width,

$$H = 2\left[\frac{B_{mn}^{1V}}{n B^{0\Theta} q'} \right]^{1/2} \qquad (2\text{-}39)$$

with all quantities evaluted at V=Vmn.

2.4 Magnetic Island Effects

Given the results of the previous section, it is now possible to compute the structure of the pressure and current functions within the magnetic island and determine the axisymmetric coeficients to be used in the differential equation.

Near the magnetic island the function

$$(nB^{0\zeta} - mB^{0\theta}) = (nq - m)B^{0\theta} = 0 \qquad (2\text{-}40)$$

passes through zero and equation (2-28) has an apparent singular point. This singularity is only apparent however, since the radial magnetic field at the mode rational surface modifies the background equilibrium in such a way as to eliminate the singularity. This nonlinear effect is a charateristic of magnetic islands and its effect will be examined in this section.

From equation (2-36) a solution to $\vec{B}\cdot\nabla f$ in the vicinity of a magnetic island was shown to be of the form:

$$f = f^{0} + a\sin\phi = 2u^{2} + f_{0} + a\sin\phi \qquad (2\text{-}41)$$

where $U=(V-Vmn)/H$, $\phi = m\theta - n\zeta$, f_0 is a constant, and H is

the half width. Since f is a surface mapped out by the magnetic field lines, to a first approximation the pressure and current density are constant on a surface of f=constant. In this case P would be a function of f; however, the differential equations (to first order) require dP°/dv which may be thought of as the first term in a Fourier expansion of P(f). To obtain an expression for dP°/dv note that P(f) can be expanded in a Taylor series around f as

$$P(f) = P(f^{\circ}) + \frac{dP(f^{\circ})}{df}\sin\phi + \frac{1}{2}\frac{d^2P(f^{\circ})}{df^2}\sin^2\phi + \cdots \qquad (2\text{-}42)$$

Note that this is also a Fourier expansion in phi so that

$$P^{\circ}(v) = \oint P(f)\frac{d\phi}{2\pi} \qquad (2\text{-}43)$$

The higher order terms in the Fourier expansion are involved with the neglected terms in $\vec{J}^1 \times \vec{B}^1$ and with the higher harmonics in phi. This thesis will approximate the island structure by using only the first term in the expansion; greater accurary in the island structure could be obtained by considering the higher harmonics and nonlinear terms, but only at the expense of a much greater computational effort.

Of special interest and the topic of this thesis is

the force free case where $\vec{J} \times \vec{B} = 0$. In that case,

$$\vec{J} = K(f)\vec{B} \tag{2-44}$$

and

$$\frac{J^{\theta}}{B^{\theta}} = K(f) \tag{2-45}$$

The above analysis applied to (2-45) leads to

$$\frac{J^{0\theta}}{B^{0\theta}} = \oint K(f)\frac{d\phi}{2\pi} \tag{2-46}$$

Note that $\frac{d}{dv}\left(\frac{J^{0\theta}}{B^{0\theta}}\right)$ is required in the differential equation also.

A pressure (or current) profile in the neighborhood of a magnetic island may be locally approximated at the widest point of the island as:

$$P = \begin{cases} P_0 + P_0' H(u-1) & u > 1 \\ P_0 + \alpha P_0' H(1-u^2) & -1 \leq u \leq 1 \\ P_0 + P_0' H(u+1) & u < -1 \end{cases} \tag{2-47}$$

where P=P(Vmn), P'=dP(Vmn)/dV, and alpha is the "peaking" in the island. In terms of f (2-47) becomes:

$$P_o = \begin{cases} P_o + P_o' H\left[\left(\frac{f-f_o+1}{2}\right)^{1/2} - 1\right] & \text{INNER EDGE} \\ P_o + \alpha P_o' H\left[1 - \frac{f-f_o+1}{2}\right] & \text{INSIDE ISLAND} \\ P_o + P_o' H\left[\left(\frac{f-f_o+1}{2}\right)^{1/2} + 1\right] & \text{OUTER EDGE} \end{cases} \quad (2\text{-}48)$$

See figure 2-1.

The interest is in the average of (2-48) since this provides the coefficients to be used in the differential equation. Using $\phi = 2w + \pi/2$ the following form for the average pressure can be obtained:

$$P^\circ = P_o + \frac{2P_o'H}{\pi}\int_{w=\frac{1}{2}(\sin^{-1}(1-2u^2)-\pi/2)}^{0}\left[(u^2+\cos^2 w)^{1/2}-1\right]dw \qquad (2\text{-}49)$$

$$+\frac{2\alpha}{\pi}\int_{w=\frac{1}{2}(\sin^{-1}(1-2u^2)-\pi/2)}^{\pi/2}\left[1-(u^2+\cos^2 w)\right]dw$$

See figure 2-2 for the path of integration.

The second integral can be computed and the first approximated to give:

$$\frac{dP^\circ}{dV} = P_o'\left(u^2+\frac{2\alpha u}{\pi}\left(g-\frac{3\pi}{2}\right)\right.$$

$$\left.+\frac{4\alpha u}{\pi}\frac{\left(\sin^2\left(\frac{g-\pi/2}{2}\right)-u^2\right)}{\cos(\pi-g)}\right) \qquad |u|<1$$

$$\frac{dP^\circ}{dV} = P_o' \qquad |u|=1 \qquad (2\text{-}50)$$

$$g = \pi - \sin^{-1}(1-2u^2)$$

$$-\pi/2 \leq \sin^{-1}(1-2u^2) \leq \pi/2$$

An examination of equation (2-28) will show that unless the equilibrium magnetic fields have a special form the pressure cannot be peaked in a magnetic island or the singularity will still be present; this condition does not apply to the force free current which can be peaked in the magnetic island. Using (2-50), very near the island center (2-28) becomes

$$\frac{d}{dV} B^1_{\theta mn} = im B^1_{vmn} + F'_g B^{1q}_{mn} - \frac{i2g B^{1v}_{mn} \psi'_q \gamma C_0}{n H_{in\ q\ space}} \qquad (2\text{-}51)$$

where F' has an expansion similar to P, but of the form:

$$F'' = C_0\left(x^2 + \frac{2\gamma x}{\pi}\left(g - \frac{3\pi}{2}\right) + \frac{4\gamma x}{\pi}\left(\frac{\sin^2\left(\frac{g-\pi/2}{2}\right) - x^2}{\cos(\pi - g)}\right)\right) \quad |x| < 1 \qquad (2\text{-}52)$$

$$F'' = C_0 \quad |x| = 1$$

$$x = (q - q_{mn}) \Big/ H_{in\ q\ space}$$

The transformation to q space is a practical matter brought about because F'' is a function of q in the equilibrium

computations and the final algorithm for the computation of the magnetic island widths iterates on the island width in q space.

The method of solution of the tearing mode equation is to vary the widths of the islands until the boundary conditions on each of the $B^{1V\prime}_{mn}$'s can be satisfied. In the case of spontaneously growing tearing modes, which are the subject of this effort, the boundary conditions are:

$$B^{1V}_{mn}(0) = 0 \tag{2-53}$$

$$B^{1V}_{mn}(edge) = 0 \tag{2-54}$$

where it is assumed that there is a conducting wall at the edge of the plasma. In general it is possible for a nonzero magnetic perturbation to exist at the plasma edge because of magnetic field errors in the applied magnetic field and these nonzero boundary conditions may effect the stability of otherwise stable modes. [68] This thesis will consider only the conducting wall case since a reasonably high speed rotation of a tearing mode will limit the magnetic penetration of the tearing mode in the wall to a very thin region. [77]

2.5 Asymptotic Approximation

To determine the limit of (2-12) and (2-21) near the orgin, the following low beta, large aspect ratio limit is taken:

$$P^1_{mn} \sim 0 \,, \quad B^{1\varrho}_{mn} \sim k^2 \,, \quad \mathcal{J} \sim \frac{VE}{k} \qquad k = \frac{1}{\text{MAJOR RADIUS}}$$

This produces from (2-12)

$$\frac{d}{dv}\left(-i\mathcal{J} B^{1V}_{mn}\right) = -m\mathcal{J} B^{1\theta}_{mn} \tag{2-55}$$

and from (2-21)

$$\begin{aligned}(nB^{0\varrho} - mB^{0\theta})\left[\frac{d}{dv} B^1_{\theta mn} - im B^1_{vmn}\right] \\ = i\mathcal{J} B^{1V}_{mn} B^{0\varrho} \frac{d}{dv}\left(\frac{\mu_0 J^{0\varrho}}{B^{0\varrho}}\right)\end{aligned} \tag{2-56}$$

Near v=0 (2-22) and (2-23) can be approximated as

$$B^1_{vmn} = \frac{2E^2 B^{1V}_{mn}}{(E^2+1)} \tag{2-57}$$

$$B^{1\theta}_{mn} = \frac{(E^2+1)\,B^{1}_{\theta mn}}{2E^2V^2} \qquad (2\text{-}58)$$

where E is the plasma elongation; see Chapter III for the details of the equilibrium.

To find the limiting tearing mode equation use (2-55), (2-57), and (2-58) in (2-56) along with $\chi_{mn} = -i\vartheta B^{1V}_{mn}$ to get

$$(nB^{0\zeta} - mB^{0\theta})\left[-\frac{d}{dV}V\frac{d}{dV}\chi_{mn} + \frac{m^2}{V}\chi_{mn}\right]$$

$$= \frac{m(E^2+1)}{2kE^2}\chi_{mn}B^{0\zeta}\frac{d}{dV}\left(\frac{\mu_0 J^{0\zeta}}{B^{0\zeta}}\right) \qquad (2\text{-}59)$$

Near V=0 the Right hand side of (2-59) vanishes since the current density gradient near the orgin is small for the cases of interest and (2-59) takes on the final form

$$\frac{d}{dV}V\frac{d}{dV}\chi_{mn} - \frac{m^2}{V}\chi_{mn} = 0 \qquad (2\text{-}60)$$

The solution for B^{1V}_{mn} is thus

$$B^{1V}_{mn} \sim V^{m-1} \qquad (2\text{-}61)$$

near the magnetic axis. [12,14]

Using (2-55) and (2-61) it can be shown that

$$-k\chi_{mn} = B^{1}_{\theta mn} \tag{2-62}$$

Equations (2-61) and (2-62) are used as starting values near the magnetic axis in the computational form of the tearing mode equations to avoid the regular singularity at the magnetic axis.

2.6 Functional Behavior

The large aspect ratio limit suitable for the circular cylinder approximation is obtained by setting E=1 in equation (2-59) giving

$$\begin{aligned}(nB^{0\varphi}-mB^{0\theta})\left[-\frac{d}{dv}v\frac{d}{dv}\chi+\frac{m^2}{v}\chi\right]\\ =\frac{m}{k}\chi B^{0\varphi}\frac{d}{dv}\left(\frac{\mu_0 J^{0\varphi}}{B^{0\varphi}}\right)\end{aligned} \tag{2-63}$$

where the subscripts have been dropped. [12] By letting,

$$\chi = wv^{-1/2} \tag{2-64}$$

(2-63) may be written in standard 2nd order form [63]:

$$w'' + g(v)\,w = 0 \qquad (2\text{-}65)$$

with

$$g(v) = \frac{m B^{0\varphi} \frac{d}{dv}\left(\frac{\mu_0 J^{0\varphi}}{B^{0\varphi}}\right)}{vk\left(nB^{0\varphi} - mB^{0\theta}\right)} + \frac{1-4m^2}{4v^2}$$

One can assume with no loss of generality that $B^{0\varphi}$, $B^{0\theta}$, m, v, k are all greater than or equal to zero and that for the center peaked current profiles of interest $\frac{d}{dv}\left(\frac{\mu_0 J^{0\varphi}}{B^{0\varphi}}\right)$ is less than or equal to zero. Thus for q greater than the q at the rational surface, g(v) will always be negative; for q less than q at the rational surface and v small, g(v) will again be negative unless $\frac{d}{dv}\left(\frac{\mu_0 J^{0\varphi}}{B^{0\varphi}}\right)$ is large near the magnetic axis (which is unlikely) since the second term in g(v) is large and negative. The only region in which g(v) may be positive is on the inner edge of the island where the first term in g(v) is positive and only if this term can overcome the second negative term. A crude qualitative solution to (2-63) may be formed by approximating g(v) as a constant in the three regions; negative from the magnetic axis to a region near the inner edge of the island, positive from the region near the inner edge of the island to the center of the island, and finally negative from the center of the island to the plasma edge. This crude method of analysis leads to a qualitative solution of (2-63); when g(v) is

negative w will be locally exponental; when positive w will be locally oscillatory. If g(v) is always negative, which may be the case for large m numbers, the solution to (2-63) will have (roughly) an exponentally growing like solution which cannot be matched to the desired boundary conditions. If g(v) is sufficiently positive somewhere, the locally oscillatory solution will be strong enough to "turn" the solution around so that the boundary conditions can be matched. Note that the only region where this is possible is in the region just before the inner edge of the island; in other words the slope of the current profile on the inner edge of the island is a major factor in determining the solution to (2-63). [13,46,48]

2.7 Summary

The quasilinear equations are derived as a perturbation analysis of the ideal MHD equations and these equations contain an apparent singularity at the mode rational surface. This singularity is shown not to exist because of the effect the magnetic island has on the background equilibrium at the mode rational surface; furthermore a specific form for the current and pressure is shown to apply in the magnetic island region. The method of solution of the tearing mode equation is to vary the widths

of the magnetic islands until the boundary conditions on each radial perturbation term can be satisfied. Finally a qualitative analysis of the tearing mode equation reveals that the current density gradient on the inner edge of the island is of importance since it is in this region that the solution is "bent" to accomodate the boundary conditions.

CHAPTER III

Computational Equilibria

3.1 Introduction

Up to this point it has been assumed that the background equilibrium existed in a form suitable for use in the tearing mode equations. This section will outline the developement of two new numerical subroutines for the computation of a two dimensional MHD equilibrium. These subroutines were developed by the author because the currently available routines did not use the functions F and F' in forms that could be utilized in the tearing mode calculations. These new subroutines are completely general and may be used outside the context of the tearing mode problem. The equilibrium for the tearing mode calculation is

obtained in a two step process; first, the equilibrium is obtained by taking moments of the Grad-Shafranov equation; then this equilibrium is converted to a Hamada coordinate system.

3.2 Moment Equations

Two FORTRAN computer programs were developed to compute a background MHD equilibrium for the tearing mode calculations. These two programs, subroutine MHD and its companion subroutine, HAMEQ, are numerical algorithms for computing a two dimensional MHD equilibrium. MHD solves the inverse Grad-Shafranov equation by a variational moments method and HAMEQ converts this equilibrium to a Hamada coordinate system. MHD is unusual in that it requires the user to specify F'' rather that the more usual FF'. Furthermore F'' may be a function of ψ , q, or both. This provides a large degree of flexibility and is useful for the solution of problems that require functions that depend on the q of the flux surface rather the the flux function.

MHD solves the inverse Grad-Shafranov equation:

$$\hat{G}=0=\frac{1}{\sqrt{g}}\left(\frac{\partial}{\partial v}\left(\frac{g_{\theta\theta}}{\sqrt{g}}\psi'(v)\right)-\psi'(v)\frac{\partial}{\partial\theta}\left(\frac{g_{v\theta}}{\sqrt{g}}\right)\right)+\mu_0 P'+\frac{FF'}{R^2} \qquad (3\text{-}1)$$

along with

$$\frac{d^2F(\psi)}{d\psi^2} = \alpha C(\psi(\rho)) \tag{3-2}$$

and

$$q = \frac{-F(\psi)}{\psi'(v)}\left\langle \frac{Z_v R_\theta - R_v Z_\theta}{R} \right\rangle \tag{3-3}$$

where:

$$\mu_0 P' = FF' T(\psi(\rho)) \tag{3-4}$$

$$g_{\theta\theta} = R_\theta^2 + Z_\theta^2 \tag{3-5}$$

$$g_{v\theta} = R_v R_\theta + Z_v Z_\theta \tag{3-6}$$

and

$$g^{1/2} = R(R_\theta Z_v - R_v Z_\theta) \tag{3-7}$$

' means differentiation by the appropiate variable in the case of single variable functions and X_y means $\frac{\partial X}{\partial y}$ except for the metric elements ($g_{\theta\theta}, g_{v\theta}, g^{1/2}$). $C(\psi(\rho))$ and $T(\psi(\rho))$ are user specified functions and α is a parameter to be determined.

Equation (3-1) is known as the inverse Grad-Shafranov equation since one solves for R and Z as functions of V and θ rather then the other (more common) form of $\psi(R,Z)$. See figure 3-1 for the coordinate system. Note also that θ is not the geometric angle, but rather an angle that satisfies the variational properties oulined below.

R and Z are expanded in terms of V and θ as follows:

$$R = R_0(v) - R_1(v)\cos\theta + \sum_{n=2}^{N} R_n(v)\cos n\theta \qquad (3\text{-}8)$$

$$Z = E(v)\sum_{n=1}^{N} R_n(v)\sin n\theta \qquad (3\text{-}9)$$

These expressions are used in developing a variational form which involves equation (3-1) and a set of weighing functions to determine an optimal set of expansion functions for E and the R's. The reader is assumed to be familiar with this proceedure and is referred to the references. [54,55]

The result of this variational proceedure is the following set of integrals involving the inverse Grad-Shafranov equation and a set of weighting functions:

$$\langle W_n \hat{G} \rangle = 0 \tag{3-10}$$

where

$$\langle A \rangle = \frac{1}{2\pi} \int_0^{2\pi} A \, d\theta$$

and the weighting functions for Ro, Rn, E, and are respectively:

$$W_o = M_{RO} \tag{3-11}$$

$$W_n = (E M_{zn} - M_{Rn}) \qquad 1 \leq n \leq N \tag{3-12}$$

$$W_{N+1} = \sum_{n=1}^{N} R_n M_{zn} \tag{3-13}$$

$$W_{N+2} = \sqrt{g} \tag{3-14}$$

where

$$M_{zn} = R R_\theta \sin n\theta \tag{3-15}$$

$$M_{Rn} = R Z_\theta \cos n\theta \tag{3-16}$$

In the case of MHD the amplitude of the first harmonic has been chosen to be the coordinate V. This determines the remainder of the system and equations (3-1) to (3-14) produce the following matrix equation for the second derivatives of the expansion functions:

$$\begin{bmatrix} a_{11} \cdots a_{1m} \cdots a_{1(N+2)} \\ \vdots \\ a_{n1} \\ \vdots \\ a_{(N+2)1} \end{bmatrix} \begin{bmatrix} R_0'' \\ R_2'' \\ \vdots \\ R_n'' \\ E'' \\ \psi'' \end{bmatrix} = \begin{bmatrix} C_1 \\ C_2 \\ \vdots \\ C_{N+1} \\ C_{N+2} \end{bmatrix} \qquad (3\text{-}17)$$

with:

$$a_{n1} = -\left\langle \frac{W_n g_{\theta\theta} R Z_\theta}{g^{3/2}} \right\rangle \qquad (3\text{-}18)$$

$$a_{n(N+1)} = \left\langle \frac{W_n g_{\theta\theta} R R_\theta}{g^{3/2}} \left(\sum_{K=1}^{N} R_K \sin K\theta \right) \right\rangle \qquad (3\text{-}19)$$

$$a_{n(N+2)} = -\left\langle \frac{W_n g_{\theta\theta}}{g \psi'} \right\rangle \qquad (3\text{-}20)$$

$$a_{nm} = \left\langle \frac{W_n g_{\theta\theta} R}{g^{3/2}} \left(E R_\theta \sin m\theta - Z_\theta \cos m\theta \right) \right\rangle \qquad (3\text{-}21)$$

and

$$C_n = \left\langle \frac{W_n}{g} \left(\frac{\partial}{\partial V} g_{\theta\theta} - \frac{\partial}{\partial \theta} g_{V\theta} + \frac{g_{V\theta}}{g^{1/2}} \frac{\partial}{\partial \theta} g^{1/2} \right) \right.$$

$$+ \frac{W_n}{\psi'} \left(\mu_0 P' + \frac{FF'}{R^2} \right) - \frac{W_n g_{\theta\theta}}{g^{3/2}} \left(R_V \left(R_\theta Z_V \right. \right. \qquad (3\text{-}22)$$

$$\left. - R_V Z_\theta \right) + R \left(R_{\theta V} Z_V - R_V Z_{\theta V} \right)$$

$$\left. + R R_\theta \left(\sum_{K=1}^{N} 2 E' R_K' \sin K\theta \right) \right) \Big\rangle$$

The averaging over theta is done by a 10 point Gauss quadature routine and the integration is done using an Adams ODE method. More Gauss points do not appear to be useful in terms of accuracy with 4 or less harmonics. The Adams method appears to be the best choice for this problem since the matrix in equation (3-17) is time consuming to evaluate. [56,58] The only difficulty with (3-17) is that certain combinations of initial conditions can cause the determinate of the matrix to become singular within the region of integration. This may be the result of a separatrix creeping into the plasma region. The only practical way to deal with this situation is to select a different starting point for the nonlinear equation solver (detailed below) should problems arise.

The boundary conditons are :

Near V=0

$$R_0 = R_{ma} + R_{02} V^2 \tag{3-23}$$

$$E = E_{ma} + E_{02} V^2 \tag{3-24}$$

$$R_n = R_{nma} V^n \tag{3-25}$$

$$FF' = C_{ma} \tag{3-26}$$

$$F = \frac{2\psi_2 q_{ma}}{E_{ma}} \tag{3-27}$$

$$\psi = \psi_2 V^2 \tag{3-28}$$

where

$$\psi_2 = \frac{-E_{ma}^2 C_{ma}}{2(E_{ma}^2+1)} \left(R_{ma}^2 T(0, q_{ma}) + 1 \right) \tag{3-29}$$

and E_{02} and R_{02} are 2nd order expansion terms.

In actual practice setting R_{02} and E_{02} equal to zero makes little, if any difference in the solution; the code is not sensitive to their values. In MHD E_{02} is set equal to zero and R_{02} is determined by solving (3-17) with the Rn's set equal to zero, Ro set equal to (3-23), ψ set equal to (3-28), F set equal to (3-27), and V equal to 1.0 percent of a, where a is the upper limit of the variable V. The approximate minor radius of the plasma is a if the higher harmonics are small.

At V=a

$$R_0 = R_a \tag{3-30}$$

$$E = E_a \tag{3-31}$$

$$R_n = R_{na} \tag{3-32}$$

$$F' = 0 \tag{3-33}$$

Ra, Ea, Rna, Cma, qma, and a are given boundary conditions and Rma, Ema, Rnma, and alpha are to be determined. Ra is the major radius, Ea is the elongation at the plasma boundary, Rna's are the amplitudes of the harmonics at the plasma boundary, Cma is a measure of the toroidal current at the magnetic axis ($RJ_\phi(0) = R_0^2 \mu_0 P'(0) + C_{ma}$), qma is the q value at the magnetic axis, and a is the upper limit of V.

This set of equations is solved by using a shooting and matching technique. [56] The equations are first integrated from V=0 to V=a using an initial guess for Rma, Ema, Rnma, and alpha. The following residual vector is then generated:

$$\vec{\mathcal{R}} = \begin{bmatrix} (R_0(a) - R_a)/\psi'(a) \\ (R_2(a) - R_{2a})/\psi'(a) \\ \vdots \\ (R_n(a) - R_{na})/\psi'(a) \\ (E(a) - E_a)/\psi'(a) \\ F'(a) \end{bmatrix} \tag{3-34}$$

The division by $\psi'(a)$ is to factor out the $\psi' \equiv 0$ solution - a source of trouble. A hybrid nonlinear equation solver then attempts to reduce $\vec{\mathcal{R}}$ to the zero vector by varying Rma, Ema, Rnma's, and alpha until $|\vec{\mathcal{R}}_{k+1} - \mathcal{R}_k| / |\mathcal{R}_{k+1}|$ is less than some specified tolerance. (k coresponds to the iteration number) It does this by choosing a step length and step direction that is a combination of a newton step and a gradient step. The particular algorithm used is that contained in the NAG library routine C05NBF. [57] The process is usually successful, but many times care must be taken in selecting the initial guess.

3.3 Hamada like coordinates

Given an arbitrary two dimensional magnetic field this section will detail its tranformation into a coordinate system such that:

$$\left(\nabla V \times \nabla \theta_h\right) \cdot \nabla \varsigma_h = \mathcal{J}_h^{-1}(V) \tag{3-35}$$

Since $\mathcal{J}$ is only a function of V this system is known as a Hamada coordinate system. [49] To perform this transformation first write $\vec{B}$ in action angle form

$$\vec{B} = (\mathcal{J}\vec{B}\cdot\nabla\varsigma)(\nabla V\times\nabla\theta) + (\mathcal{J}\vec{B}\cdot\nabla\theta)(\nabla\varsigma\times\nabla V) \qquad (3\text{-}36)$$

where θ and ς are angle like coordinates. The goal of this section is to write the magnetic field in the form:

$$\vec{B} = \mathcal{J}_h B^{\varsigma}(\nabla V\times\nabla\theta_h) + \mathcal{J}_h B^{\theta}(\nabla\varsigma_h\times\nabla V) \qquad (3\text{-}37)$$

where B^{ς} and B^{θ} are only functions of V. [2,49,59,60]

Let θ_h be a function of V and θ. Also let ς_h be a function of V, θ, and ς. Use θ_h and ς_h in (3-37) to produce

$$\vec{B} = \mathcal{J}_h\left(B^{\varsigma}\frac{\partial\theta_h}{\partial\theta} - B^{\theta}\frac{\partial\varsigma_h}{\partial\theta}\right)(\nabla V\times\nabla\theta) + B^{\theta}\mathcal{J}_h\frac{\partial\varsigma_h}{\partial\varsigma}(\nabla\varsigma\times\nabla V) \qquad (3\text{-}38)$$

From (3-36) and (3-38) the following two equations can be produced:

$$\mathcal{J}\vec{B}\cdot\nabla\varsigma = \mathcal{J}_h\left(B^{\varsigma}\frac{\partial\theta_h}{\partial\theta} - B^{\theta}\frac{\partial\varsigma_h}{\partial\theta}\right) \qquad (3\text{-}39)$$

$$\vartheta \vec{B} \cdot \nabla\theta = \vartheta_h B^\theta \frac{\partial \varsigma_h}{\partial \varsigma} \tag{3-40}$$

Expanding (3-35) gives:

$$\frac{\partial \theta_h}{\partial \theta} = \frac{\vartheta}{\vartheta_h} \frac{\partial \varsigma_h}{\partial \varsigma} \tag{3-41}$$

Use (3-40) in (3-41) to get an expression involving θ and θ_h :

$$\frac{\partial \theta_h}{\partial \theta} = \frac{B^\theta}{\vec{B} \cdot \nabla\theta} \tag{3-42}$$

Next integrate (3-42) from $\theta = 0$ to θ and set any constant terms equal to zero since the reference angle is arbitrary. This gives:

$$\theta_h = \int_0^\theta \frac{B^\theta \, d\theta}{(\vec{B} \cdot \nabla\theta)} \tag{3-43}$$

In general $\nabla\theta_h$ will be multivalued in θ . To avoid this problem note that B^θ has yet to be determined. If one sets

$$B^\theta = \frac{\rho}{\oint \frac{d\theta}{(\vec{B} \cdot \nabla\theta)}} \tag{3-44}$$

where P is the period, the multivalued problem is avoided and the equation for θ_h becomes:

$$\theta_h = \frac{\int_0^{\theta} \frac{d\theta}{(\vec{B}\cdot\nabla\theta)}}{\frac{1}{P}\oint \frac{d\theta}{(\vec{B}\cdot\nabla\theta)}} \qquad (3\text{-}45)$$

To find the remaining angle ς_h, use (3-41) in (3-39) to produce the following equation for ς_h.

$$\frac{\partial \varsigma_h}{\partial \theta} = \frac{B^{\varsigma}\partial}{B^{\theta}\partial_h}\frac{\partial \varsigma_h}{\partial \varsigma} - \frac{\partial(\vec{B}\cdot\nabla\varsigma)}{\partial_h B^{\theta}} \qquad (3\text{-}46)$$

Choosing $\varsigma_h \sim \varsigma + G(\theta, v)$ as a form for ς_h and using this relation in (3-46) gives

$$\frac{\partial \varsigma_h}{\partial \theta} = \frac{B^{\varsigma}}{B^{\theta}}\frac{\partial}{\partial_h} - \frac{\partial(\vec{B}\cdot\nabla\varsigma)}{\partial_h B^{\theta}} \qquad (3\text{-}47)$$

Integrating as before gives the equation for ς_h.

$$\varsigma_h = \int_0^{\theta} \frac{\partial d\theta}{\partial_h B^{\theta}}\left(B^{\varsigma} - (\vec{B}\cdot\nabla\varsigma)\right) + \varsigma \qquad (3\text{-}48)$$

Again the multivalued problem is apparent and it can be avoided by choosing:

$$\oint \vartheta \left(B^{\varsigma} - \left(B^{\varsigma} \cdot \nabla \varsigma \right) \right) d\theta = 0 \tag{3-49}$$

Finally, using (3-49), B^{ς} is determined.

$$B^{\varsigma} = \frac{\oint \vartheta (\vec{B} \cdot \nabla \varsigma) d\theta}{\oint \vartheta \, d\theta} \tag{3-50}$$

From (3-40) ϑ_h is produced.

$$\vartheta_h = \frac{\vartheta (\vec{B} \cdot \nabla \theta)}{B^{\theta}} \tag{3-51}$$

The fact that we can not independently select ϑ_h arises from the fact that $\nabla \theta_h$ and $\nabla \varsigma_h$ are both required to be single valued in θ . If ϑ_h is not a function of V, the forms for θ_h and ς_h may not be general enough and different forms for θ_h and ς_h may be inferred. Also note that the transformation from V to a V' and thus $\vartheta(V)$ to $\vartheta'(V')$ will allow one to choose any $\vartheta'(V')$ desired. However, the former forms are general enough for the purposes of this work.

Finally, using (3-40) in (3-48) the final form for ς_h is:

$$\varsigma_h = B^{\varsigma} \int_0^{\theta} \frac{d\theta}{(\vec{B}\cdot\nabla\theta)} - \int_0^{\theta} \frac{(\vec{B}\cdot\nabla\varsigma)\,d\theta}{(\vec{B}\cdot\nabla\theta)} + \varsigma \qquad (3\text{-}52)$$

3.4 Transformation from moment equilibrium to Hamada equilibrium

The Grad-Shafranov representation of the magnetic field is [1,7]

$$\vec{B} = \frac{d\psi}{dv}(\nabla v \times \nabla\phi) + F(\psi)\nabla\phi \qquad (3\text{-}53)$$

which when dotted into $\nabla\theta$ and $\nabla\phi$ gives

$$\vec{B}\cdot\nabla\theta = -\psi'/\mathcal{J} \qquad (3\text{-}54)$$

$$\vec{B}\cdot\nabla\phi = F/R^2 \qquad (3\text{-}55)$$

where

$$\mathcal{J} = R\left(Z_V R_\theta - R_V Z_\theta\right) \tag{3-56}$$

Using equations (3-44),(3-45),(3-50),(3-51),(3-52),(3-54),(3-55) the following equations can be derived for the Hamada quantities:

$$\theta_h = \frac{1}{\partial h}\int_0^\theta \mathcal{J}\, d\theta \tag{3-57}$$

$$B^\theta = -\psi'/\partial h \tag{3-58}$$

$$B^\zeta = \frac{F}{2\pi \partial h}\oint \frac{\mathcal{J}}{R^2}\, d\theta \tag{3-59}$$

$$\partial h = \frac{1}{2\pi}\int_0^{2\pi} \mathcal{J}\, d\theta \tag{3-60}$$

$$\zeta_h = \frac{-B^\zeta}{\psi'}\int_0^\theta \mathcal{J}\, d\theta + \frac{F}{\psi'}\int_0^\theta \frac{\mathcal{J}}{R^2}\, d\theta + \phi \tag{3-61}$$

The representation of the current density in the Hamada form is also determined by HAMEQ. To derive it start with

$$\vec{J} = \partial h\, J^\theta\left(\nabla \zeta_h \times \nabla V\right) + \partial h\, J^\zeta\left(\nabla V \times \nabla \theta_h\right) \tag{3-62}$$

where J^{θ} and J^{ζ} are to be determined. J^{θ} may be determined by taking the curl of equation (3-53) and dotting $\mu_0 \nabla\theta$ into the result thus producing

$$\mu_0 \vec{J}\cdot\nabla\theta = \mu_0 J^{\theta} = \psi' F' (\nabla V \times \nabla\phi)\cdot\nabla\theta \qquad (3\text{-}63)$$

which becomes

$$\mu_0 J^{\theta} = \frac{-\psi' F'(\psi)}{\partial h} \qquad (3\text{-}64)$$

J^{ζ} can be determined from the force balance equation in Hamada coordinates:

$$\partial h \left(J^{\theta} B^{\zeta} - J^{\zeta} B^{\theta}\right) = \psi' p'(\psi) \qquad (3\text{-}65)$$

giving:

$$\mu_0 J^{\zeta} = \left(\frac{\mu_0 J^{\theta} B^{\zeta}}{B^{\theta}} - \frac{\mu_0 \psi' p'}{\partial h B^{\theta}}\right) \qquad (3\text{-}66)$$

Near the magnetic axis (3-57) to (3-61), (3-64), and (3-66) may be approximated as

$$B^{\theta} \approx -2\psi_2 / R_{ma} E_{ma} \tag{3-67}$$

$$B^{\varphi} \approx F(v=0) / R_{ma}^2 \tag{3-68}$$

$$\vartheta_h \approx R_{ma} E_{ma} V \tag{3-69}$$

$$\theta_h \approx \theta \tag{3-70}$$

$$\varphi_h \approx \phi \tag{3-71}$$

$$\mu_0 J^{\theta} \approx -2\psi_2 F'(v=0) / R_{ma} E_{ma} \tag{3-72}$$

$$\mu_0 J^{\varphi} \approx F'(v=0) F(v=0) / R_{ma}^2 - \mu_0 P'(v=0) \tag{3-73}$$

HAMEQ accomplishes the conversion from moment to Hamada equilibrium by first Fourier expanding ϑ and ϑ / R^2 (by means of fast Fourier transforms) in the following way:

$$\vartheta = \vartheta_0(v) + \sum_{n=1}^{N} \vartheta_n(v) \cos n\theta \tag{3-74}$$

$$\vartheta/R^2 = \vartheta_{R0}(v) + \sum_{n=1}^{N} \vartheta_{Rn}(v) \cos n\theta \qquad (3\text{-}75)$$

Using (3-74) and (3-75) in (3-57)-(3-61), (3-64) and (3-66) the following expansions in theta are obtained:

$$\vartheta_h = \vartheta_0 \qquad (3\text{-}76)$$

$$\theta_h = \theta + \sum_{n=1}^{N} \frac{\vartheta_n}{\vartheta_0 n} \sin n\theta \qquad (3\text{-}77)$$

$$\frac{\partial \theta_h}{\partial v} = \sum_{n=1}^{N} \left(\frac{\vartheta_n'}{\vartheta_0} - \frac{\vartheta_n \vartheta_0'}{\vartheta_0^2} \right) \frac{\sin n\theta}{n} \qquad (3\text{-}78)$$

$$\frac{\partial \theta_h}{\partial \theta} = 1 + \sum_{n=1}^{N} \frac{\vartheta_n}{\vartheta_0} \cos n\theta \qquad (3\text{-}79)$$

$$\varsigma_h = \sum_{n=1}^{N} \frac{F}{\psi'} \left(\vartheta_{Rn} - \frac{\vartheta_{Rn} \vartheta_n}{\vartheta_0} \right) \frac{\sin n\theta}{n} + \phi \qquad (3\text{-}80)$$

$$\frac{\partial \xi_h}{\partial V} = \sum_{n=1}^{N} \frac{1}{n} \left\{ \frac{F}{\psi'} \left[\vartheta'_{Rn} - \frac{1}{\vartheta_0} \left(\vartheta'_{R0} \vartheta_n + \vartheta_{R0} \vartheta'_n \right) \right. \right. \tag{3-81}$$

$$\left. \left. \frac{\vartheta_{R0} \vartheta_n \vartheta'_0}{\vartheta_0^2} \right] + \left(\vartheta_{Rn} - \frac{\vartheta_{R0} \vartheta_n}{\vartheta_0} \right) \left(F' - \frac{F \psi''}{\psi'^2} \right) \right\}$$

$$\frac{\partial \xi_h}{\partial \theta} = \sum_{n=1}^{N} \frac{F}{\psi'} \left(\vartheta_{Rn} - \frac{\vartheta_{R0} \vartheta_n}{\vartheta_0} \right) \cos n\theta + \phi \tag{3-82}$$

$$B^\theta = -\psi' / \vartheta_0 \tag{3-83}$$

$$\frac{dB^\theta}{dV} = -\frac{1}{\vartheta_0} \left(\psi'' - \frac{\vartheta_0' \psi'}{\vartheta_0} \right) \tag{3-84}$$

$$B^\zeta = F \vartheta_{R0} / \vartheta_0 \tag{3-85}$$

$$\frac{dB^\zeta}{dV} = F' \psi' \vartheta_{R0} / \vartheta_0 + \frac{F}{\vartheta_0} \left(\vartheta'_{R0} - \frac{\vartheta_{R0} \vartheta_0'}{\vartheta_0} \right) \tag{3-86}$$

$$\mu_0 \overline{J}^\theta = -\psi' F' / \vartheta_0 \tag{3-87}$$

$$\mu_0 \overline{J}^\zeta = \frac{\mu_0 \overline{J}^\theta B^\zeta}{B^\theta} - \frac{\mu_0 \psi' p'}{\vartheta_0 B^\theta} \tag{3-88}$$

The above form the complete set of equations used in HAMEQ. ϑ' and $(\vartheta/R^2)'$ are determined by using (3-17); no finite differencing is used so that the accuracy of the Hamada quanities is determined by the accuracy of the fast Fourier decomposition and the accuracy of the terms delivered by MHD.

3.5 Hamada Metric Elements

The above details the transformation from the moment coordinate system to the Hamada coordinate system; however, the Hamada metric elements are in terms of the moment coordinate system rather than the Hamada system. In order to do the contravarient/covariant conversions the metric elements must be functions of the Hamada variables; in particular it may be useful to have them expanded in a Fourier series. This may be accomplished as follows: With:

$$g(v,\theta_h) = \sum_m g_m \exp(im\theta_h) \tag{3-89}$$

the expansion functions are determined by:

$$g_m = \frac{1}{2\pi}\int_0^{2\pi} g(v,\theta)\frac{\partial\theta_h}{\partial\theta}d\theta \exp(im\theta_h(\theta)) \tag{3-90}$$

keeping V constant. θ_h is the Hamada angle, θ is the moment angle, and $g(V,\theta)$ is the metric element in the moment system.

3.6 Asymptotic Metric Element Approximations

In order to find the asymptotic limit of the tearing mode equation in section 2.5, it is necessary to determine the asymptotic limit of equations (2-22) and (2-23). Note that one is interested in $\nabla V \cdot \nabla V$, $\nabla\theta \cdot \nabla\theta$, and $\nabla\theta \cdot \nabla V$, since the other terms have been discarded in the limit. $\nabla V \cdot \nabla V$, $\nabla\theta \cdot \nabla\theta$, and $\nabla\theta \cdot \nabla V$ can be obtained by inverting and taking the appropiate dot products of the following expressions:

$$\nabla R = \frac{\partial R}{\partial V}\nabla V + \frac{\partial R}{\partial \theta}\nabla\theta \tag{3-91}$$

$$\nabla Z = \frac{\partial Z}{\partial V}\nabla V + \frac{\partial Z}{\partial \theta}\nabla\theta \tag{3-92}$$

giving:

$$\nabla V \cdot \nabla V = R^2\left(Z_\theta^2 + R_\theta^2\right)/g^2 \tag{3-93}$$

$$\nabla\theta\cdot\nabla\theta = R^2\left(Z_V^2 + R_V^2\right)/\mathcal{J}^2 \tag{3-94}$$

$$\nabla\theta\cdot\nabla V = -R^2\left(Z_V Z_\theta + R_V R_\theta\right)/\mathcal{J}^2 \tag{3-95}$$

Using equations (3-8), (3-9), and (3-69) in (3-93) through (3-95), discarding terms of order V and smaller, and finally Fourier analyzing gives the following approximations near the magnetic axis:

$$\nabla V\cdot\nabla V \approx \frac{E^2+1}{2E^2} \tag{3-96}$$

$$\nabla\theta\cdot\nabla\theta \approx \frac{E^2+1}{2V^2E^2} \tag{3-97}$$

$$\nabla\theta\cdot\nabla V \approx 0 \tag{3-98}$$

CHAPTER IV

Solution of the Tearing Mode Equations

4.1 General

The method of solution of the tearing mode equations is to treat them as eigenfunctions and the island widths as nonlinear eigenvalues. A shooting technique is used as the numerical method; the tearing mode equations are integrated from the magnetic axis to the edge of the plasma and the deviation from the desired boundary conditions computed. The magnitude of this deviation or residual is to determine the island width for the next iteration by a quasi-newton method. [56,57] Each iteration involves recomputing the equilibrium using the new island widths, determining the amplitudes of the B^{1V}_{mn}'s that coorespond to the island widths, and finally

integrating the tearing mode equations to determine the new residual at the plasma edge. This proceedure is repeated until convergence is obtained by the perturbation field components approaching zero at the plasma edge. Determination of the amplitudes of the B^{iV}_{mn}'S expansions near the magnetic axis (See section 2.5) is also done using an iterative quasi-newton method. The amplitudes of the B^{iV}_{mn}'S expansions are varied until they coorespond to the appropiate magnetic island widths and, since all modes are done simultaneously, the mode mixing and nonlinear interactions due to the current density profile modifications are included. It should be noted that the iterations on the magnetic island halfwidth are done in q space rather than V space because the equilibrium subroutines require F''(q). All numerical integrations are done using an Adams ODE method and all integrations to determine the Fourier decompositions of equations (2-22), (2-23), and (2-24) are done by using Gauss quadature. [56]

4.2 Limitations

One of the major difficultes experienced in the use of this method is numerical accurary. Magnetic island widths can be determined to a maximum accurary of about 1 part in 1000; since the island widths are products of mulitiple

integrations and iterations on nonlinear functions, both in the equilibrium routines as well as in the tearing computations, it is necessary that all routines be run at limiting or near limiting accurary to achieve useful results. This accurary limit is also manifest in a lower limit on the smallest island that can be computed. Experience indicates that the minimum island width that can be consistantly handled is approximately 0.02 times the q at the edge of the plasma; if an island is smaller than this, or if no island appears to exist, the amplitude of the appropiate perturbation is set equal to zero. The program is constructed in such a way that zero island width can be easily handled and that the island width can return to a finite value during the course of the iteration if necessary. The smallest island that can be determined is related to the number of radial grid points. The equilibrium subroutines return the functions as a sequence of values on a radial grid and since an adaptive integration routine is used in the integration of the tearing mode equation, functional values between the grid points must be determined by interpolation. In this program linear interpolation is used and experience indicates that at least 25 points across the magnetic island region are necessary for decent resolution and stability of the shooting method. Unequal grid point spacing has been tried, but the most practical solution is to use a large number of grid points - in the neighborhood of 501 to 2001

points.

Another more general problem is the ability of the equilibrium subroutine to compute an equilibrium given an arbitrary set of magnetic island widths and the ability of the tearing mode shooting method to converge to the correct magnetic island width given an arbitrary starting value for the width. Occasionally a magnetic island width will be generated for which no equilibrium can found (note that this does not mean that the equilibrium does not exist); in this case the program stops and gives an error message. If a starting guess for a magnetic island is too small the program may incorrectly indicate that no magnetic island exists; this problem may be overcome by trying a new, larger set of initial guesses for the island widths. If the starting guess is far too large, the program may find itself trapped in a local minimum and falsely indicate convergence; this can be noted by examining the residuals which are printed out for each iteration. Both of these problems seem to be more severe as the number of islands increase and as the saturated magnetic island width becomes smaller. Other than the above concerns, which can be easily identified, the numercial method works well in a reasonable amount of time.

Figure 4-1 illustrates the program flow and control. The actual computer program makes use of several external libraries as well as being constructed in a modular fashion to aid in trouble shooting and modification. All input is in

the form of namelists and an extensive graphics capability is provided as will be shown in the next chapter. The ouput includes all the equilibrium function values as well as the magnetic island information.

CHAPTER V

Results

5.1 Interpretation of Model

This chapter will detail the effects of plasma global current density profile, current density peaking within a magnetic island, plasma toroidicity, plasma elongation, nonlinear magnetic island coupling, and linear magnetic island coupling on the saturated width of the resulting magnetic islands. The most important new finding is that the saturated width of a magnetic island is sensitive to the amount of current density peaking within the magnetic island and this new finding may make prediction of magnetic island widths more difficult because of the great accurary required in modelling the current density profile.

The results presented in this section are obtained by starting with a consistant background axisymmetric equilibrium, modifing a parameter such as island current profile, and letting the computer algorithm find a neighboring three dimensional equilibrium from this two dimensional starting equilibrium. Note that this does not coorrespond to a time evolving process, but rather a search to determine what equilibrium near the starting equilibrium can satisfy the mathematical model.

In the cases studied the form for F'' was chosen to be:

$$F'' = \alpha \left(C_0 + C_1 x + C_2 x^2 + C_3 x^3 \right)^S \qquad (5\text{-}1)$$

where C0 through C3 are coeficients chosen by the user and they are usually in the range 0.0 to 5.0; S is a user selected exponent, and X = (q-qaxis). In all the cases presented in this chapter S was set equal to -0.5, qaxis was 1.0, and the C's are shown on each seperate run. (alpha is selected by the equilibrium subroutines - see chapter III) This form for F'' allowed a wide range of current profiles to be represented as well as being fast and convenient to compute. Also note that because of the boundary conditions on F' (see chapter III) the current profile is always zero at the wall; this corresponds to the physical situation.

The examples presented in this chapter are the results of a parameter study to determine the effects of various plasma attributes upon saturated magnetic island widths. This approach was chosen rather than detailed studies of particular equilibria because:

1. It was found that the magnetic island width is very sensitive to the current density profile near and within the magnetic island. To simulate this situation with the computer model would require very accurate data in a very narrow region of the plasma; this requirement is probably beyond what could be actually measured because current density profiles are indirectly inferred from the observation of other parameters such as the electron temperature. This proceedure is subject to the limitations of the electron scattering data and to the specific relationship between the current density profile and the electron temperature. [78,79] With this type of situation a parameter study is useful because generic behavior may be deduced.

2. It was the most efficient way to use the computer resources available. Since a single computer run could take as long as 15 minutes, which was the

weekly allocation of this author, it was not fesible to do several runs in an attempt to match a particular current density profile. Again, useful qualitative and generic information may be obtained with the parameter search approach.

Before proceeding with a discussion of the results, it is necessary to explain some nomenclature. In figures 5-1 to 5-24, Vmn refers to the position of the mode rational surface, in V space, under discussion; Qe is the q value at the edge of the plasma; E is the elongation of the plasma; the width of the island is in V space; and all results are for a low beta plasma. Since it was not possible to do a parametric study encompassing all possible plasma configurations, a subset was selected that enabled the desired characteristics to be examined consistant with the numerical stability of the method and reasonable computing time.

Figures 5-1a through 5-2d and figures 5-24a-e are the graphical output of the computer program. RØ, R1, R2, and E coorrespond to the moment expansion (see equations 3-8 and 3-9); a limited number of expansion harmonics were used and in all cases one moment expansion harmonic and two hamada expansion harmonics were found to be adequate. Psi is ψ, bzeta is $B^{0\zeta}$, btheta is $B^{0\theta}$, ujzeta is $\mu_0 J^{0\zeta}$, ujtheta is $\mu_0 J^{0\theta}$, bvmn is B^{1V}_{mn}, ujvmn is $\mu_0 J^{1V}_{mn}$, and F'' is shown in

the region of the magnetic island. All variables are plotted in V space. Finally, dq/(dq/dv) is the width of the magnetic island in V space, the halfwidth in q space being just above it; "amp of this harmonic" refers to the coeficient of the asymtotic expansion of the radial perturbation near the magnetic axis; note that the parameters for a given island are confined to the page that contains its graph.

5.2 Global Current Profile

One important parameter to be examined in the context of magnetic island widths is the effect of the shape of the background current density profile; in particular one is interested in the influence of "rounded", low q edge value current density profiles vs the influence of "peaked", high q edge value current density profiles. This study was accomplished by varying the parameter C3 in equation (5-1) to produce a set of profiles that had the current increasingly "peaked" or concentrated near the magnetic axis. The trend produced was a reduction in the width of the magnetic island as the profile became more highly peaked in a way qualitively similar to reference [13]. Two widely different cases are illustrated in figures 5-1a-d and 5-2a-d. This reduction in magnetic island width is not, in general, monotonic however, and should be viewed in the light of the next section which will examine local effects.

Comparison of the two profiles is somewhat complicated because it is desirable to keep the q on the magnetic axis the same for each run both for physical reasons as well as minimizing the number of variables to be modified for each run. Since the q on the magnetic axis was kept the same, the mode rational surface was closer to the magnetic axis for the peaked current density case than for the rounded case and the effect of the inward shift of the magnetic axis could not be eliminated; it was desired to keep the q on axis near 1.0 since much lower values may be unphysical due to the sawtooth oscillation and much larger values are not representative of most tokamak discharges. Nonetheless it is possible to outline the trend and make some comparisons.

In the cases presented in this section, the 2/1 magnetic island was selected since it was found to be the most unstable which is consistant with the experimental observations. [16,71,75] The plasma parameters were: aspect ratio=4.0, plasma elongation=1.0, flat island current density profile, C0=1.0, C1=0.3, C2=0.0, and C3 was varied to produce various degrees of current density localization near the magnetic axis. C3 was selected to be varied because a smooth series of profiles could be generated; the cubic term has its greatest effect in the outer regions of the plasma and these resulting profiles covered a wide range of current density localization. A plot of q at the plasma edge vs C3 is shown in figure 5-3; an increase in C3 resulted in greater

"peaking" and less total current, thus the higher q edge values. Figure 5-4 shows that outside of a small maximum near C3=1.0, the 2/1 magnetic island width generally decreased with increasing current density localization at the magnetic axis and the resultant q edge increase. Note that as C3 is increased the mode rational surface shifts inward because of the reduction in total current - see figure 5-5. Finally, observe that outside of a small peak in the curve, figure 5-6 demonstrates that the width of the 2/1 magnetic island shrinks as the mode rational surface shifts inward and q edge increases. The peak in figure 5-6 may be due to the effects discussed in the next section. Note that in the peaked case (see figure 5-2a-d) the perturbed magnetic field has a long decaying tail and a sharper slope near the rational surface than does the rounded case (see figure 5-1a-d); these two effects combine to produce a smaller value for the perturbed magnetic field at the mode rational surface and thus a smaller island. This seems to indicate that the plasma current makes its largest contribution to the perturbation on the inside of the mode rational surface since the long tail is characteristic of a vacuum like solution. In general, it appears that the more "rounded", low q edge value current density profiles are the most unstable to tearing modes. This is consistant with the observed experimental results from a number of tokamaks:

1. The TOSCA Tokamak group indicated that special helical coils were necessary to suppress the 2/1 mode so that a plasma with a low q value at the edge could be obtained. [67]

2. The DIVA Tokamak could sustain low q discharges only if the impurity concentration of the plasma could be kept low - a disruption could be initiated by the injection of neon gas which caused the plasma radiation loss to jump from 15 percent of the Ohmic input power to about 100 percent of the Ohmic input power. The 2/1 mode is observed to rapidly grow just before the disruption indicating a connection between the current density profile, suddenly modified by the neon impurity, and the 2/1 magnetic island. [71]

3. In the DITE Tokamkak soft disruptions are suspected to be caused by impurities cooling the plasma edge and forcing the current channel to contract which raises the effective q of the discharge. This combination generates an unfavorable current density profile and the resulting growth of the 2/1 magnetic island. [73]

All these observations should also be reviewed in the context of the next section which will examine the local

current density gradient in the neighborhood of a mode rational surface.

5.3 Island Current Profile

The preceeding section concerned itself with the effects of modification of the global current density profile. This section, in contrast, will consider the effects of local current density modifications within the magnetic island itself and to the equilibrium current density profile at the mode rational surface. Both cases will be examined while holding the equilibrium global current density profile constant.

The current density profile effects within a magnetic island may be studied in a parametric manner by varying gamma in equation (2-52). Figure 5-7 is a plot of the 2/1 magnetic island width vs gamma; note that as gamma increases , the mganetic island width increases. The plasma parameters for this series of runs were: aspect ratio=4.0, elongation=1.0, C0=1.0, C1=0.5, C2=0.0, and C3=1.25. Figure 5-8 illustrates the trend of q at the plasma edge vs gamma; figure 5-9 shows how the mode rational surface shifted with gamma; note that figures 5-8 and 5-9 depict changes in the range of 12 percent, while figure 5-7 shows a change in the magnetic island width of about 60 percent.

In order to understand the influence of different current density profiles within a magnetic island, keeping the global current density profile constant, it is useful to compare the difference in the derivatives of B^{1V}_{mn} across the island for different local current density forms. With the assumption that the local magnetic island current profile will only locally modify the form of B^{1V}_{mn}, one would expect that the form of B^{1V}_{mn} will remain independent of the magnetic island current profile outside the magnetic island. Since the equation for the magnetic perturbation is linear, a difference in the derivative of B^{1V}_{mn} would imply a scaling of B^{1V}_{mn} if it were of the proper sign. A larger difference in the derivative, if of the proper sign, would imply a larger B^{1V}_{mn} and consequensely a larger island. If the difference were large but of the wrong sign, it would indicate the possible elimination of the island.

To estimate this difference for a given magnetic island current density profile, start with the large aspect ratio limit and assume all terms except J^{0q}/B^{0q} to be constant along an island so that

$$\chi''_{mn} = \frac{\chi_{mn0}}{V_{mn}}\left[\frac{m^2}{V_{mn}} - \frac{m q_0}{n k q_0' x}\frac{d}{dx}\left(\frac{\mu_0 J^{0q}}{B^{0q}}\right)\right] \qquad (5\text{-}2)$$

where $x = V - V_{mn}$, $(nq-m) \sim nq'x$, V_{mn} is the location of the mode rational surface, q_0, q_0', χ_{mn0} are the terms evaluated at

Vmn. Define the normalized difference in the derivative across the magnetic island as:

$$\Delta' = \left[X'_{mn}(V_{mn}+H) - X'_{mn}(V_{mn}-H) \right] \Big/ X_{mn}(V_{mn})$$

$$= \frac{1}{V_{mn}} \int_{-H}^{H} \left[\frac{m^2}{V_{mn}} - \frac{m q_0}{n k q_0' x} \frac{d}{dx} \left(\frac{\mu_0 J^{0q}}{B^{0q}} \right) \right] dx \qquad (5\text{-}3)$$

where H is the halfwidth. With a flat island $\frac{d}{dx}(\mu_0 J^{0q}/B^{0q}) \sim x^2/H^2$ so that (see section 2.4)

$$\Delta_f' = \frac{2m^2 H}{V_{mn}^2} \qquad (5\text{-}4)$$

where the f signifies the "flat" island profile. With a peaked island $\frac{d}{dx}(\mu_0 J^{0q}/B^{0q}) \sim -\gamma K_0' x/H$ so that

$$\Delta_p' = \Delta_f' + \frac{2m q_0 \gamma K_0'}{V_{mn} n k q_0'} \qquad (5\text{-}5)$$

where the p signifies the "peaked" island profile. Note that this definition of Δ' is somewhat different than the Δ' used in the literature since (5-3) uses the modified, rather than the orginal current density density profile. Asymptotically in the island halfwidth H, the order of Δ'_p is smaller than that of Δ'_f ; in fact the island peaking can completely dominate the Δ'_f term. By making gamma larger in magnitude and of the correct sign the edges of the island are forced farther apart. The computation model supports this result and the numerical results for a typical profile with a 2/1 magnetic island are shown in figure 5-7. Note that since Ko' is negative in the center peaked current profiles of interest, a positive gamma corresponds to a local current dip within a magnetic island; a negative gamma corresponds to a local current profile peak within a magnetic island. For the purposes of this thesis, any nonzero gamma will be refered to as "peaking". Also of interest is the observation that the island peaking can destabilize otherwise stable islands; figure 5-10 illustrates this behavior with a 3/2 island. Note that with gamma equal to zero no magnetic island was found; the plasma parameters for this series of runs were: aspect ratio=4.0, elongation=1.0, C0=1.0, C1=0.0, C2=0.0, and C3=0.5. Figure 5-11 shows that the q at the plasma edge varied little with gamma and figure 5-12 plots the mode rational surface vs gamma. Note that by changing the sign of gamma (figure 5-7) the island can be reduced in

width which leads to speculation of a possible means of magnetic island control. In the large aspect ratio approximation suppression of magnetic islands is shown to occur by the unique current distribution caused by RF driven currents. [61,72,74] If specific regions could be selectively heated (by perhaps RF) or cooled (impurities?) it may be possible to control the width of a magnetic island. This remains to be seen, since controlling the proper position of this heating or cooling may be very difficult.

It is useful to estimate the magnitude of the possible current peaking within an island. The gradient of the current density profile at the rational surface is $J^{0\prime}$; within the island it is approximately $\gamma J^{0\prime}$. Assuming that the current gradient within the island has the same magnitude as that within the plasma proper, one can equate the two terms and estimate that gamma is of order one. Thus while the current peaking is moderate, the fact that F''/(nq-m) is no longer zero at the mode rational surface is of great consequence. This implies that the second derivative of the current density is important near the mode rational surface.

Another related phenomena of interest is the effect of local peaking of the background equilibrium current density profile. In these cases the current density profile in the magnetic island is flat and only the equilibrium current density profile is peaked in the vicinity of the mode rational surface by means of a step function placed on F''.

The step function is of amplitude Si across the island, decaying exponentially to zero on either side of the island. See figure 5-13. This function produces a large local change in J_{OS}' on the scale length of a magnetic island width. Such great local current gradients may not be entirely physical, but this study is useful because it allows one to examine the sensitivity of island widths to the local current gradient. Figure 5-14 shows this relationship. The current density gradient effect is not unique; different local profiles can give somewhat different results, but figure 5-14 illustrates the trend that larger local current density gradients give larger island widths. The other plasma parameters were: aspect ratio=4.0, elongation=1.0, C0=1.0, C1=0.0, C2=0.0, and C3=0.5. This result and the previous one show that the current density profile within and around the magnetic island is of the same importance, or perhaps more important, than the gobal profile and should be seriously considered.

Comparing the above conditions with experiment is spectulative because both conditions demand highly detailed information about a discharge, but some parallels may be drawn:

1. The impurity neon injections in DIVA noted in the previous section may also modify the gradient of the

current density profile near the q=2 surface and cause a radiation loss within the island itself. Note that both a current density dip within an island and an increased current density gardient at the mode rational surface cause larger islands; thus a very complicated series of current density modifications involving both global and local effects may be taking place in this set of experiments. [71]

2. The JIPP T-II Tokamak group has achieved low q edge operation by a combination of gas puffing and a second transformer current rise. By controlling the rise time of the second plasma current pulse, its penetration into the plasma can be limited to the plasma edge regions; this provides a means of controlling the current density profile. The rise time of the pulse controls where the current is induced and the gas puffing adds an electron power loss term; thus by appropiate controls on both the current pulse rise time and gas puffing the current density gradient in the neighborhood of the mode rational surface as well as the global current density profile may be controlled. By careful control, low q edge discharges have been obtained. [70]

5.4 Nonlinear Coupling of Magnetic Islands

The effect of two magnetic islands of different helicity n numbers coupling through the background current density profile is of great importance. When a magnetic island exists, it modifies the background current profile and in some cases may radically steepen the current density gradients on either side of it and nonlinearly couple to and destablize nearby islands. This type of behavior can be illustrated by examining the interaction of the 3/2 and 2/1 magnetic islands. When the 3/2 island is present, the 2/1 island is found to be larger than it was without the 3/2 island; figures 5-15a-e show the effect of both islands on the background current profile. The width of the 3/2 island is approximately the same as before the existence of the 2/1 island, but its presence modifies the current density gradient between the two islands and this effect further destablizes the 2/1 island. As the current density peaking within the 2/1 island is increased, the combination of current density gradient destablization and current density peaking cause a large increase in the width of the 2/1 island and a small reduction in the width of the 3/2 island. The total region occupied by magnetic islands increases however. The net result is that the two islands begin to coalesce as the coupling increases and the background equilibrium current density profile shows a high degree of modification by the

islands - a "ledge" begins to appear in the plasma middle region. The location of the mode rational surfaces seem to be important - the closer they are the greater the coupling effect - however, because of the limited number of runs done it was difficult to evaluate this topic. The plasma parameters were: aspect ratio=4.0, elongation=1.0, C0=1.0, C1=0.0, C2=0.0, and C3=0.50. Unfortunately, the nonlinear coupling can make convergence of the computer program difficult and time consuming, so only a limited number of runs could be done. The major problem is that the time spent on a computer run grows rapidly as the number of islands increase. Nonetheless the nonlinear coupling demonstrated by this series of runs shows the importance of the phenomenon and it is interesting to note that one scenario for the major disruption is the interaction of the 3/2 and 2/1 islands which may overlap and destroy a major portion of the plasma confinement volume. [16,67] Another importance effect is the interaction of the 1/1 and 2/1 islands, but since the simulation of the 1/1 island requires inertial terms, the interaction could not be modelled. In general it is very difficult to model the time dependent behavior of two islands overlapping and the resulting plasma disruption; however, the quasilinear model can demonstrate the nature of this instability. One interesting topic that could not be adressed was the combination of the following three islands: 3/2, 5/3, and 2/1. Since the 5/3 island is in between the

3/2 and 2/1 islands the possiblity exists that it may be destablized by the presence of the 3/2 and 2/1 islands and make a further contribution to the chaos of island overlaping and destablization.

Even though the actual time dependence of the current density coupling of magnetic islands can not be represented with this model, useful qualitative explanations of experiments can be shown:

1. Observed disruptions in the PDX Tokamak are preceeded by the growth of a 2/1 island which is often preceeded by an internal disruption; this may be as a result of both linear and nonlinear coupling of the 2/1 island to the 1/1 island which is beyond the scope of this thesis. [69]

2. In the JIPP T-II Tokamak disruptions of a low q edge value plasma are observed to be preceeded by an abrupt growth of the 3/2 and 2/1 modes. [70]

3. The low q edge discharges in DIVA disrupt with the sudden growth of a 2/1 mode; other modes exist, but disruption only occurs with the presence of a 2/1 mode. [71]

4. When a low q edge discharge with q edge less than 2 and when impurity control to stablize the 2/1 kink mode is obtained, no major disruptions are observed in the DIVA Tokamak. [71]

5. Soft disruptions in the DITE Tokamak are caused by the interaction and overlap of the 1/1 and 2/1 island. [73]

5.5 Metric Element Mixing

Since equation (2-21) is a relationship involving both the contravarient and covariant vector components one would expect harmonic mixing when converting from one form to another. Equations (2-22)-(2-24) detail this conversion. The analysis of these equations proceeds along the following line: Starting with:

$$B_x = g(\theta) \sum_{n,m} B^x_{mn} \exp\left[i(m\theta - n\zeta)\right] \tag{5-6}$$

where $g(\theta)$ represents a metric element term. Rewritting using the decomposed form of B_x gives

$$\sum_{n,m} B_{xmn} \exp\left[i(m\theta - n\zeta)\right] = g(\theta) \sum_{n,m} B^x_{mn} \exp\left[i(m\theta - n\zeta)\right] \tag{5-7}$$

Since g is not a function of φ one may write for each n :

$$\sum_m B_{xmn} \exp[im\theta] = g(\theta) \sum_m B^{x}_{mn} \exp[im\theta] \qquad (5\text{-}8)$$

or

$$B_{xmn} = \frac{1}{2\pi} \int_0^{2\pi} \left\{ g(\theta) \left[\sum_{m'} B_{m'n} \exp[i(m'-m)\theta] \right] d\theta \right\} \qquad (5\text{-}9)$$

The metric elements provide cross harmonic driving terms and modes with the same n number may influence each other through this coupling. The principle coupling elements are toroidicity and plasma elongation both of which are expected to be present in future Tokamaks. Figure 5-17 shows the 2/1 magnetic island width vs inverse aspect ratio and figure 5-21 shows the 2/1 magnetic island width vs elongation. In both of these graphs the q on axis remained constant, C0=1.0, C1=0.5, C2=0.0, C3=1.25, gamma=0.0, and both consider the 2/1 mode. With the method of equilibrium computation used (see chapter III) it is not possible to keep q edge constant; it increases both with a decrease in aspect ratio and an increase in elongation, and thus the family of equilibria generated in the aspect ratio study differs

somewhat in the magnetic field configuration as well as the aspect ratio. See figures 5-16, 5-18, 5-20, and 5-22. The effects of toroidicity and elongation on the magnetic island width depend on the position of the magnetic island to some degree, being somewhat greater for islands nearer the edge of the plasma where the metric elements have the strongest dependance on theta; however, again this is profile dependent. The effect of toroidicity is to reduce the saturated magnetic island width as the aspect ratio decreases; this is qualitatively consistant with reference [64]. As the aspect ratio was decreased, the mode rational surface shifted (see figure 5-18) into the plasma and the 2/1 perturbation developed a decaying tail similar to the center peaked current case. Since the form of the current density profile changed as the aspect ratio changed, it being dependent upon the specific equilibrium solution, there may be some question as to whether the toroidicity causes the current density profile to change which then causes the reduction in magnetic island width, rather than a direct connection between the island width and toroidicity. Plasma elongation also appears to reduce the saturated magnetic island width, but care should be taken when interpretating these results since the equilibrium current density profile changes radically with large changes in plasma elongation. As the elongation increases the mode rational surface also shifts inward as in the toroidal case (see figure 5-22), but

to a lesser extent. With either current peaking, toroidicity, or elongation, a reduction in the magnetic island width has generally been associated with the inward shift of the mode rational surface. See figure 5-19 for the aspect ratio case and figure 5-23 for the elongation case. Since this inward shift of the mode rational surface cannot be separated from the equilibrium computations used in this model, a further examination of elongation and toroidicity with a global plasma transport model would be a useful extension of this work.

5.6 Mode Mixing

Mode mixing occurs when perturbations of the same n number interact through metric element coupling to enhance or suppress each other and thus modify the magnetic island width. In the cases studied the effect of the 2/1 island on the 3/1 island was examined and it was found that the 2/1 island could drive a 3/1 island in equilibria that could not otherwise support a 3/1 island provided that there was a large amount of plasma elongation present. With only small amounts of elongation no effects could be detected; even with large amounts of elongation the 3/1 island width was only about one percent of the minor radius; the 2/1 magnetic island remained essentially the same. See figures 5-24a-e.

In this case the plasma parameters were: aspect ratio=4.0, elongation=2.0, C0=1.0, C1=0.0, C2=0.0, and C3=0.0. The aspect ratio had only a minor effect on the mode mixing.

Unlike some work done using the reduced MHD equations, the 1/1 mode could not be generated (because in general it oscillates in time and does not saturate) and thus what may be the major harmonic driving term could not be modelled. [62,73] Another difference is that the magnetic island is allowed to modify the background current density profile in the model of this thesis, while the background resistively remained only a function of the radial coordinate rather than a function of the magnetic surfaces in the work of many of the references; this may result in differences in the functional form of the perturbed radial magnetic field components. [65,66] The 3/1 island has been observed to play a roll in a limited number of disruptions in the PDX Tokamak; however, the 2/1 island is considered to be the most active mode in disruptions. [69] Other tokamak groups have observed a large number of MHD modes; however, these higher m number modes do not appear to cause any major problems. [16,70,71,73,75]

5.7 Summary

The major parameter effecting the magnetic island

width is the local current density gradient and the current profile within the magnetic island. Modification of the background current profile by the presence of multiple islands can and does destablize otherwise stable islands; it may be the major coupling effect. Toroidicity and elongation are shown to modestly reduce the saturated magnetic island width and a general trend of smaller magnetic island width with the inward shift of the mode rational surface is noted. Mode mixing coupling has been shown to exist, but its effect has been very modest. Possibily the inclusion of the 1/1 mode, which this work cannot address, would show a greater influence. Overall, good qualitative agreement with experiment has been shown.

CHAPTER VI

Conclusions

The quasilnear model has proven to be useful in the computation of saturated magnetic island widths. Unlike the reduced MHD equations, the quaslinear equations consider only the asymtotic time limit and thus do not follow the evolution of the equilibrium as a function of time. They can, however, handle cases of greater geometric complexity within a reasonable computing time limit and this factor along with a somewhat simplier equation set is their source of attraction. One major limitation is the inability of the equations to model tearing modes that oscillate in time such as the m=1,n=1 mode. In order to include the modes that oscillate in time it is necessary to consider the inertial terms of the MHD equations, such as the mass density and velocity, with the consequence of greater complexity. [17,18,65,66]

In the course of the derivation of the quasilinear

equations it has been shown that the magnetic island influences the background current density profile and, using a simple approximation for the pressure and current density within a magnetic island, the effect of the magnetic island on the background equilibrium has been quantified and a self consistant set of equations formed. This set of equations has been solved for a varity of parameters, including torodicity, plasma elongation, equilibrium current density profile, and current density profile within a magnetic island. The new results of greatest interest are the effects of the current density gradient local to the magnetic island and the current density profile within a magnetic island itself.

The large aspect ratio limit has been used to provide a qualitative analysis of the structure of the radial magnetic field perturbation and this analysis points to the region on the inner side of the magnetic island as important to the existence of the radial perturbation. It is in this region that the solution is forced to "bend" or turn to meet the boundary conditions at the edge of the plasma and this effect is found to depend on the local gradient of the current density. It has been demonstrated that the magnetic island width increases as the local current gradient at the mode rational surfaces increases.

The most unexpected effect is the fact that peaking the current density profile within a magnetic island can

cause a large increase in the width of a magnetic island and can also destablize otherwise stable magnetic islands. This result enables speculation on a possible means of magnetic island control - devise some means to locally heat or cool the plasma so that the local current density profiles can be modified to suppress the existence of the magnetic islands. Local heating by RF, or perhaps, beams could be used, but control may be difficult - this is an open issue.

The nonlinear coupling of magnetic islands through the background current density profile has been found to increase the saturated width of magnetic islands when the current density gradient at the inner edge of the island is increased by the presence of another magnetic island. This effect is independent of the mode numbers of the islands involved and thus all the islands within a plasma will be coupled to a degree which depends on the relative spacing between the islands and the width of the islands themselves. Linear coupling of magnetic islands with the same n number occures when toroidicity and/or elongation is present. This linear coupling can cause normally stable islands to be driven unstable by their unstable neighbors and thus increase the amount of the plasma that is occupied by magnetic islands. In the work done, however, this was found to be a relatively minor effect possibly because the 1/1 magnetic island could not be included. When toroidicity and/or elongation is increased in a plasma with only a single mode present, the

saturated magnetic island width showed a small decrease. In all the cases studied it was noted that, in general, the magnetic island width decreased as the mode rational surface drifted inward pointing to low q edqe plasma as being the most unstable to tearing modes.

Since the saturated magnetic island width and even its existence depends to a large extent on the local current density profile, knowledge of the global current density profile may not be sufficient to predict magnetic island behavior. In cases such as these the predicition of the saturated magnetic island width may, by necessity, take on a probabalistic nature unless the appropiate current profiles can be externally controlled, perhaps by operation in restructed regions of Tokamak discharge phase space.

References

[1] L.S. Solov'ev, V.D. Shafranov, Reviews of Plasma Physics , Volume 5, Consultants Bureau, New York, 1, (1970)

[2] G. Bateman, MHD Instabilities , The M.I.T. Press, Cambridge, 1978

[3] J.D. Callen, et al., "Magnetic "Islandography" in Tokamaks", Oak Ridge National Laboratory, ORNL/TM-6564

[3] H.P. Furth, P.H. Rutherford, H. Selberg, Physics of Fluids , 16 , (1973) 1054

[4] B.B. Kadomtsev, O.P. Pogutse, Sov. Phys-JETP, Vol. 38, (1974) 283

[5] J.L. Johnston, J.M. Greene, Plasma Physics, 9 , (1967), 611

[6] A.H. Glasser, J.M. Greene, J.L. Johnson, Physics of Fluids , 18 , (1975) 875

[7] A.H. Glasser, J.M. Greene, J.L. Johnson, Physics of Fluids , 19 , (1976) 567

[8] H. Tasso, J.T. Virtamo, Plasma Physics,22 , (1980) 1003

[9] R.B. Paris, "Lectures on Resistive Instabilities in MHD", Departement de Recherches Sur La Fusion Controlee, Association Euratom - C.E.A. (February 1982)

[10] P.H. Rutherford, H.P. Furth, "Nonlinear Properties of Kink and Tearing Instabilities in Tokamaks", MATT-872, Plasma Physics Laboratory, Princeton University (December 1971)

[11] R.B. White, "Resistive Instabilities and Field Line Reconnection", Princeton University, PPPl-1655

[12] G. Bateman, R.N. Morris, "Effect of a Localized Magnetic Perturbation on Magnetic Islands in a Cylindrical Plasma", Georgia Tech GTFR-15 (May 1980)

[13] R.B. White, D.A. Monticelo, M.N. Rosenbluth, B.V. Waddell, Physics of Fluids 20 (1977) 800

[14] G. Bateman, R.N. Morris, "Model for Saturated Tearing Modes in Toroidal Geometry", Georgia Tech GTFR-31, (April 1982)

[15] W. Kerner, H. Tasso, Plasma Physics 24, 97 (1982)

[16] K. Toi, K. Sakurai, S. Tanahashi, S. Yasue, Nucl. Fusion, 22 , 465, (1982)

[17] H.R. Hicks, J.A. Holmes, B.A. Carreras, D.J. Tetreault, G. Berge, J.P. Freidberg, P.A. Politzer, D. Sherwell, in Eighth Int. Conf. on Plasma Physics and Controlled Nuclear Fusion Research (IAEA, Brussels), Vol. I, 259 (1980)

[18] H.R. Hicks, B. Carreras, J.A. Holmes, B.V. Waddell, "Interaction of Tearing Modes of Different Pitch in Cylindrical Geometry", Oak Ridge National Labrotory Report ORNL/TM-6096, (December 1977)

[19] F. Karger, et al., in Sixth Int. Conf. on Plasma Physics and Controlled Nuclear Fusion Research (IAEA, Berchtesgaden), Volume I, 267 (1976)

[20] K. Bol, et al., in Seventh Int. Conf. on Plasma Physics and Controlled Nuclear Fusion Research (IAEA, Innsbruck) Volume I, 11 (1978)

[21] N.R. Sauthoff, S. Von Goeler, W. Stodiek, Nuclear Fusion 18 , 1445 (1978)

[22] B.V. Waddell, B. Carreras, H.R. Hicks, J.A. Holmes, D.K. Lee, Phys. Rev. Lett. 41 , 1386 (1978)

[23] J.D. Callen, et al., in Seventh Int. Conf. on Plasma Physics and Controlled Nuclear Fusion Research (IAEA, Innsbruck) Volume I, 415 (1978)

[24] B.V. Waddell, B. Carreras, H.R. Hicks, J.A. Holmes, Physics of Fluids 22 , 896 (1979)

[25] B. Carreras, B.V. Waddell, H.R. Hicks, Nuclear Fusion 19 , 1423 (1979)

[26] B. Carreras, H.R. Hicks, J.A. Holmes, B.V. Waddell, Physics of Fluids 23 ,1811 (1980)

[27] A. Sykes, J.A. Wesson, Phys. Rev. Lett. 44 , 1215 (1980)

[28] J.A. Holmes, et al., "Tearing Mode Calculations for Noncircular Tokamak Plasmas", Proc. IEEE Int. Conf. on Plasma Science, Madison Wisconsin, (May 1980)

[29] B. Carreras, B.V. Waddell, and H.R. Hicks, "Poloidal Magnetic Field Fluctuations in Tokamaks", ORNL/TM-6403, (July 1978)

[30] B.V. Waddell, G.L. Jahns, J.D. Callen, H.R. Hicks, Nuclear Fusion 18 , (1978) 735

[31] G.L. Jahns, M. Soler, B.V. Waddell, J.D. Callen, H.R. Hicks, Nuclear Fusion 18 , (1978) 609

[32] S.J. Zweben, B.V. Waddell, D.W. Swain, H.H. Fleischman, "High Energy Runaway Orbits in the Presence of m=2 Magnetic Islands", ORNL/TM-6216, July 1973

[33] M.V. Berry, in "Topics in Nonlinear Dynamics", (JORNA, S., ed.), (Am. Inst. Phys. New York, 1978) 16-120

[34] A.N. Kolmogorov, in Proceeding of the International Congress of Mathematicians , Amsterdam (North Holland, Amsterdam, 1957) Volume I, p. 315

[35] V.I. Arnol'd, Russ. Math. Sor. 18 (1963), 9

[36] J. Moser, Nachr. Akad. Wiss Gottingen II Math. Phys. Kl, 1 (1962)

[37] A.H. Boozer, R.B. White, "Particle Diffusion in Tokamaks with Partially Destroyed Magnetic Surfaces", Princeton University, PPPL-1872, (1982)

[38] H. Goldstein, Classical Mechanics , 2nd Edition, Addison-Wesley Publishing Company, Reading Massachusetts

[39] H.P. Furth, J. Killeen, M.N. Rosenbluth, Physics of Fluids 6 , (1963) ,459

[40] G. Schmidt, Physics of High Temperature Plasmas , 2nd Edition, Academic Press, New York, (1979)

[41] S.P. Hirshman, "Curvilinear Coordinates for Magnetic Confinement Geometries", ORNL/TM-8393, (1982)

[42] H.R. Strauss, Physics of Fluids 19 , (1976), 134

[43] H. Tasso, Plasma Physics, 17 , 1131, (1975)

[44] R.B. White, D.A. Monticello, M.N. Rosenbluth, Phys. Rev. Leters, 39 , (1977)

[45] S. Yoshikawa, Phys. Rev. Letters, 27 , (1971)

[46] B. Carreras, H.R. Hicks, D.K. Lee, "The Effects of Toroidal Coupling on the Stability of Tearing Modes", Oak Ridge National Laboratory Report ORNL/TM-7281, (1980)

[47] D. Edery, J.L. Soule, R. Pellat, M. Frey, J.P. Somon, "Non-Linear Evolution of Tearing Modes in Toroidal Geometry", in Eighth Conference Proceeding on Plasma Physics and Controlled Nuclear Fusion Research, (IAEA, Brussels), Volume I, 269, (1980)

[48] W. Kerner, H. Tasso, "Stability of Multihelical Tearing Modes in Shaped Tokamaks", Max-Planck-Institut Fur Plasmaphysik, IPP 6/211, (March 1982)

[49] S. Hamada, Nuclear Fusion, 2 , (1962) 22

[50] P.H. Rutherford, Phys. Fluids 16 , 1903, (1973)

[51] A.H. Nayfeh, Perturbation Methods , Wiley, New York, (1973)

[52] M.N. Rosenbluth, D.A. Monticello, H. Strauss, R.B. White, Phys. Fluids, 19 , (1976), 1987

[53] D. Biskamp, H. Welter, "Numerical Studies of Resistive Instabilities", in Sixth Conference Proceeding on Plasma Physics and Controlled Nuclear Fusion Research, (IAEA, Berchtesgaden), Volume I, 579, (1976)

[54] L.L. Lao, S.P. Hirshman, R.M. Wieland, Phys. Fluids, 24 , 1431 (1981)

[55] L.L. Lao, R.M. Wieland, W.A. Houlberg, S.P. Hirshman, Oak Ridge National Laboratory Report ORNL/TM-7871 (1982)

[56] J.H. Ferziger, Numerical Methods for Engineering Applications , John Wiley and Sons, New York (1981)

[57] P. Rabinowitz, Numerical Methods for Non-linear Algebraic Equations , Gordon and Breach, 1970

[58] L.F. Shampine, M.K. Gordon, Computer Solution of Ordinary Differential Equations: The Initial Value Problem

[59] A.H. Glasser, Lecture Notes

[60] J.M. Greene, J.L. Johnson, Phys. Fluids, 5 , 510 (1962)

[61] A.H. Reiman, Phys. Fluids, 26 , 1338 (1983)

[62] B.A. Carreras, et al, "MHD Activity in the ISX-B Tokamak: Experimental Results and Theoretical Interpretation", ORNL/TM-8648, June 1983

[63] R. Bellman, Stability Theory of Differential Equations , Mc Graw Hill, New York, (1953)

[64] R. Izzo, A. Monticello, W. Park, J. Manickam, H.R. Strauss, R. Grimm, K. McGuire, Phys. Fluids, 26 , 2240 (1983)

[65] J.A. Holmes, B.A. Carreras, T.C. Hender, H.R. Hicks, V.E. Lynch, and B.F. Masden, Phys. Fluids, 26 , 2569 (1983)

[66] H.R. Hicks, B.A. Carreras, J.A. Holmes, D.K. Lee, and B.V. Waddell, J. Comput. Phys. 44 , 46 (1981)

[67] J.J. Ellis, K. McGuire, R. Peacock, D.C. Robinson, I. Stares, in Eighth Int. Conf. on Plasma Physics and Controlled Nuclear Fusion Research (IAEA,Brussels), Vol. I 731 (1980)

[68] J.K. Lee, H. Ikezi, F.W. Mclain, N. Ohyabu, "Island Driven by an External Source", General Atomic Company, GA-A16777, (1982)

[69] P. Couture, K. Okano, K. McGuire, Bull. of the Am. Phys. Soc., Vol. 28, No. 8, 1174 (1983)

[70] K. Toi, S. Itoh, K. Kadota, K. Kawahata, N. Noda, K. Sakurai, K. Sato, S. Tanahashi, S. Yasue, Nucl. Fusion 19 , 1643, (1979)

[71] DIVA Group, Nucl. Fusion 20 , 271, (1980)

[72] V. Chan, G. Guest, Nucl. Fusion 22 , 272, (1982)

[73] M.F. Turner, J.A. Wesson, Nucl. Fusion, 22 , 1069, (1982)

[74] F. De Luca, A. Jacchia, E. Lazzaro, G. Ramponi, Nucl. Fusion, 22 , 1664, (1982)

[75] S.V. Mirnov, I.B. Semenov, Sov. At. Energy 30 , (1971), 22

[76] J.W. Eastwood, K.I. Hopcraft, Bull. of the Am. Phys. Soc., Vol. 28, No. 8, 1174 (1983)

[77] Smythe, Static and Dynamic Electricity , McGraw-Hill, New York, (1950)

[78] Sheffield, Plasma Scattering of Electromagnetic Radiation , Academic Press, (1975)

[79] E.A. Lazarus, Plasma Phys., 25 , 1271 (1983)

Vita

Robert Morris was born in Detroit, Michigan on August 24, 1956. He attended Aero Mechanics High School where, in addition to earning a High School Diploma, he became a certified aircraft mechanic. After graduating from High School in June of 1974, he attended Wayne State University (also in Detroit) , majored in electrical engineering, and graduated in December of 1978 with a B.S.E.E. He began his studies at Georgia Tech in January of 1979 and recieved his M.S.N.E. in December of 1979; he immediately began his doctoral studies in January of 1980. He is currently married and has no children.

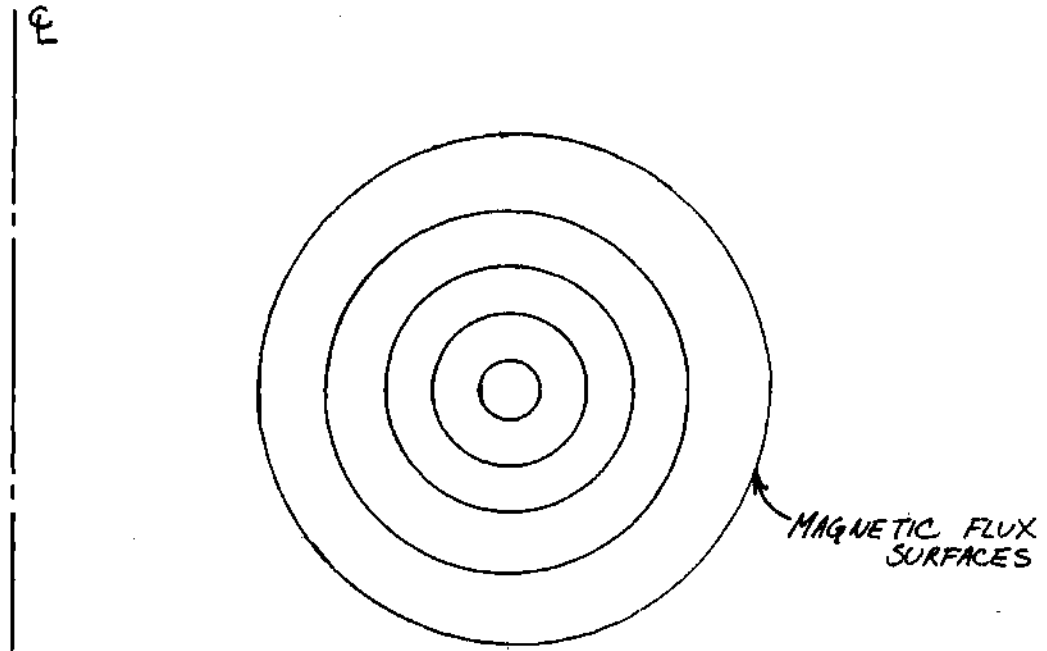

Figure 1-1. Ideal MHD Equilibrium

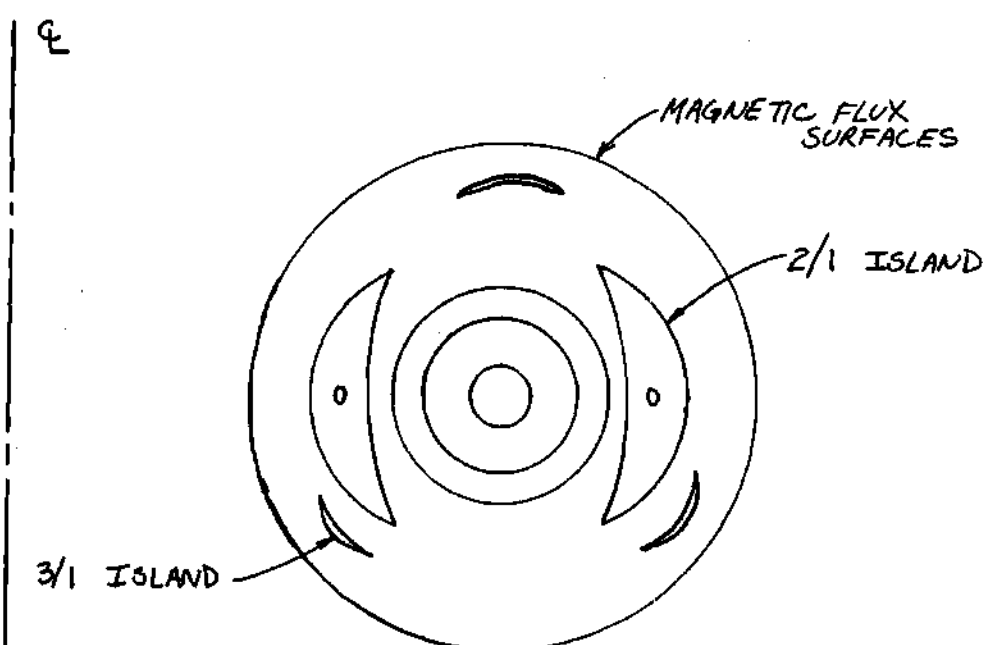

Figure 1-2. Equilibrium with Magnetic Islands

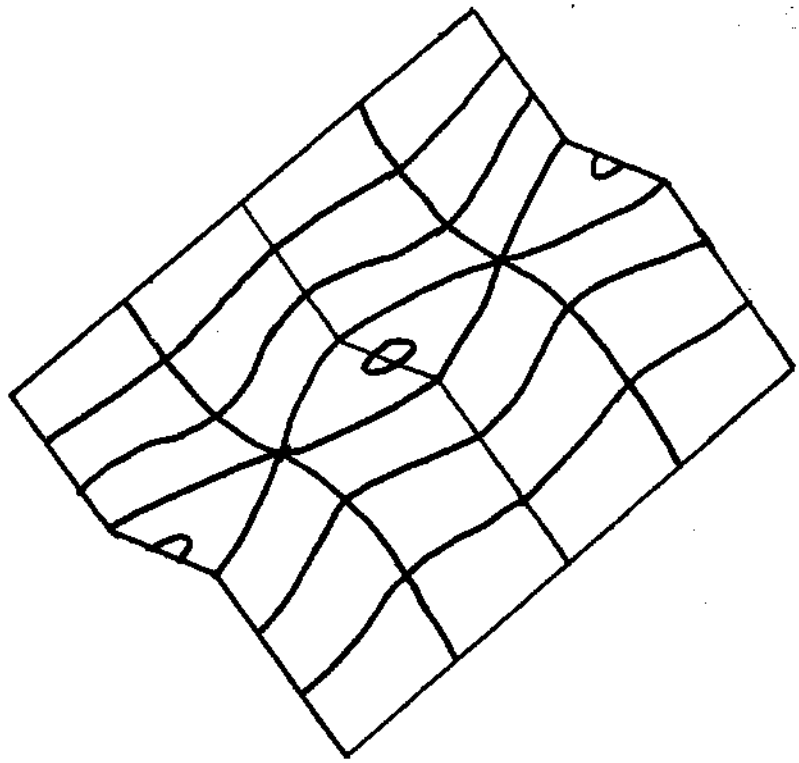

Figure 2-1. Magnetic Island Pressure Profile

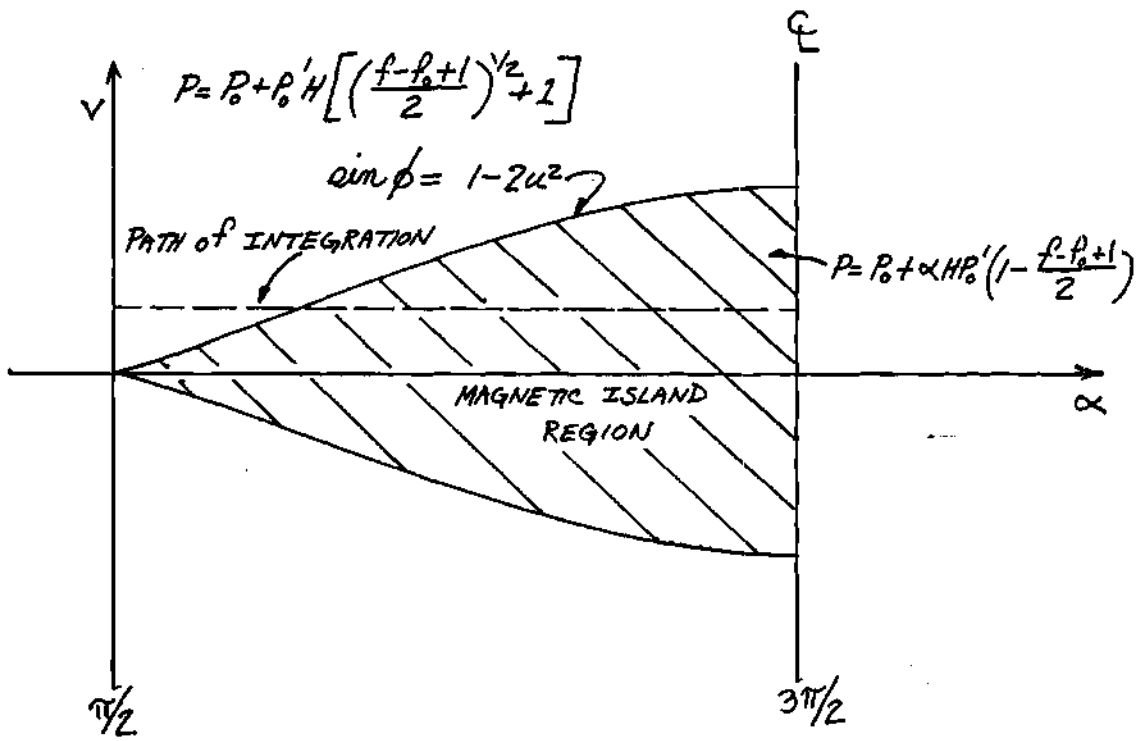

Figure 2-2. Path of Pressure Integration.

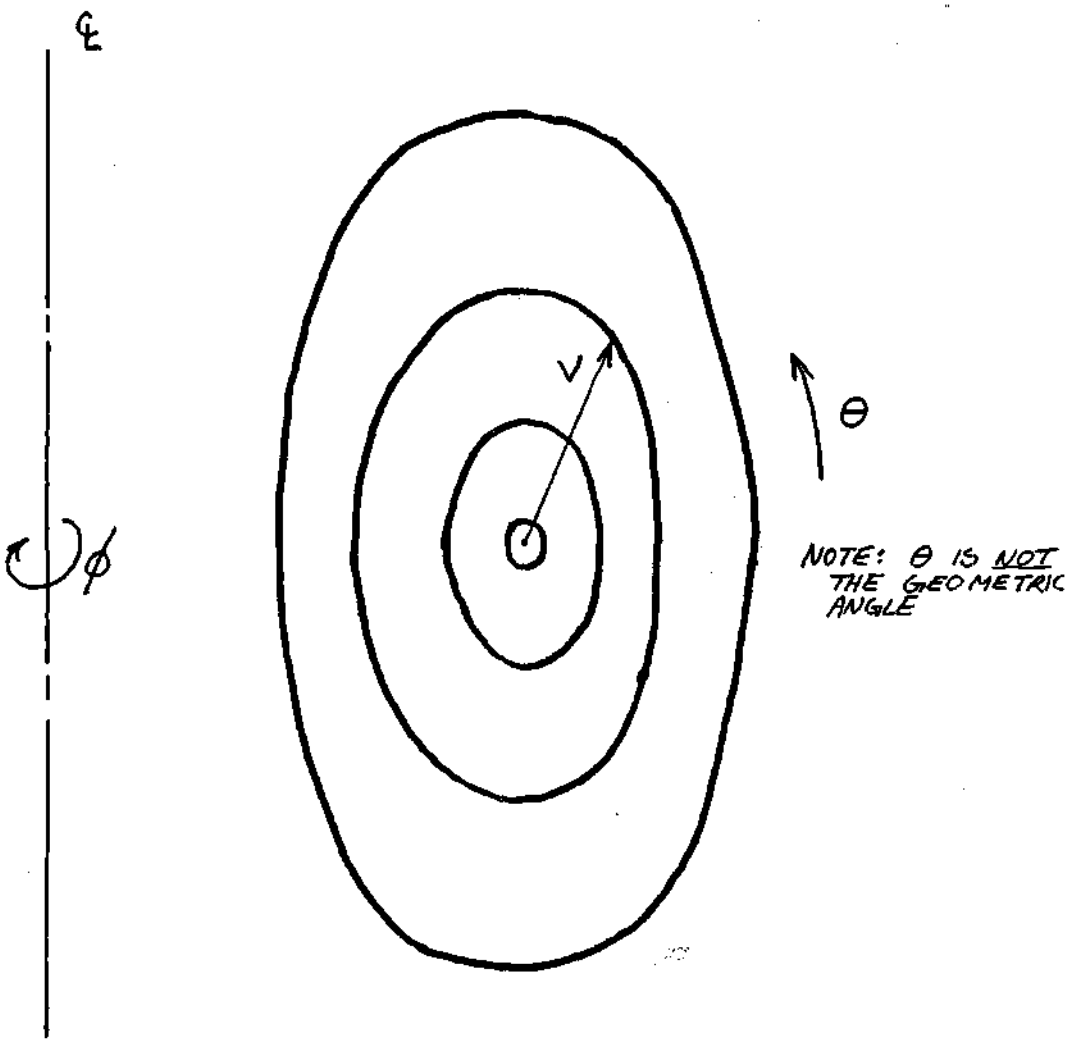

Figure 3-1. Moment Coordinate System.

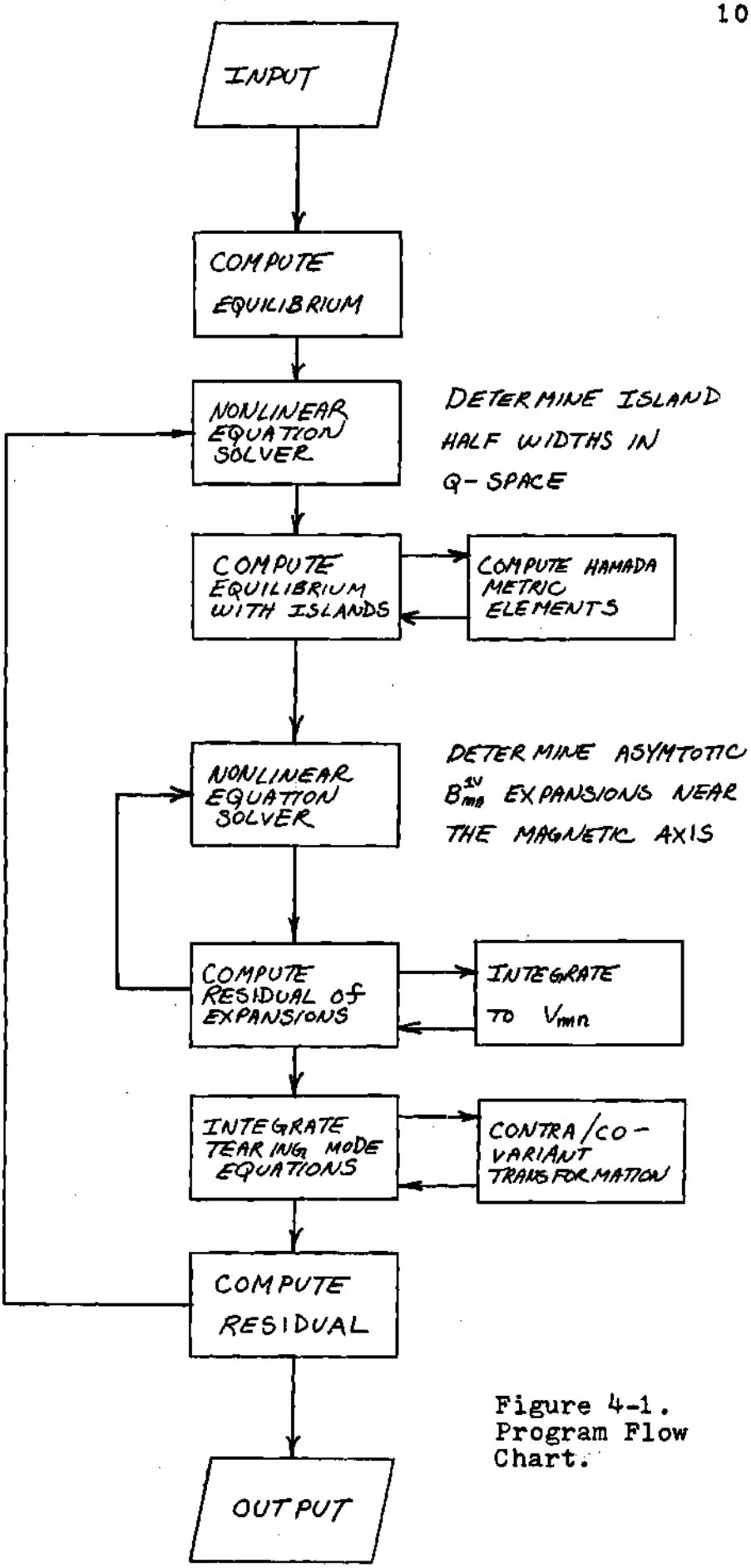

Figure 4-1. Program Flow Chart.

```
12:12:30  12/10/83  page  1

georgia tech eq1rm/tearing
code  1983  by r. morris

        r0  4.000e+00
        e   1.000e+00
        r1  1.000e+00
        r2  0.

  1  moment harmonics
  2  hamada harmonics
c0  1.000e+00  c1  3.000e-01
c2  0.         c3  0.
ex -5.000e-01
```

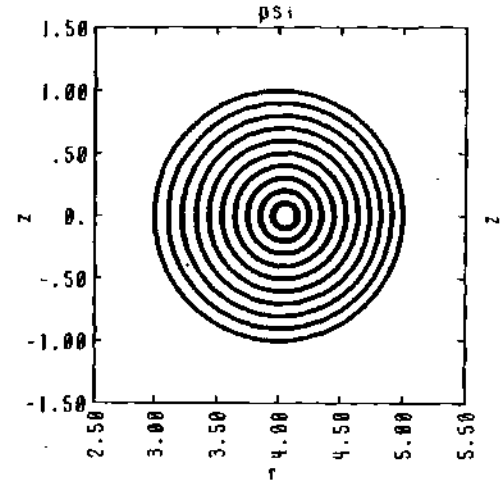

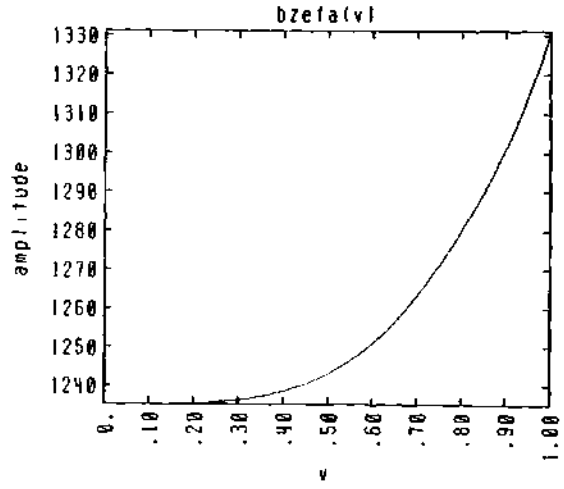

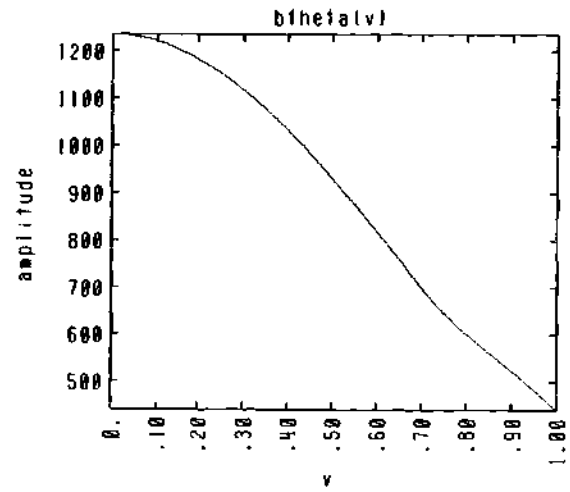

Figure 5-1a. Rounded Current Profile Case / P1.

```
12:12:30  12/10/83  page  2

georgia tech eqlim/tearing
code  1983  by r. morris

        r0  4.000e+00
        e   1.000e+00
        r1  1.000e+00
        r2  0.

  1  moment harmonics
  2  hamada harmonics
c0  1.000e+00  c1  3.000e-01
c2  0.         c3  0.
ex -5.000e-01
```

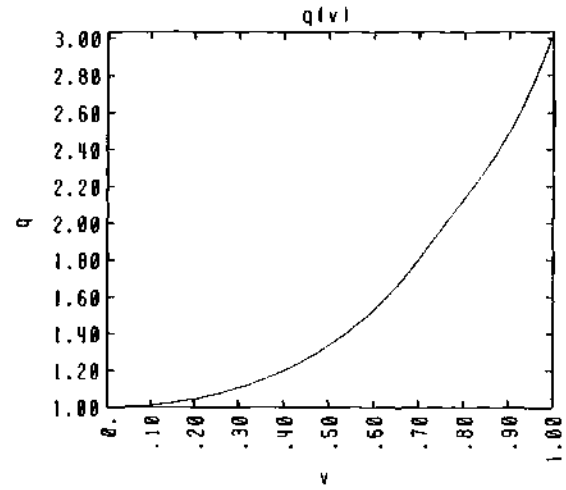

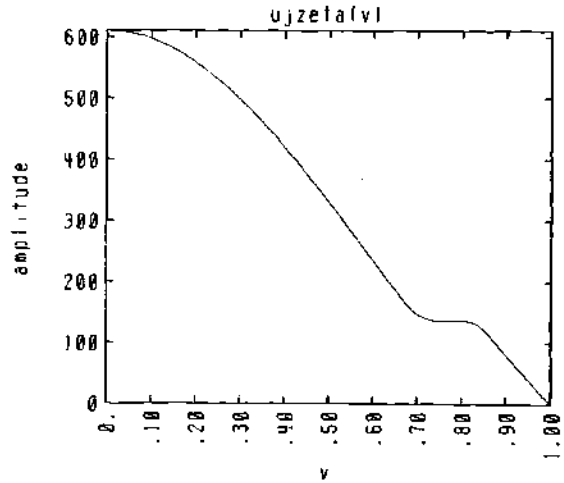

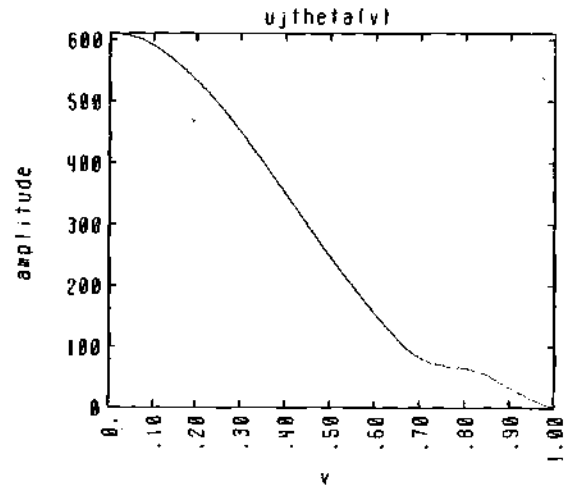

Figure 5-1b. Rounded Current Profile Case / P2.

```
12:12:30  12/10/83  page  3

georgia tech eqlim/tearing
code  1983  by r. morris

        r0  4.000e+00
        e   1.000e+00
        r1  1.000e+00
        r2  0.

  1  moment harmonics
  2  hamada harmonics
c0  1.000e+00  c1  3.000e-01
c2  0.         c3  0.
ex -5.000e-01 pex  2.000e+00
s1  0.         s2  0.
```

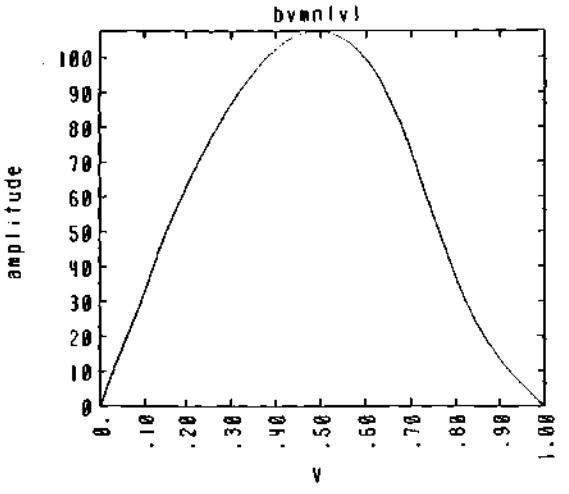

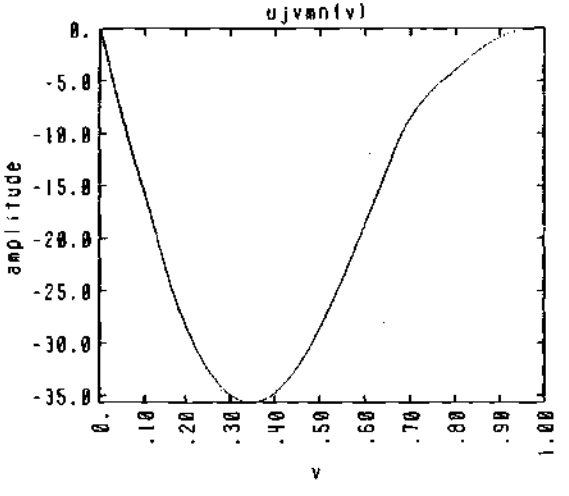


```
total number of modes          1
this mode                      2/ 1
halfwidth in q space           3.121e-01
dq/(dq/dv)                     1.894e-01
amp of this harmonic           2.627e+02
v rational for this mode       7.592e-01
gamma(1)                       2.000e-01
gamma(2)                       5.000e-01
```

Figure 5-1c. Rounded Current Profile Case / P3.

```
12:12:30  12/10/83  page  4

georgia tech eqlim/tearing
code  1983  by r. morris

        r0  4.000e+00
        e   1.000e+00
        r1  1.000e+00
        r2  0.

  1  moment harmonics
  2  hamada harmonics
c0  1.000e+00  c1  3.000e-01
c2  0.         c3  0.
ex -5.000e-01 pex  2.000e+00
s1  0.        s2  0.
```

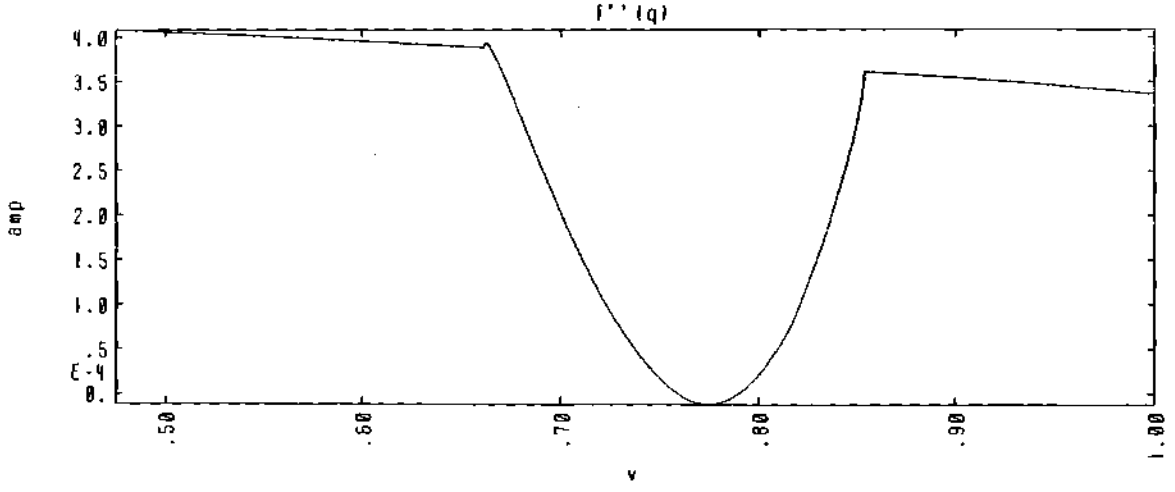

Figure 5-1d. Rounded Current Profile Case / P4.

13:49:52 12/10/83 page 1

georgia tech eqlim/tearing
code 1983 by r. morris

r0 4.000e+00
e 1.000e+00
r1 1.000e+00
r2 0.

1 moment harmonics
2 hamada harmonics
c0 1.000e+00 c1 3.000e-01
c2 0. c3 3.000e+00
ex -5.000e-01

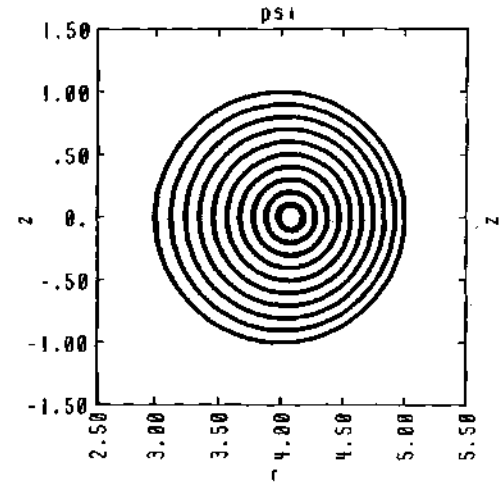

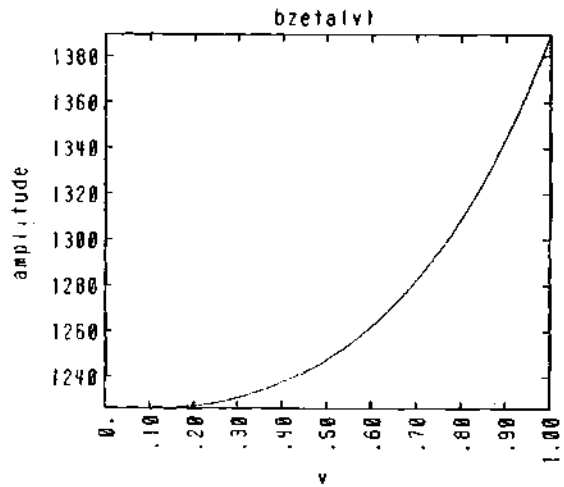

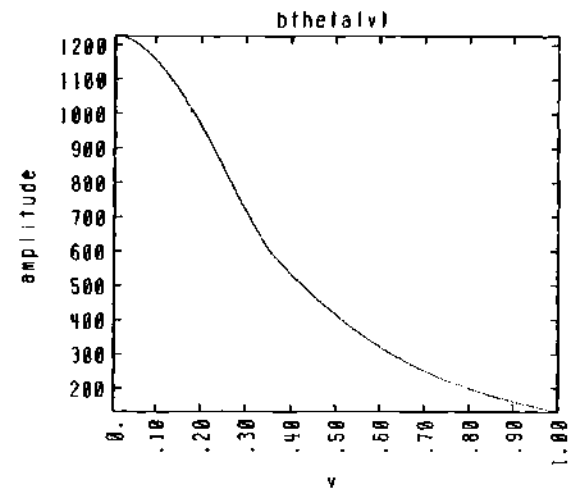

Figure 5-2a. Peaked Current Profile Case / P1.

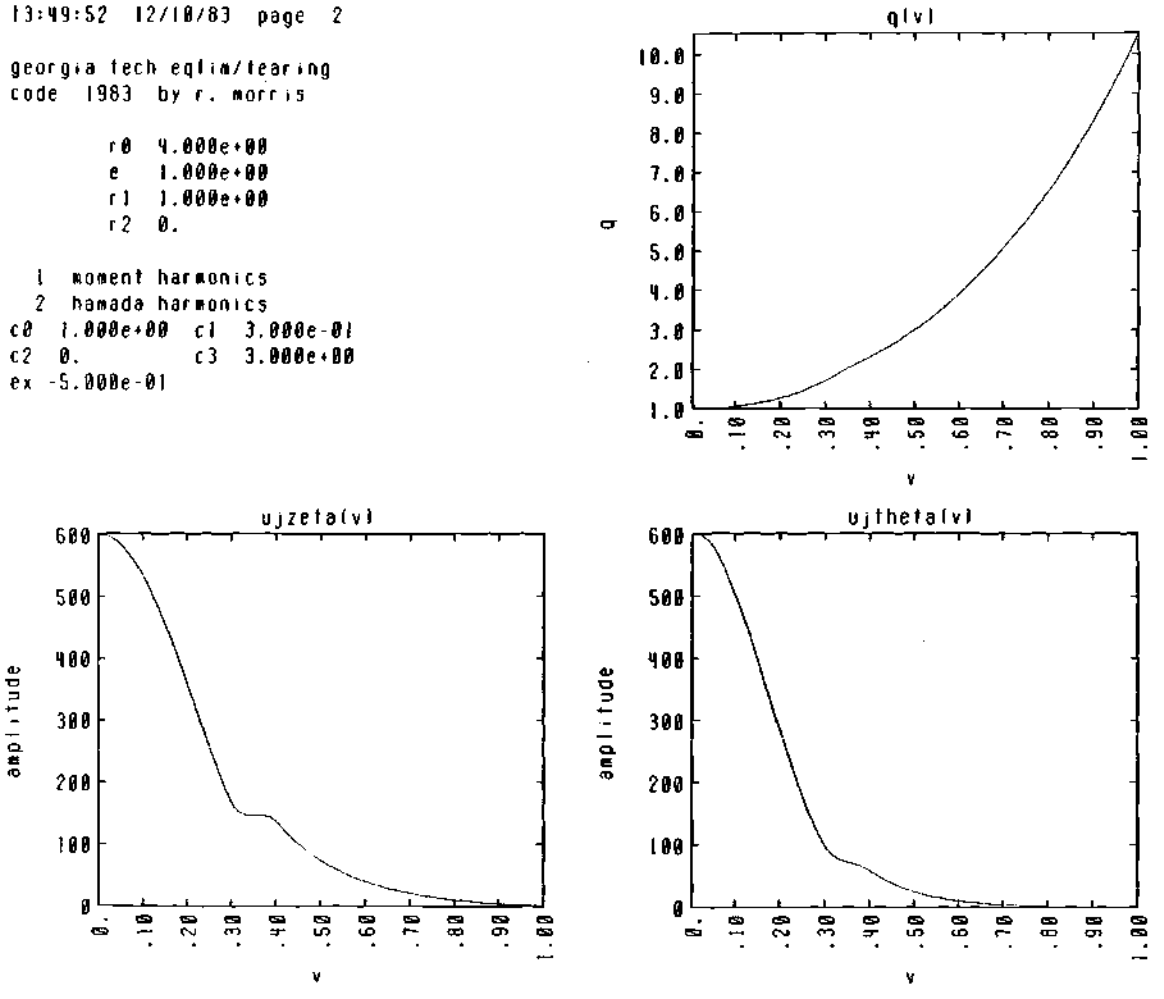

Figure 5-2b. Peaked Current Profile Case. / P2.

13:49:52 12/10/83 page 3

georgia tech eql+m/tearing
code 1983 by r. morris

r0 4.000e+00
e 1.000e+00
r1 1.000e+00
r2 0.

1 moment harmonics
2 hamada harmonics

c0	1.000e+00	c1	3.000e-01
c2	0.	c3	3.000e+00
ex	-5.000e-01	pex	2.000e+00
si1	0.	si2	0.

total number of modes	1
this mode	2/ 1
halfwidth in q space	3.336e-01
dq/(dq/dv)	1.000e-01
amp of this harmonic	1.162e+03
v rational for this mode	3.455e-01
gamma(1)	2.000e-01
gamma(2)	5.000e-01

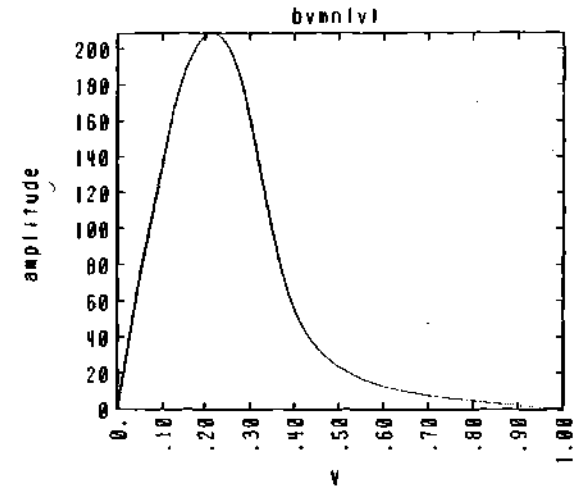

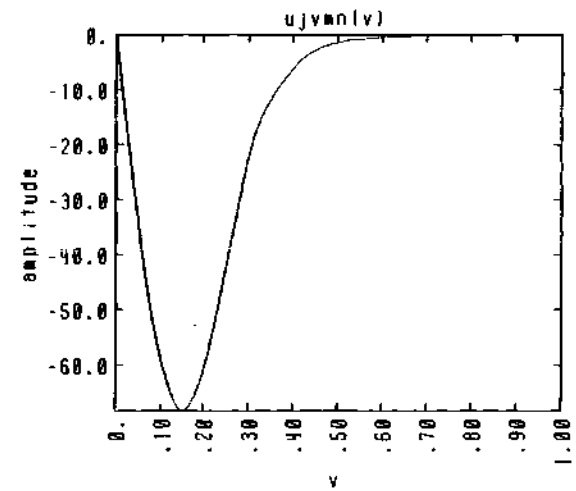

Figure 5-2c. Peaked Current Profile Case / P3.

```
13:49:52  12/10/83  page  4

georgia tech eqlim/tearing
code  1983  by r. morris

        r0  4.000e+00
        e   1.000e+00
        r1  1.000e+00
        r2  0.

  1  moment harmonics
  2  hamada harmonics
c0  1.000e+00  c1  3.000e-01
c2  0.         c3  3.000e+00
ex -5.000e-01 pex  2.000e+00
si1  0.        si2  0.
```

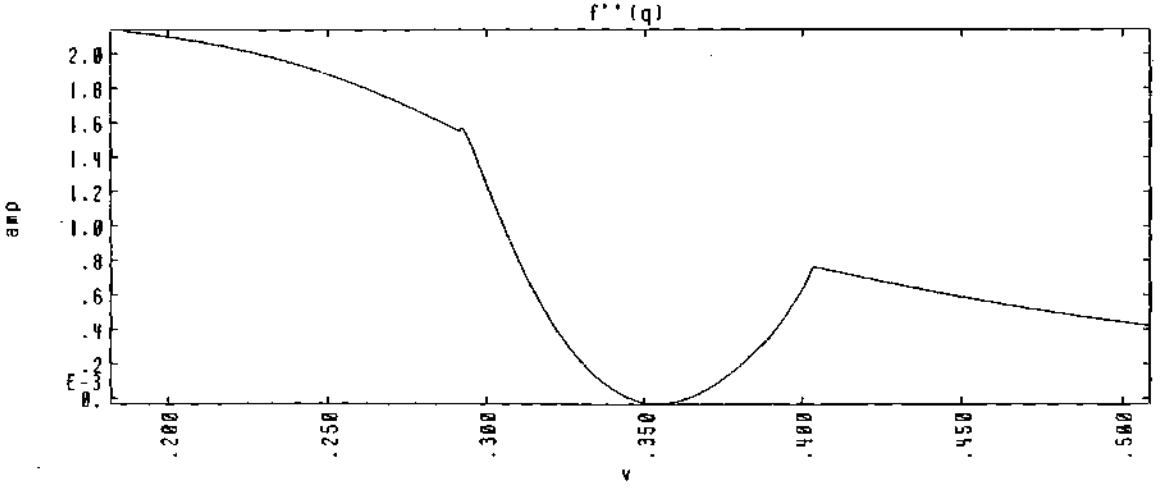

Figure 5-2d. Peaked Current Profile Case / P4

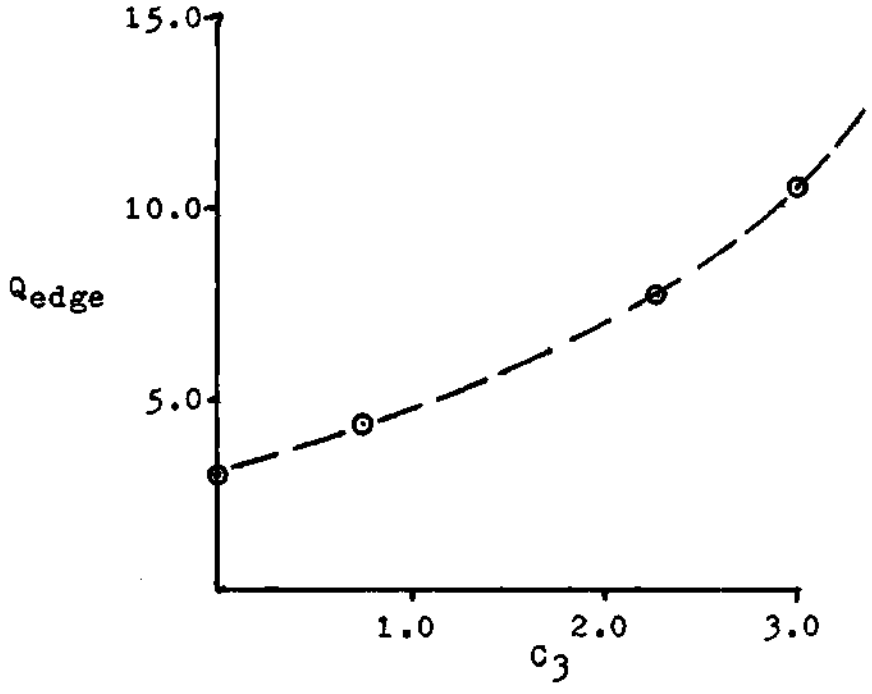

Figure 5-3. Q_{edge} vs C_3.

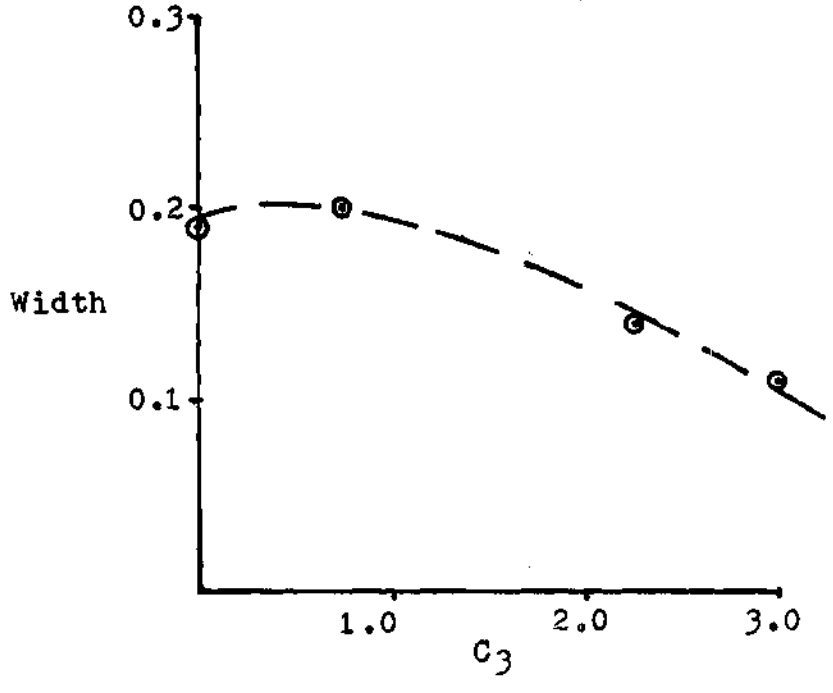

Figure 5-4. 2/1 Island width vs C_3.

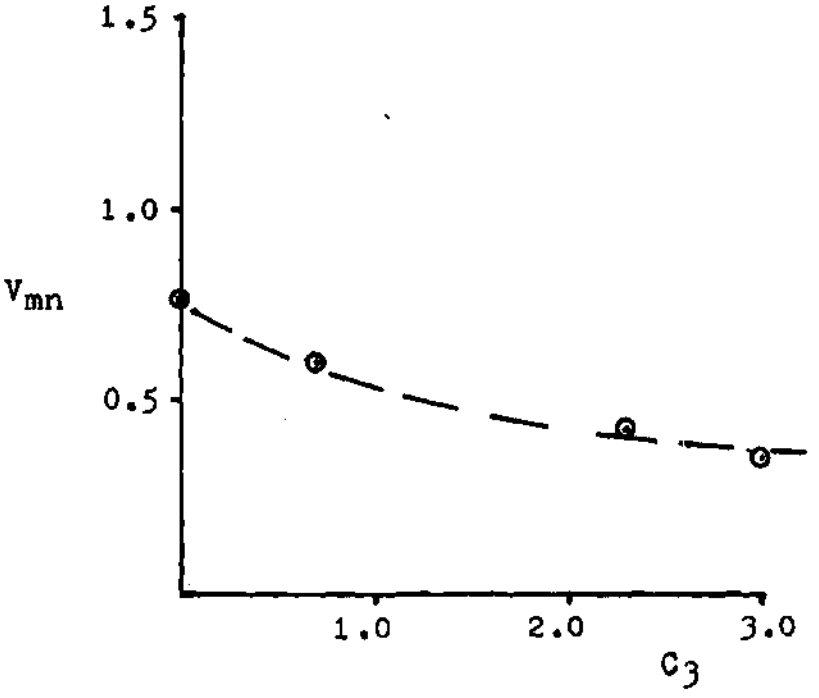

Figure 5-5. Position of Mode Rational Surface vs C_3.

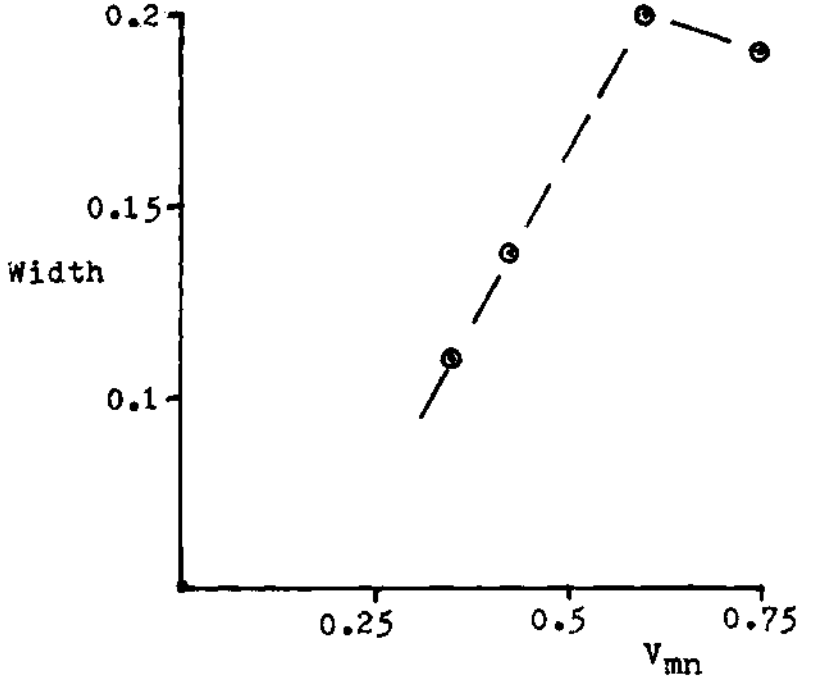

Figure 5-6. 2/1 Island Width vs Position of Mode Rational Surface.

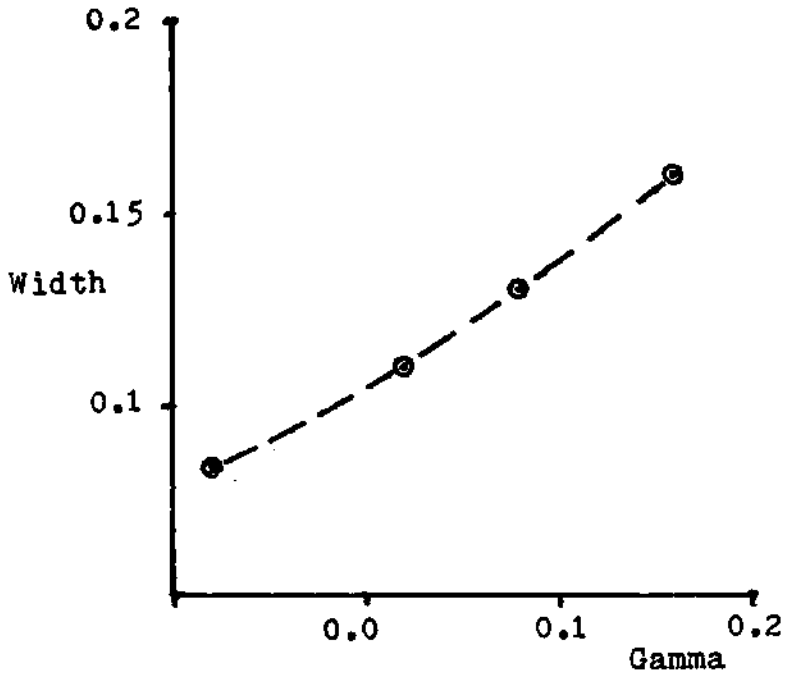

Figure 5-7. 2/1 Island Width vs Gamma.

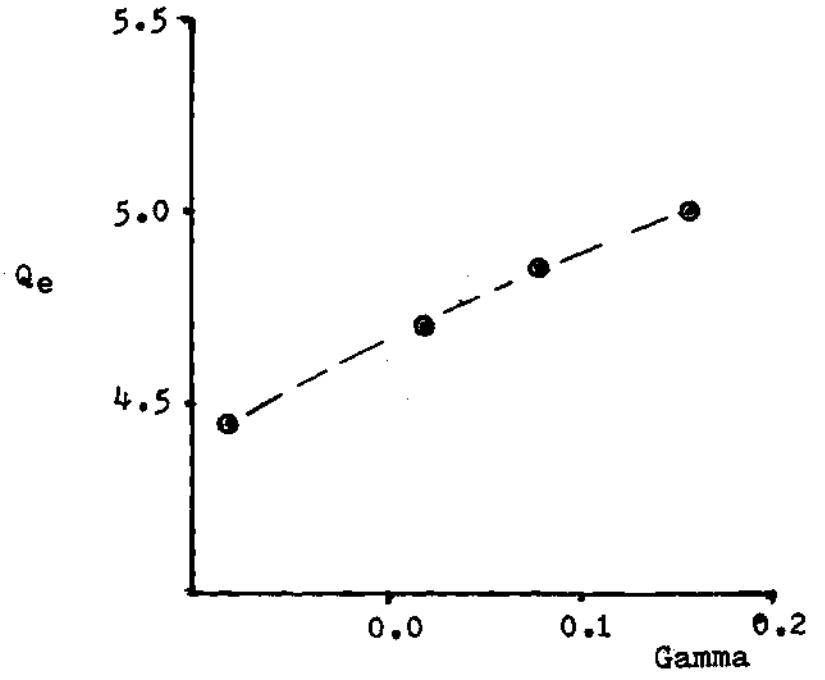

Figure 5-8. Q_e vs Gamma for 2/1 Island.

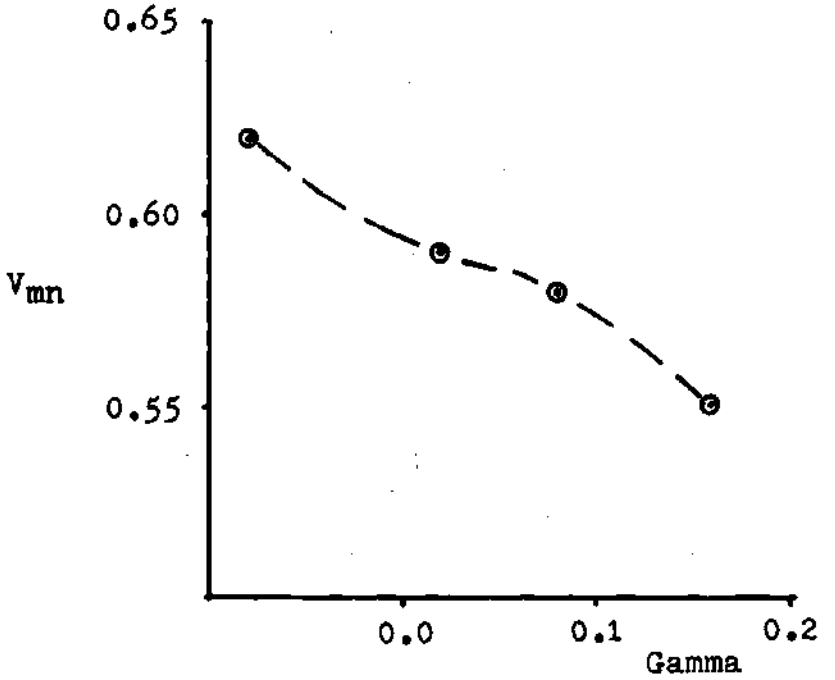

Figure 5-9. V_{mn} vs Gamma for 2/1 Island.

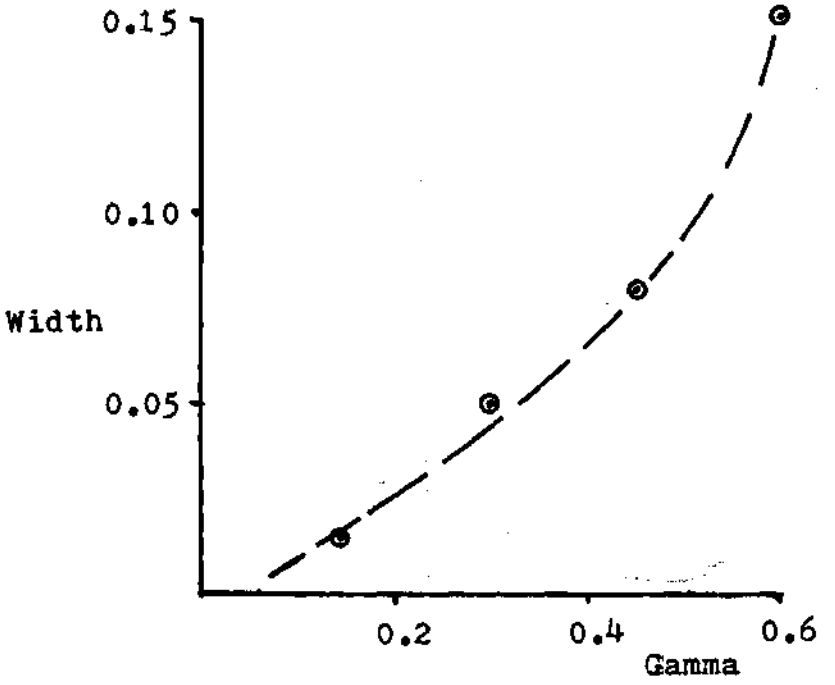

Figure 5-10. 3/2 Island Width vs Gamma.

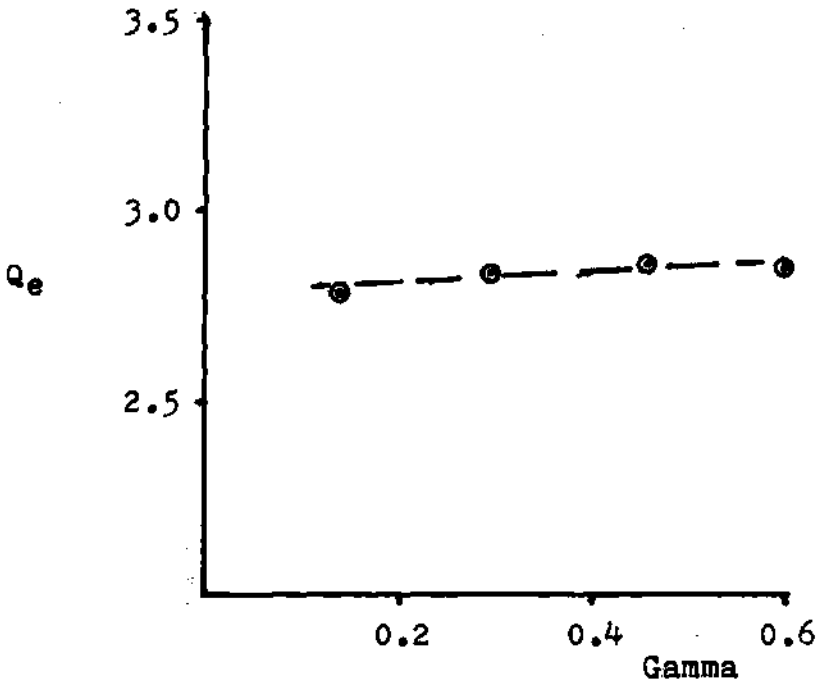

Figure 5-11. Q_e vs Gamma for 3/2 Island.

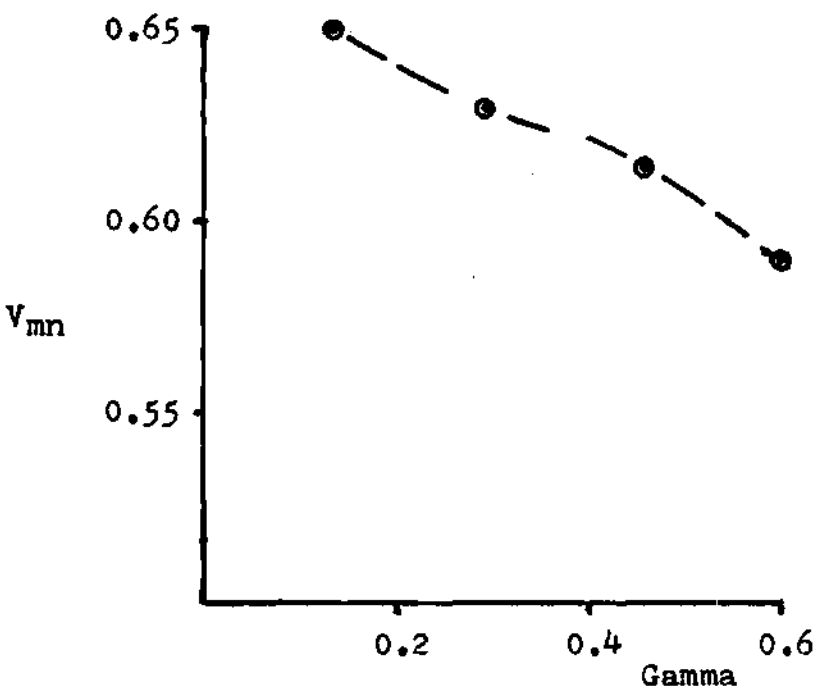

Figure 5-12. V_{mn} vs Gamma for 3/2 Island.

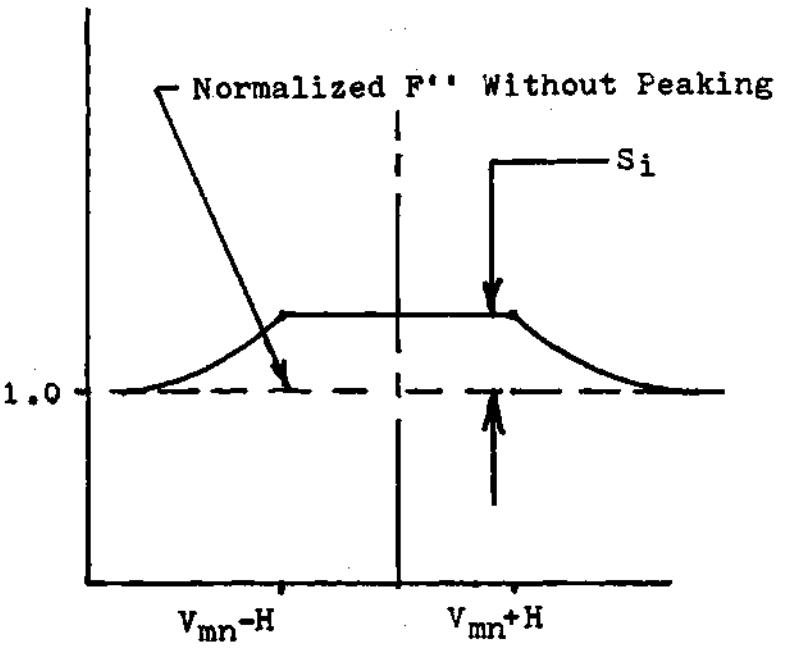

Figure 5-13. Normalized F'' with Peaking.

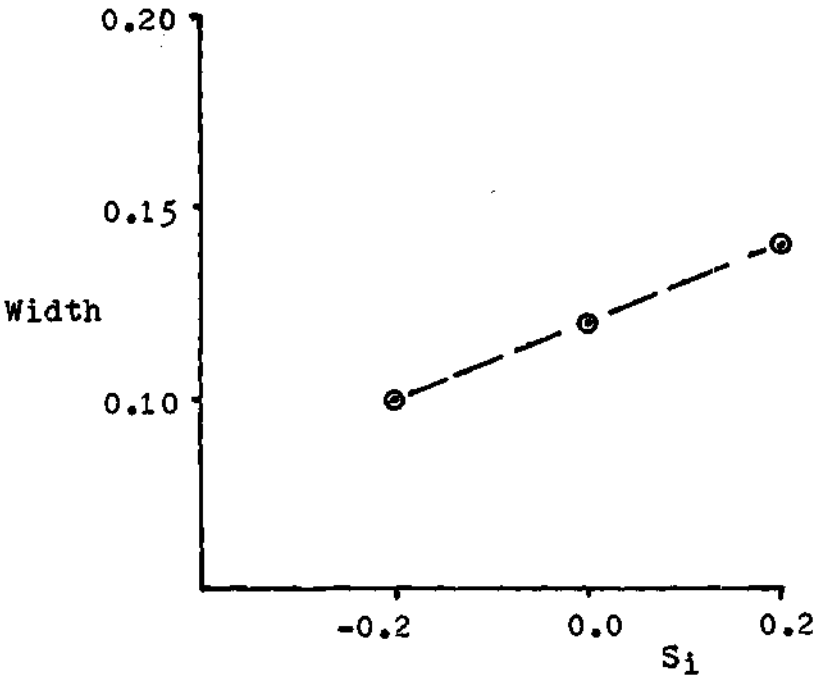

Figure 5-14. 2/1 Island Width vs S_i.

```
05:22:35  11/30/83  page  1

georgia tech eqlib/tearing
code  1983  by r. morris

        r0  4.000e+00
        e   1.000e+00
        r1  1.000e+00
        r2  0.

  1  moment harmonics
  2  hamada harmonics
c0  1.000e+00  c1  0.
c2  0.         c3  5.000e-01
ex -5.000e-01
```

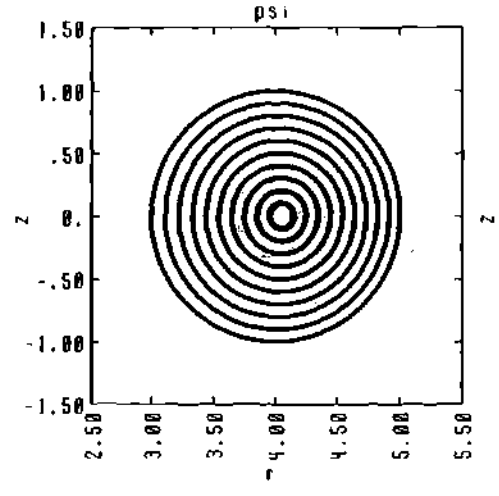

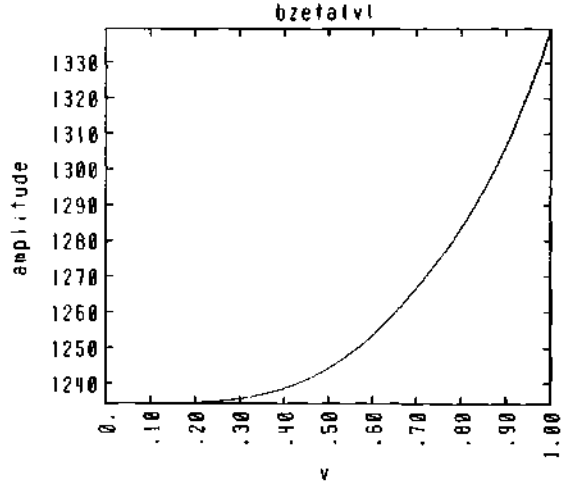

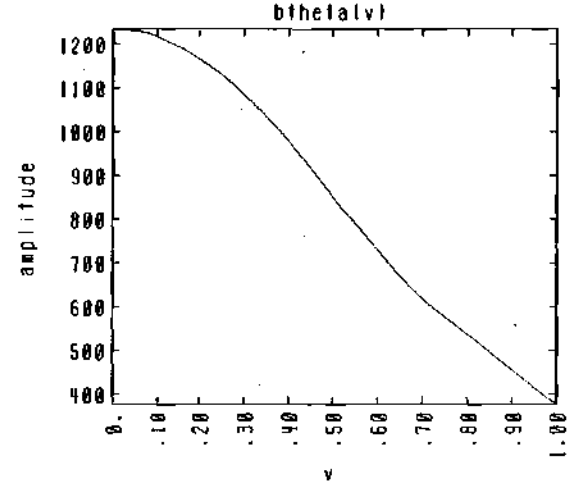

Figure 5-15a. Nonlinear 3/2 and 2/1 Island Coupling / P1.

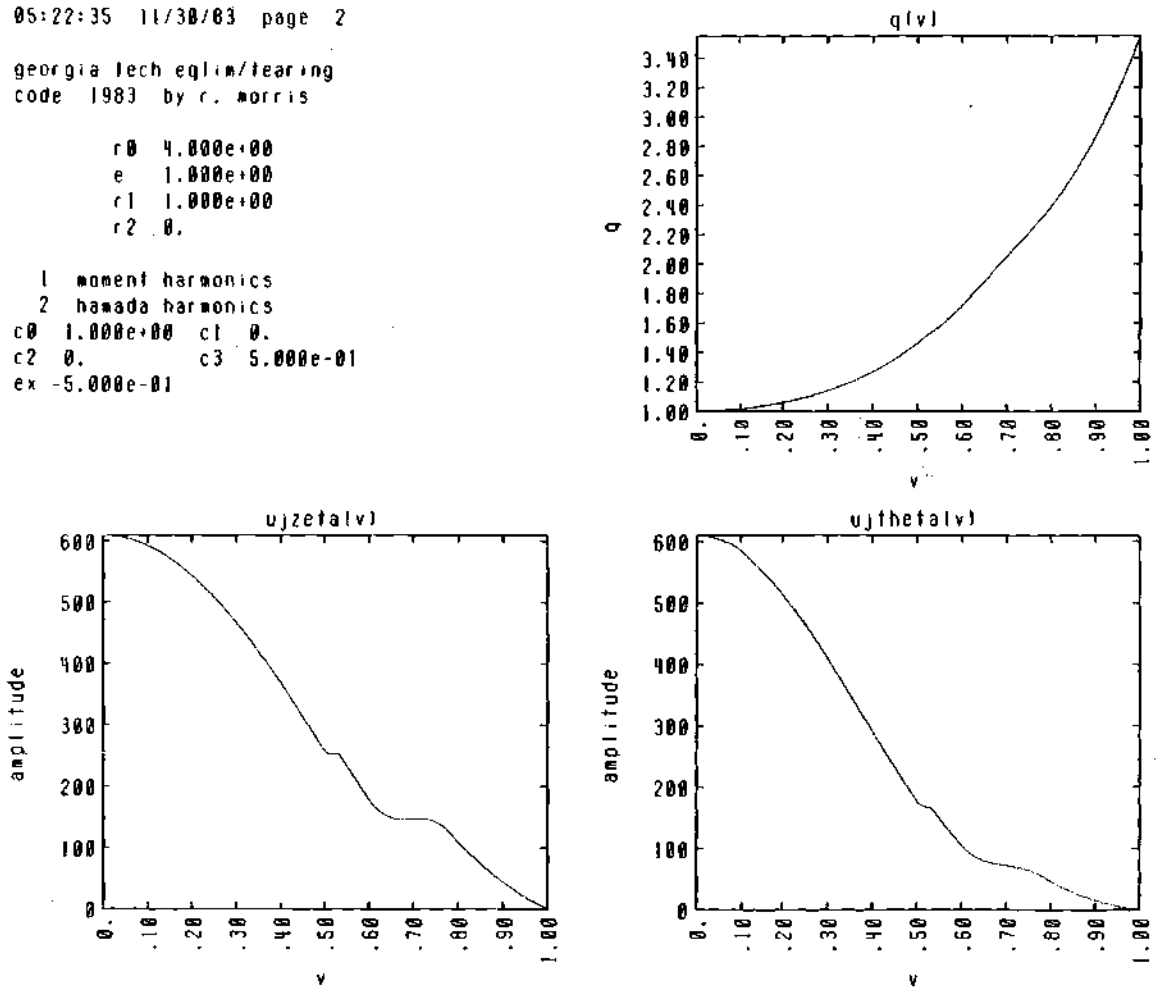

Figure 5-15b. Nonlinear 3/2 and 2/1 Island Coupling / P2.

```
05:22:35  11/30/83  page  3

georgia tech eqlim/tearing
code  1983  by r. morris

        r0  4.000e+00
        e   1.000e+00
        r1  1.000e+00
        r2  0.

  1  moment harmonics
  2  hamada harmonics
c0  1.000e+00  c1  0.
c2  0.         c3  5.000e-01
ex -5.000e-01 pex  2.500e+00
si1  0.        si2  0.
```

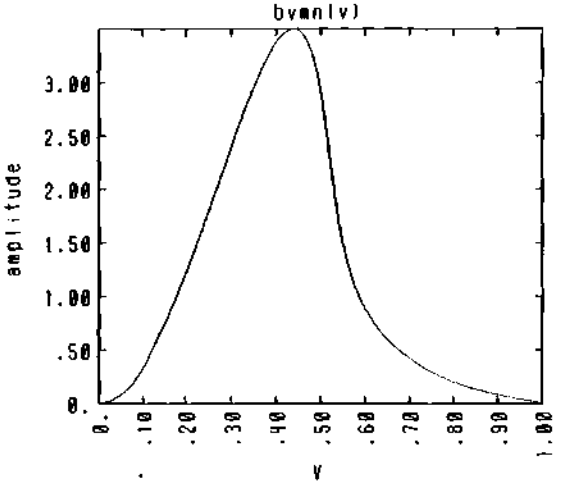

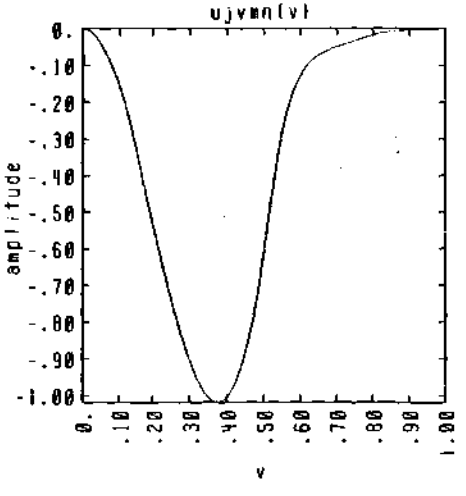


```
total number of modes          2
this mode                      3/ 2
halfwidth in q space           4.992e-02
dq/(dq/dv)                     4.223e-02
amp of this harmonic           2.338e+01
v rational for this mode       5.156e-01
gamma(1)                       3.000e-01
gamma(2)                       1.500e-01
```

Figure 5-15c. Nonlinear 3/2 and 2/1 Island Coupling / P3.

```
05:22:35  11/30/83  page  4

georgia tech eqlim/tearing
code  1983  by r. morris

        r0  4.000e+00
        e   1.000e+00
        r1  1.000e+00
        r2  0.

  1  moment harmonics
  2  hamada harmonics
c0  1.000e+00  c1  0.
c2  0.         c3  5.000e-01
ex -5.000e-01 pex  2.500e+00
si1  0.        si2  0.
```

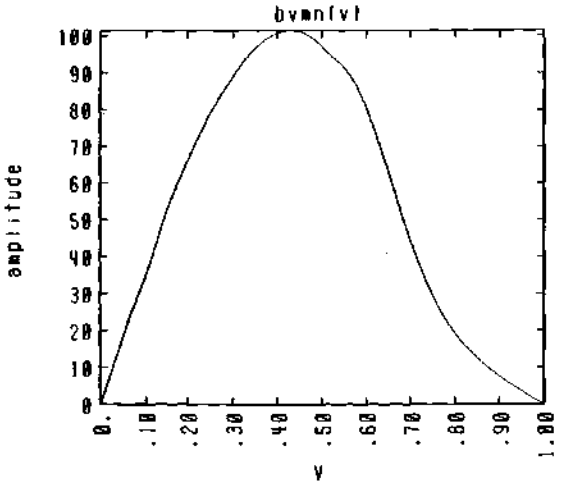

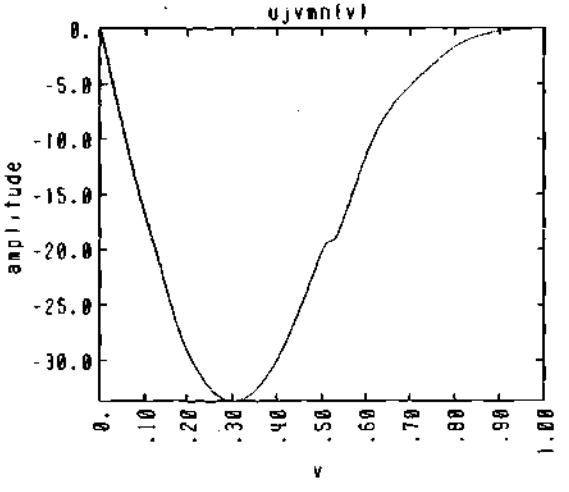

total number of modes	2
this mode	2/ 1
halfwidth in q space	3.868e-01
dq/(dq/dv)	1.820e-01
amp of this harmonic	2.824e+02
v rational for this mode	6.845e-01
gamma(1)	3.000e-01
gamma(2)	1.500e-01

Figure 5-15d. Nonlinear 3/2 and 2/1 Island Coupling / P4.

```
05:22:35  11/30/83  page  5

georgia tech eqlrm/tearing
code  1983  by r. morris

        r0  4.000e+00
        e   1.000e+00
        rt  1.000e+00
        r2  0.

  1  moment harmonics
  2  hamada harmonics
c0  1.000e+00  c1  0.
c2  0.         c3  5.000e-01
ex -5.000e-01 pex  2.500e+00
si1  0.        si2  0.
```

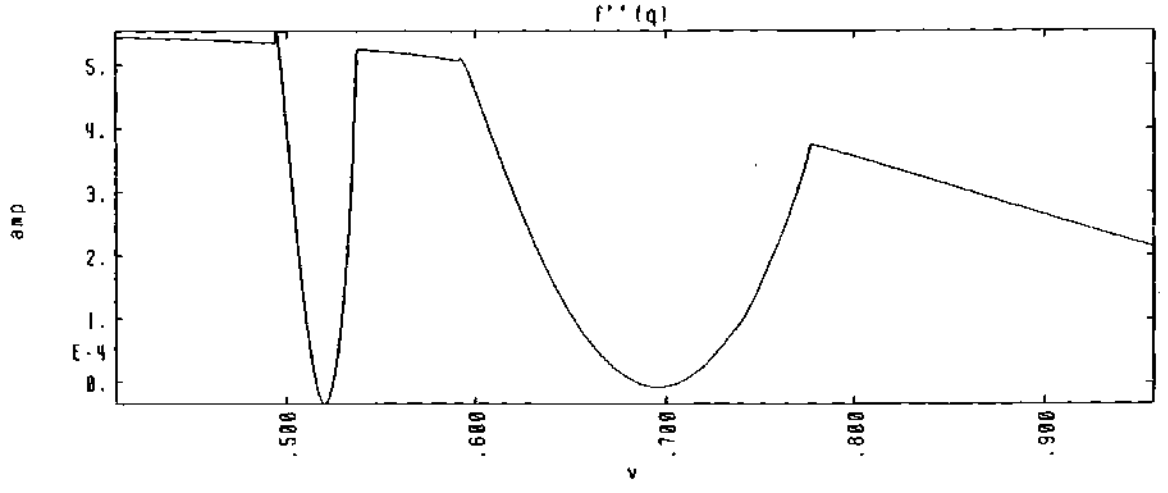

Figure 5-15e. Nonlinear 3/2 and 2/1 Island Coupling / P5.

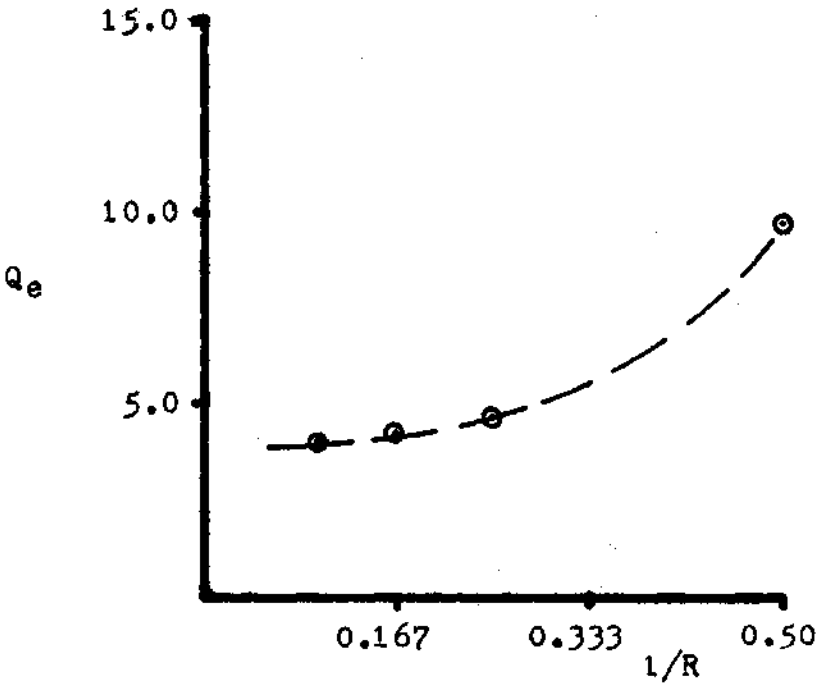

Figure 5-16. Q_e vs Inverse Aspect Ratio.

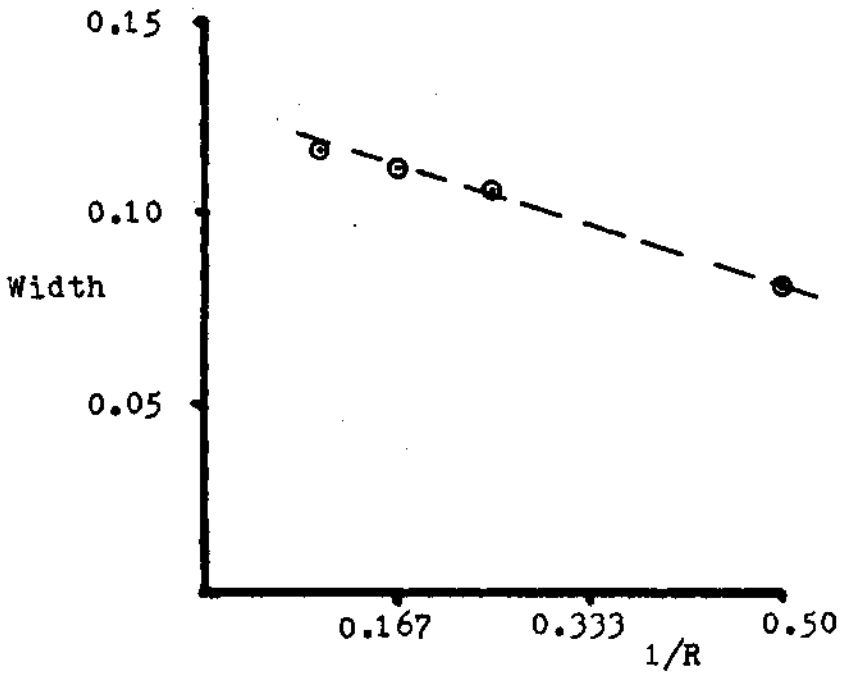

Figure 5-17. 2/1 Magnetic Island Width vs Inverse Aspect Ratio.

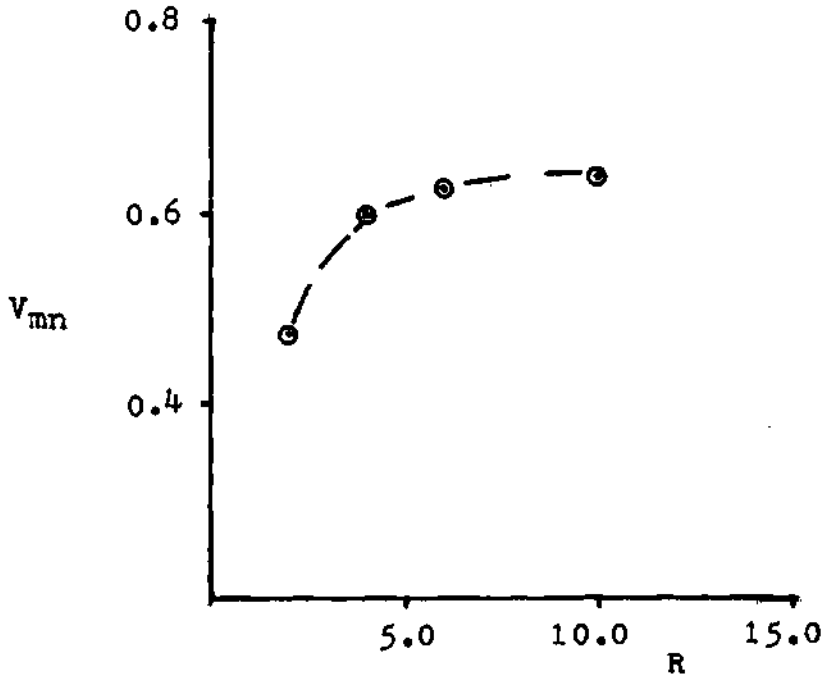

Figure 5-18. Mode Rational Surface Position vs Aspect Ratio.

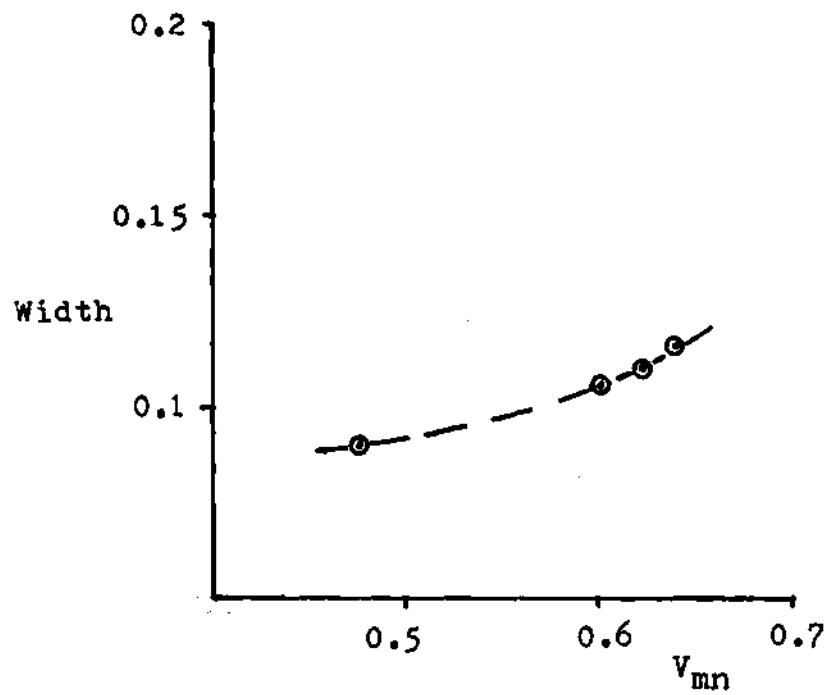

Figure 5-19. 2/1 Island Width vs V_{mn}.

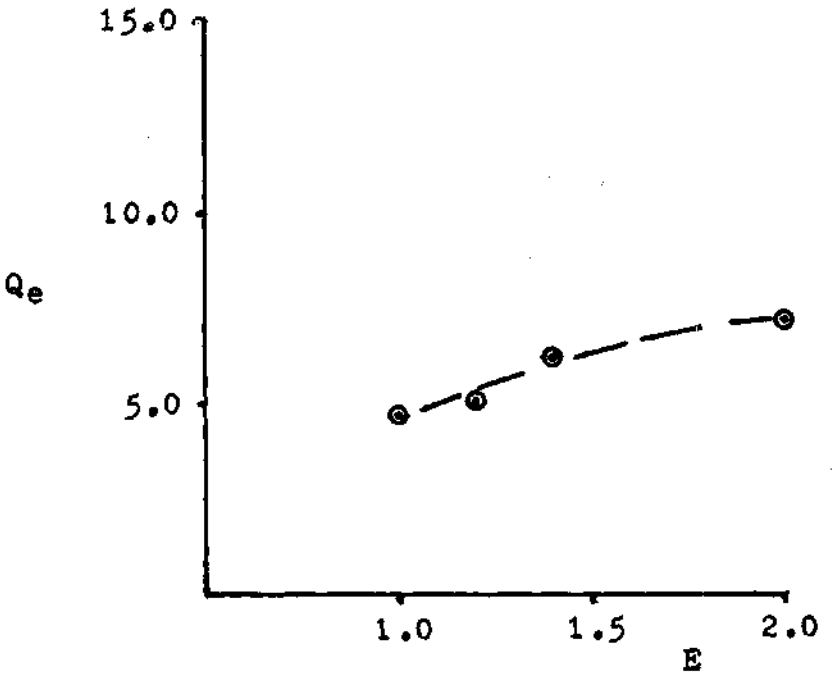

Figure 5-20. Q_e vs Elongation.

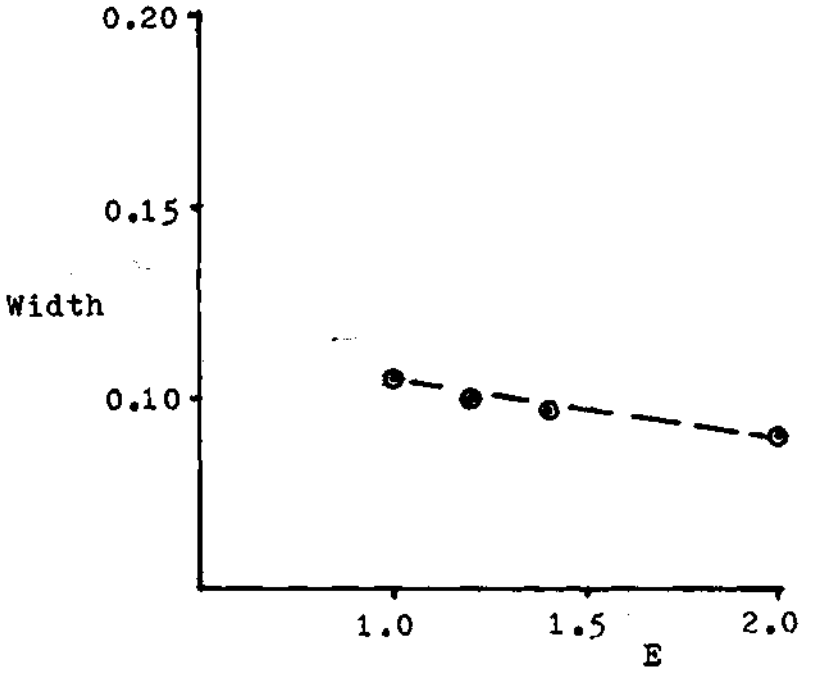

Figure 5-21. 2/1 Island Width vs Elongation.

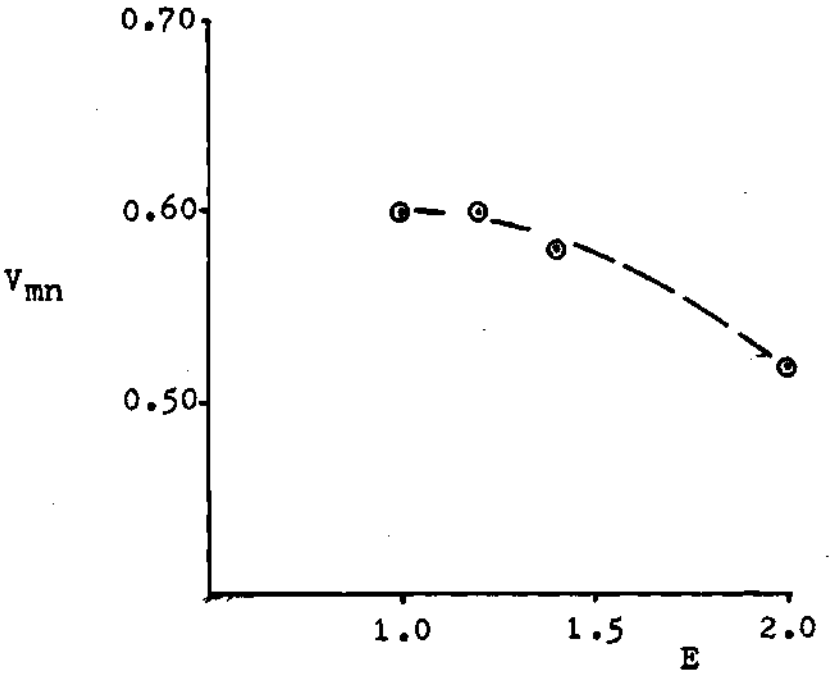

Figure 5-22. V_{mn} vs Elongation.

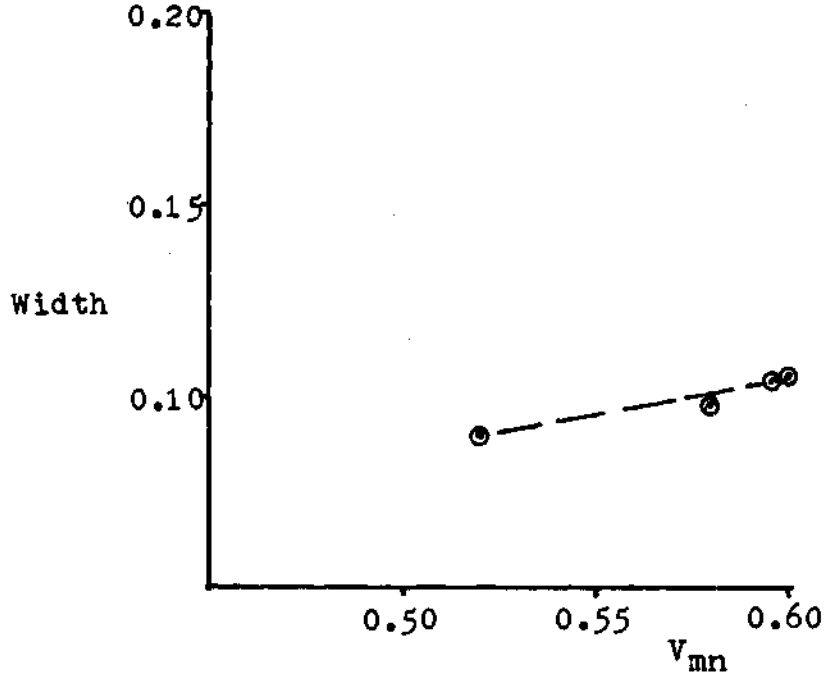

Figure 5-23. 2/1 Island Width vs V_{mn}.

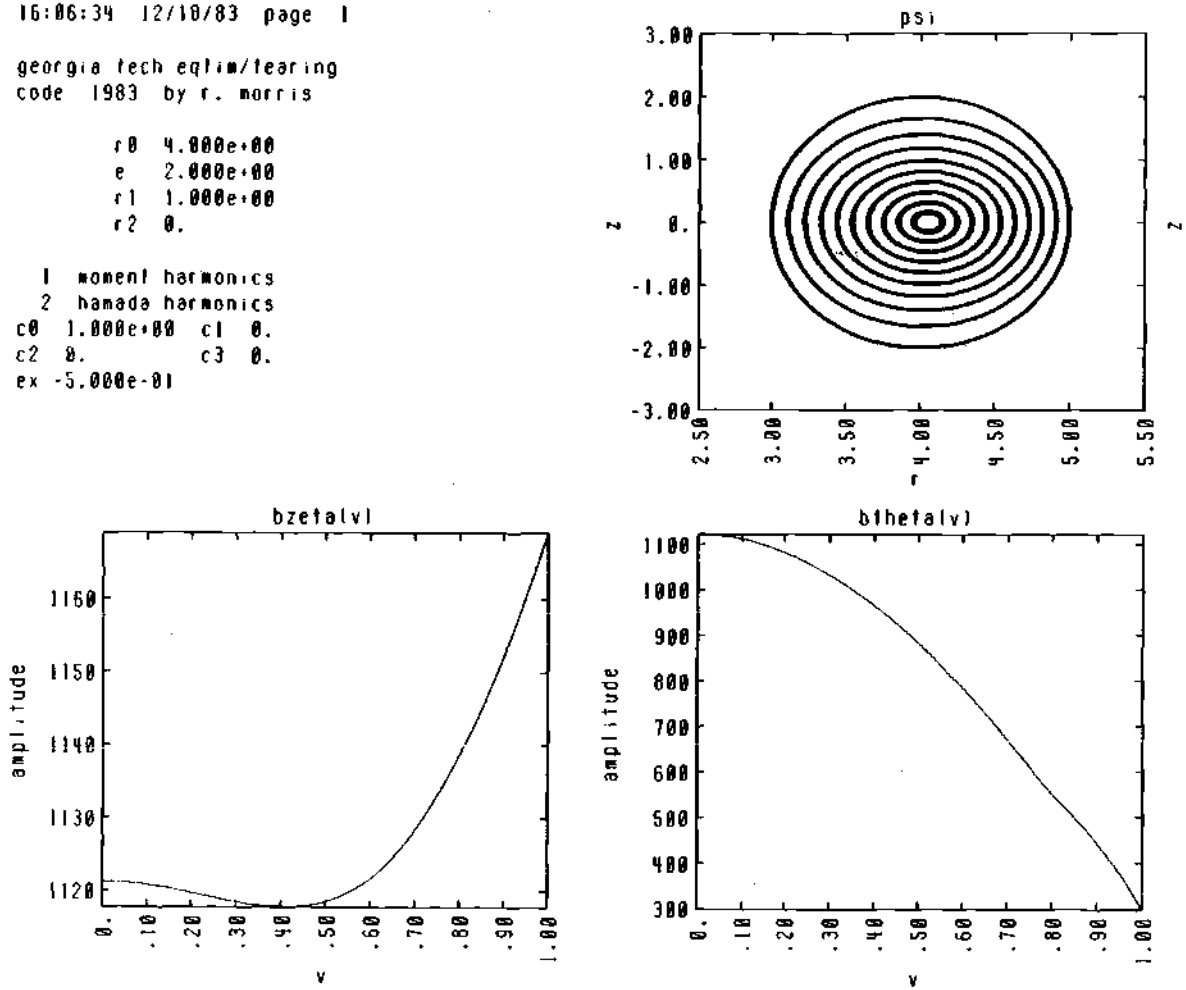

Figure 5-24a. Linear 2/1 and 3/1 Island Coupling / P1.

16:06:34 12/10/83 page 2

georgia tech eqlim/tearing
code 1983 by r. morris

r0 4.000e+00
e 2.000e+00
r1 1.000e+00
r2 0.

1 moment harmonics
2 hamada harmonics
c0 1.000e+00 c1 0.
c2 0. c3 0.
ex -5.000e-01

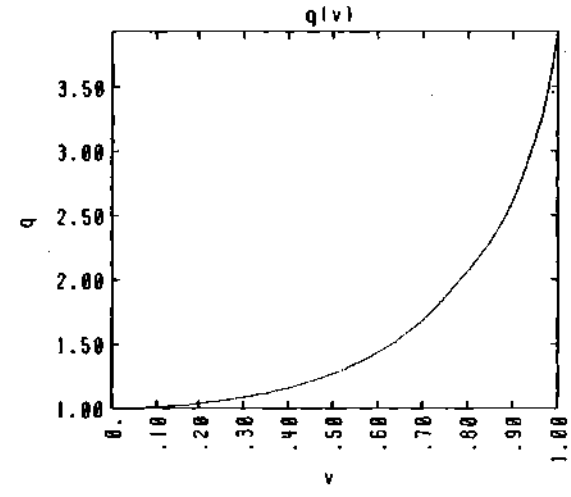

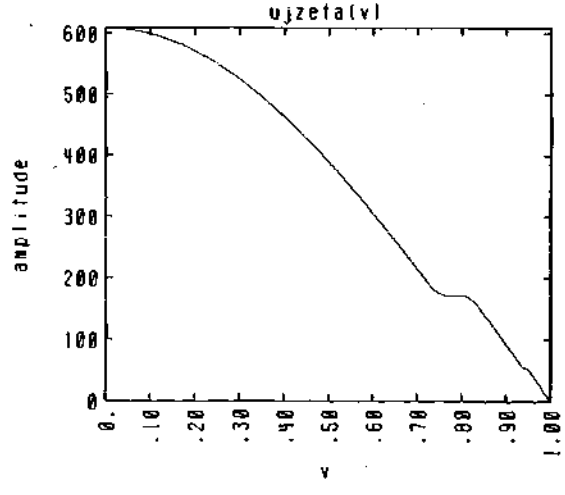

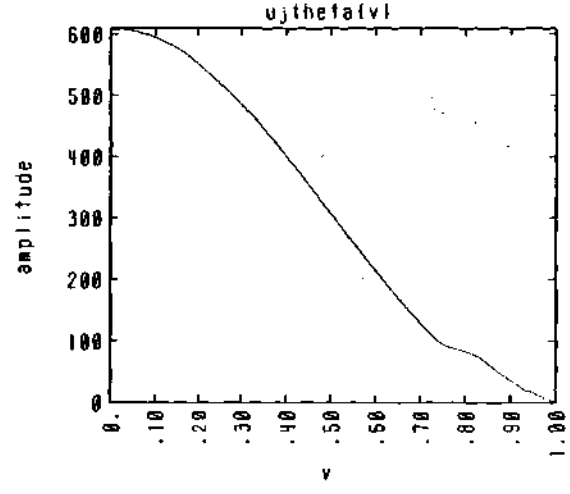

Figure 5-24b. Linear 2/1 and 3/1 Island Coupling / P2.

```
16:06:34  12/18/83  page  3

georgia tech eqlim/tearing
code  1983  by r. morris

        r0  4.000e+00
        e   2.000e+00
        rl  1.000e+00
        r2  0.

  1  moment harmonics
  2  hamada harmonics
c0  1.000e+00  cl  0.
c2  0.         c3  0.
ex -5.000e-01 pex  2.000e+00
sil  0.        si2  0.
```

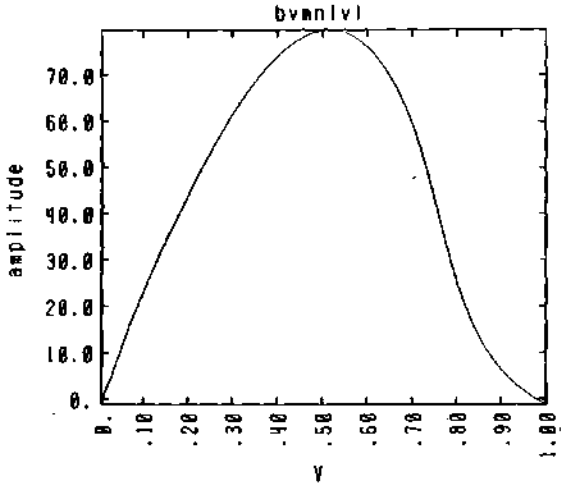

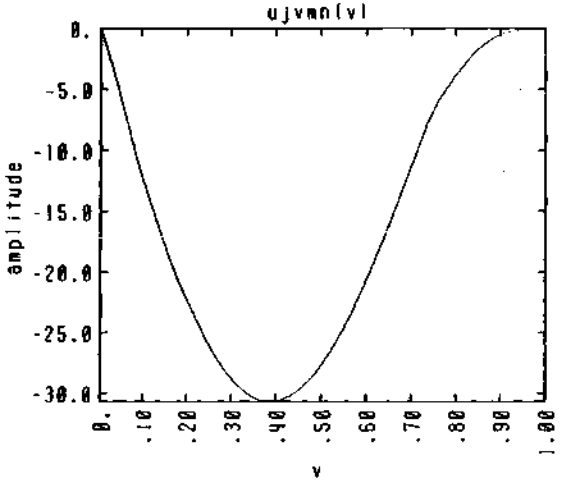


```
total number of modes          2
this mode                      2/ 1
halfwidth in q space           2.288e-01
dq/fdq/dvl                     1.103e-01
amp of this harmonic           1.757e+02
v rational for this mode       7.841e-01
gamma(1)                       0.
gamma(2)                       0.
```

Figure 5-24c. Linear 2/1 and 3/1 Island Coupling / P3.

```
16:06:34  12/10/83  page  4

georgia tech eqlim/tearing
code  1983  by r. morris

        r0  4.000e+00
        e   2.000e+00
        r1  1.000e+00
        r2  0.

  1  moment harmonics
  2  hamada harmonics
c0  1.000e+00  c1  0.
c2  0.         c3  0.
ex -5.000e-01 pex  2.000e+00
si1  0.        si2  0.
```

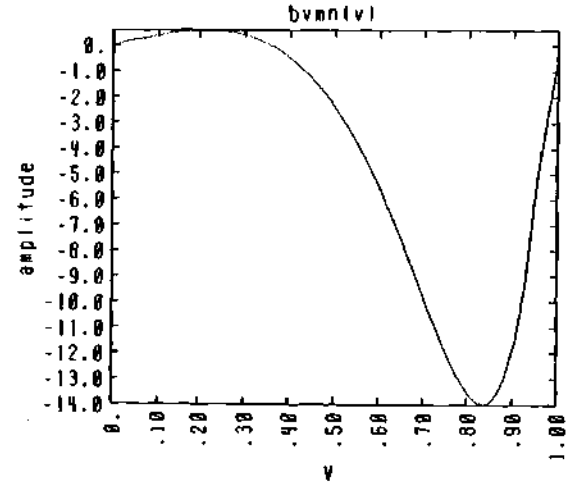

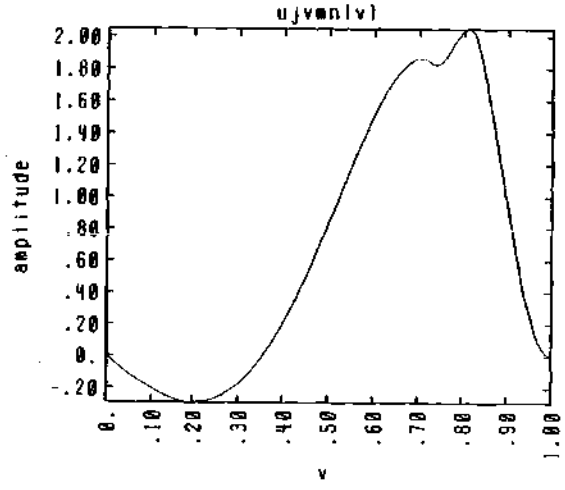


```
total number of modes          2
this mode                      3/ 1
halfwidth in q space           8.140e-02
dq/(dq/dv)                     1.455e-02
amp of this harmonic           6.582e+03
v rational for this mode       9.423e-01
gamma1(1)                      0.
gamma1(2)                      0.
```

Figure 5-24d. Linear 2/1 and 3/1 Island Coupling / P4.

```
16:06:34  12/10/83  page  5

georgia tech eqlim/tearing
code  1983  by r. morris

        r0  4.000e+00
        e   2.000e+00
        r1  1.000e+00
        r2  0.

  1  moment harmonics
  2  hamada harmonics
c0  1.000e+00  c1  0.
c2  0.         c3  0.
ex -5.000e-01 pex  2.000e+00
si1  0.        si2  0.
```

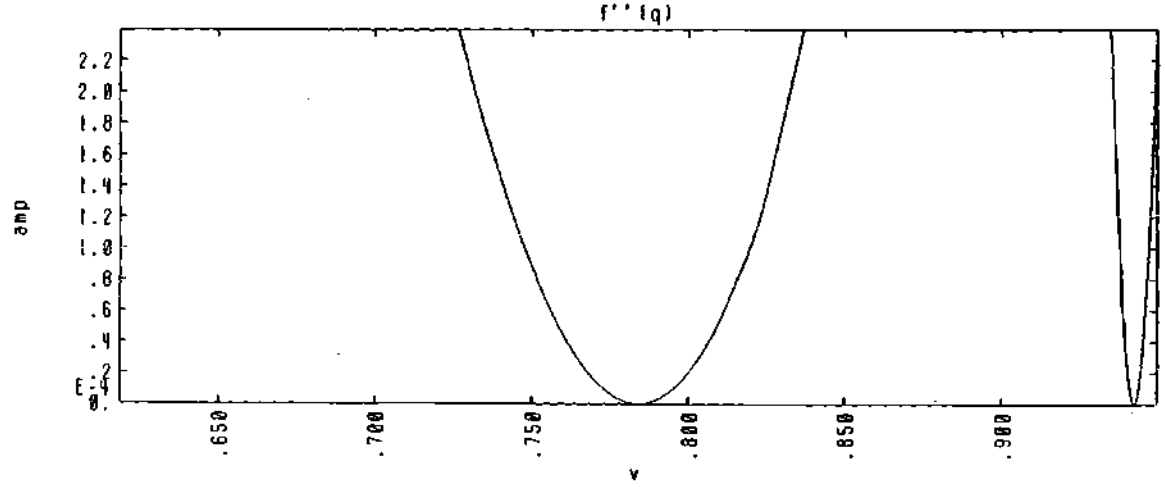

Figure 5-24e. Linear 2/1 and 3/1 Island Coupling /P5.